

HEALTH AND SCIENCE

EDITORS

Assoc. Prof. Dr. Yasemin TAŞCI
Prof. Dr. Sevi ÖZ

AUTHORS

Prof. Dr. Orhan ATAKOL
Prof. Dr. Özlem MORALOĞLU
Prof. Dr. Sevi ÖZ
Assoc. Prof. Dr. Ayşe Şebnem ERENLER
Assoc. Prof. Dr. Serkan KAHYAOĞLU
Assoc. Prof. Dr. Yasemin TAŞCI
Assist. Prof. Dr. Aykut YILMAZ
Assist. Prof. Dr. Kenan Selçuk TUNCAY
Assist. Prof. Dr. Ömer Hamit YUMUŞAK
Res. Assist. Kemal YÜCE
Res. Assist. Tuba ÜNVER
Ahmet İsmail ÖZKAN
Nagihan ÇEKİÇ
Zehra KARAPINAR ŞENTÜRK



İKSAD
Publishing House

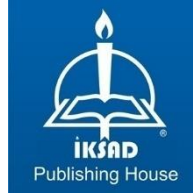
HEALTH AND SCIENCE

EDITORS

Prof. Dr. Sevi ÖZ
Assoc. Prof. Dr. Yasemin TAŞÇI

AUTHORS

Prof. Dr. Orhan ATAKOL
Prof. Dr. Özlem MORALOĞLU
Prof. Dr. Sevi ÖZ
Assoc. Prof. Dr. Ayşe Şebnem ERENLER
Assoc. Prof. Dr. Serkan KAHYAOĞLU
Assoc. Prof. Dr. Yasemin TASCI
Assist. Prof. Dr. Aykut YILMAZ
Assist. Prof. Dr. Kenan Selçuk TUNCAY
Assist. Prof. Dr. Ömer Hamit YUMUŞAK
Res. Assist. Kemal YÜCE
Res. Assist. Tuba ÜNVER
Ahmet İsmail ÖZKAN
Nagihan ÇEKİÇ
Zehra KARAPINAR ŞENTÜRK



Copyright © 2020 by iksad publishing house
All rights reserved. No part of this publication may be reproduced,
distributed or transmitted in any form or by
any means, including photocopying, recording or other electronic or
mechanical methods, without the prior written permission of the publisher,
except in the case of
brief quotations embodied in critical reviews and certain other
noncommercial uses permitted by copyright law. Institution of Economic
Development and Social
Researches Publications®
(The Licence Number of Publicator: 2014/31220)
TURKEY TR: +90 342 606 06 75
USA: +1 631 685 0 853
E mail: iksadyayinevi@gmail.com
www.iksadyayinevi.com

It is responsibility of the author to abide by the publishing ethics rules.
Iksad Publications – 2020©

ISBN: 978-625-7897-22-8
Cover Design: İbrahim KAYA
June / 2020
Ankara / Turkey
Size = 16 x 24 cm

İÇİNDEKİLER

EDITORS

FOREWORD

Assoc. Prof. Dr. Yasemin TAŞÇI, Prof. Dr. Sevi ÖZ..... 1

CHAPTER 1

SELECTED HEAVY METAL AND TRACE ELEMENT LEVELS IN WHOLE BLOOD AND PERITONEAL FLUID OF OVARIAN ENDOMETRIOSIS: A PRELIMINARY STUDY

Assist. Prof. Dr. Ömer Hamit YUMUŞAK, Assoc. Prof. Dr. Yasemin TASCİ, Prof. Dr. Özlem MORALOĞLU, Assoc. Prof. Dr. Serkan KAHYAOĞLU Serkan KAHYAOĞLU, Prof. Dr. Orhan ATAKOL, Prof. Dr. Sevi ÖZ	4
INTRODUCTION.....	5
SUBJECTS AND METHODS	7
RESULTS AND DISCUSSION.....	9
CONCLUSION	13
REFERENCES	14

CHAPTER 2

DEEP DETECTION OF CERVICAL CANCER FROM PAP SMEAR IMAGES

Zehra KARAPINAR ŞENTÜRK, Nagihan ÇEKİÇ	19
INTRODUCTION.....	21
MATERIALS AND METHODS	25
RESULTS.....	28
CONCLUSION	29
REFERENCES	30

CHAPTER 3

SPECIES IDENTIFICATION ABILITIES OF NUCLEAR AND PLASTID DNA REGIONS, THEIR IMPORTANCE IN PHYLOGENETIC RELATIONSHIPS AMONG *Colchicum L.* Species

Asst. Prof. Aykut YILMAZ.....	35
INTRODUCTION.....	37
MATERIAL AND METHODS FOR PHYLOGENETIC ANALYSIS OF COLCHICUM TAXA.....	39
NUCLEAR AND PLASTID DNA REGIONS USED FOR COLCHICUM TAXA AND THEIR ANALYSIS RESULTS.....	40
CONCLUSION	48
REFERENCES.....	52

CHAPTER 4

STRUCTURE AND FUNCTION OF THREE CLASSES OF C₂H₂ ZINC FINGER (ZNF) PROTEINS

Res. Assist. Kemal YÜCE, Ahmet İsmail ÖZKAN	65
INTRODUCTION.....	67
1. TRIPLE-C ₂ H ₂ (TC ₂ H ₂) FINGER PROTEINS.....	69
2. MULTIPLE-ADJACENT-C ₂ H ₂ (MAC ₂ H ₂) FINGER PROTEINS ..	71
3. SEPARATED-PAIRED-C ₂ H ₂ (SPC ₂ H ₂) FINGER PROTEINS	80
REFERENCES.....	84

CHAPTER 5

A VERY RARE REASON OF NASAL OBSTRUCTION: INFERIOR TURBINATE PNEUMATIZATION: REPORT OF TWO CASES

Assist. Prof. Dr. Kenan Selçuk TUNCAY	95
INTRODUCTION.....	97
CASE REPORTS	103
CASE 1.....	103
CASE 2.....	107
DISCUSSION	111
CONCLUSION	116
REFERENCES.....	117

CHAPTER 6

COMPARATIVE EVALUATION OF IN-VITRO METHODS FOR ANTIMICROBIAL ACTIVITY DETERMINATION

Res. Assist. Tuba ÜNVER, Assoc. Prof. Dr. Ayşe Şebnem ERENLER	121
INTRODUCTION.....	123
1. A SHORT HISTORY OF ANTIMICROBIAL ACTIVITY METHODS	124
2. PURPOSE OF USE OF ANTIMICROBIAL ACTIVITY	124
3. THE METHODS FOR DETERMINING ANTIMICROBIAL ACTIVITY	125
4. CORRECT USAGE OF ANTIMICROBIAL SUBSTANCES AND MANAGEMENT OF THIS TARGET	141
5. ACCURATE AND RATIONAL ANTIMICROBIAL USE IN MEDICINES	142
CONCLUSION	143
REFERENCES.....	145

FOREWORD

We are delighted to write the foreword for this health and science book. We would like to thank to whole IKSAD publication team and all the authors who contributed to the book.

It is our hope and expectation that this book will provide an effective learning experience and referenced resource for all health and science professionals.

Editors

Assoc. Prof. Dr. Yasemin TAŞÇI¹

Prof. Dr. Sevi ÖZ²

¹ Department of Obstetrics and Gynecology, Ministry of Health, Ankara City Hospital, Ankara, Turkey

² Department of Chemistry, Faculty of Science and Arts, Ankara Hacı Bayram Veli University, Turkey

CHAPTER 1

**SELECTED HEAVY METAL AND TRACE ELEMENT
LEVELS IN WHOLE BLOOD AND PERITONEAL FLUID OF
OVARIAN ENDOMETRIOSIS: A PRELIMINARY STUDY**

Ömer Hamit YUMUŞAK¹, Yasemin TASCI¹,
Özlem MORALOĞLU¹, Serkan KAHYAOĞLU¹,
Orhan ATAKOL², Sevi ÖZ³

¹ Department of Obstetrics and Gynecology, Ministry of Health, Ankara City Hospital, Ankara, Turkey

² Department of Chemistry, Faculty of Science, Ankara University, Ankara, Turkey

³ Department of Chemistry, Faculty of Science and Arts, Ankara Hacı Bayram Veli University, Turkey

INTRODUCTION

Endometriosis is a benign, estrogen-dependent, chronic inflammatory disease characterized by the presence of endometrial tissue outside the uterus. It affects 6-10% of women of reproductive age and the patients suffer from dysmenorrhea, dyspareunia, chronic pelvic pain and infertility¹. Despite a large number of studies on endometriosis, its etiology has not been clearly defined yet. Recent data suggest that a combination of factors (hormonal, genetic, environmental, anatomical and immunological) plays a role in the pathogenesis of this disorder²⁻⁴. Among these related factors, smoking, environmental factors are of particular importance because of the elevated risk of environmental contamination due to foods, consumption and exposure to industrial products.

Heavy metals is one of the most widely-distributed environmental pollutants and commonly defined as a group elements with a specific density of more than 5 g cm^{-3} , but this definition is often a definition for high-density metals such as Cd, Hg, and Pb, and there is no scientific basis for this definition because heavy metal ions are used for non-essential toxic elements for living beings, although beryllium (Be) and aluminum (Al) densities are not essential for living beings, they are considered as pollution^{5, 6}. These elements can be not destroyed and disposed in biological medium, they cause various syndromes resulting of bioaccumulation via the food chain. Some of these metals are as useful as a certain concentration for living organisms and they have physiological roles in the living body including iron (Fe), zinc (Zn),

copper (Cu), manganese (Mn), cobalt (Co), molybdenum (Mo). These elements are generally known as essential elements, but even these elements have a toxic effect after a certain concentration. Among these non-essential elements are Be, aluminum (Al), cadmium (Cd), mercury (Hg), lead (Pb), as well as other non-essential elements countable. In the current literature there are a number of human studies and animal experimental research demonstrating their direct and potential adverse effects on nervous system, bones, kidneys, reproductive function and immune system⁷⁻¹⁰. Current information based on epidemiological and experimental studies on the effects of heavy metal exposure on female reproduction is that it was negatively associated with poor ovarian follicular health, reduced fecundity, and adverse pregnancy outcomes in women¹¹⁻¹³. Among these elements cadmium, which is considered to be a metalloestrogen, has been shown in several studies that may be a potential causative agent of estrogen-dependent diseases such as breast cancer, endometrial cancer and endometriosis^{4, 14-16}. In cases of endometriosis there are a few studies evaluating the levels of heavy metals other than cadmium and these elements were measured in whole blood or urine in these studies^{15, 17-19}. A case control study by Silva et al have demonstrated the presence of cadmium, lead and nickel in ectopic endometrial tissue and they hypothesized that the hematogenous route as a possible source of heavy metals in the ectopic endometrial tissue²⁰. However, in the literature, there is no study investigating heavy metal levels in the peritoneal fluid in ovarian endometriosis.

The aim of this presented study was to evaluate the levels of heavy metals in cases of endometriosis in whole blood and peritoneal fluid which is increasing and changing content in these patients and compare with the results in healthy women. There are no other studies evaluating heavy metal and trace element levels in the peritoneal fluid in endometriosis cases in the literature.

SUBJECTS AND METHODS

Study population: This case-control trial was carried out on 22 reproductive age women who underwent laparoscopy for symptomatic ovarian endometriosis at Reproductive Endocrinology Clinic of Zekai Tahir Burak Womens Health Research Hospital. Also, 22 matched healthy women with normal pelvic anatomy without endometriosis that underwent laparoscopy for tubal sterilization served as the control group. Exclusion criteria included the presence of any acute or chronic disease, active pelvic inflammatory disease and be a current smoker. The study protocol following approval from the local ethical committee and written informed consent was obtained from all participants. All the participants of the study group were stage 3-4 endometriosis according American Fertility Society (r-ASRM) scoring system. Two patients in the control group were withdrawn the study because blood samples could not be analyzed; one patient was removed from study due to her request.

After overnight fasting, venous blood samples (5 mL) were collected from the antecubital vein from all patients before any intervention. At

laparoscopy, a lavage of the lower peritoneal cavity with 10 mL normal saline was performed and peritoneal fluid samples were collected from the cul-de-sac into a sterile syringe from all the participants at the beginning of the laparoscopic surgery after insertion of trocars.

Cr, Fe, Ni, Cu, Zn, and lead levels were determined in the samples of whole blood and peritoneal lavage fluid samples were determined by electrothermal atomic absorption (ETAAS or GFAAS) method.

Sample preparation: A part of blood or peritoneal fluid sample was weighed in an analytical balance and transferred into a Kjeldahl flask. Then, 5.00 mL of the certificated HNO₃ (63%, $d = 1.43 \text{ g mL}^{-1}$) and 5.00 mL of H₂O₂ were put in the flask and the mixture was boiled for about half an hour until colorless. Later, this solution was put in a 50.00 mL flask and diluted to 50 mL from where the samples were injected to the Atomic Absorption Spectrometer (AAS). GBC Avanta PM model AAS with GF 3000 power supply and PAL 3000 auto sampler was used and atomization was achieved by graphite furnace electrothermally (GBC Scientific Equipment Pty. Ltd., Braeside, Victoria, Australia). All solutions were prepared with de-ionized water with 0.55 mS/cm conductivity. Calibration curves were obtained for 1–200 mg/L standard solutions prepared from 1000 mg/L commercial stock solutions (Merck, Darmstadt, Germany). The graphite oven temperature programs are shown in Table 1. LOQ values were assessed with respect to standard methods designated in literature^{21,22}. The value where the standard deviation and signal/noise ratio values of the blank solution was 10, has been designated as LOQ. Also the adsorption

values were measure using 0.1–3.0 mg/L standard solutions and the linear border region of the calibration curve was determined from the graph. The obtained LOQ values are as shown below:

Cr: 1.95 $\mu\text{g L}^{-1}$ Ni: 2.20 $\mu\text{g L}^{-1}$ Cu: 1.34 $\mu\text{g L}^{-1}$ Zn: 0.68 $\mu\text{g L}^{-1}$ Cd: 0.36 $\mu\text{g L}^{-1}$ Pb: 2.70 $\mu\text{g L}^{-1}$

Table 1. Temperature programming of graphite cuvette using ETAAS method

Determined Element	Drying			Ashing			Reading			Cleaning		Inert Gas
	Ramp Time(s)	$^{\circ}\text{C}$	Hold. Time(s)	Ramp Time(s)	$^{\circ}\text{C}$		Ramp Time(s)	$^{\circ}\text{C}$	Hold. Time(s)	Ramp Time(s)	$^{\circ}\text{C}$	
Cr	5	80	5	5	750	0	1.5	2500	1.5	2600	1.5	Ar
	5	120	10									
Ni	5	80	5	5	700	0	1.5	2300	1.5	2500	1.5	Ar
	5	120	10									
Cu	5	80	5	5	600	0	1.5	2300	1.5	2500	1.5	Ar
	5	120	10									
Zn	5	80	5	5	450	0	1.5	2100	1.5	2500	1.0	Ar
	5	120	10									
Cd	5	80	5	5	400	0	1.5	1900	1.4	2500	1.0	Ar
	5	120	10									
Pb	5	80	5	5	350	0	1.5	2100	1.5	2500	1.0	Ar

In addition, due to the lack of a reference standard material, accuracy of the analysis and the effect of the matrices in the media were controlled with the standard addition method.

RESULTS AND DISCUSSION

Mean (\pm SD) age in cases and controls were 32.13 \pm 3.5 and 32.4 \pm 2.7 years respectively ($p=0.78$). Cases and controls were similar in body mass index while none of the women who participated in the study were current smokers. The mean values with standard deviations of the results of the atomic absorption study are given in Table 2.

Table 2. The results of the atomic absorption study

Measurement Group		Measured Heavy metal					
		Cr ppb*	Fe ppm*	Cu ppm	Zn ppm	Cd ppb	Pb ppm
Endometriosis group n=22	Blood	57.61±38.72 n=22	37.40±15.03 n=22	0.699±0.343 n=21	11.57±4.47 n=22	19.23 n=21	0.429±0.302 n=20
	Abdominal Fluid	4.08 n=22	15.04 n=22	0.605±0.285 n=21	4.66±3.55 n=22	18.28 n=21	0.101±0.049 n=20
Control group n=19	Blood	59.80±7.69 n=19	37.66±15.51 n=19	0.632±0.288 n=19	9.33±2.25 n=19	11.43 n=18	0.199±0.098 n=18
	Abdominal Fluid	4.51 n=19	17.56±14.85 n=19	0.194 n=19	3.35±1.23 n=19	10.03 n=18	0.116±0.041 n=18

*Measured concentration values are given as ppb and ppm according to the blood and abdominal fluid volumes

ppm: *Parts per million* ppb: *Parts per billion*

The reason of the higher numeric values at the Table 1 is that the adjustment of the measurement results. The average amounts of Fe, Zn, Pb and Cu in a human of 70 kg body weight are 4.0 g, 2.3 g, 0.12 g and 0.07 g, respectively²³. Naturally, these elements are found at different concentrations in different tissues and there is equilibrium between these tissues by means of blood and body fluids²³. However, it can be say with a practical calculation over homogeneous distribution that average concentrations of Fe, Zn, Pb and Cu are 57 ppm, 33 ppm, 1.7 ppm and 1.0 ppm, respectively. In this study, measurements are made with the prepared samples which are diluted to 50 mL suspensions following to digestion of the 2-5 g blood. The results are given as the values calculated for 1 kg of blood.

High ranges of the measurement results of the elements are bringing some calculation difficulties on standard deviations. It has seen from

the measurements that results and standard deviations of the study and control group for the Fe, Cu and Zn, which are essential for the livings, are acceptable¹⁶. However, standard deviations for Pb were high and also standard deviation of the Cd analysis couldn't be calculated from the peritoneal fluids of the patient and control group. Fe was detected from all samples except blood and peritoneal fluid samples of the two subjects from control group. While, Cu was below of the limit of detection for 1 blood and 8 peritoneal fluid samples, it was measured at essential amounts for the rest of the samples. Cr was detected at the all blood samples from study and control groups, but it was detected at only 3 peritoneal fluid samples of the study and control groups.

On the other hand, average concentrations of the relative soft metals (Zn, Cd and Pb) in both blood and peritoneal samples were seen higher in the patients than control group and this finding is consistent with the results of other studies^{4, 17, 24}. In our study, Zn are detected all study and control group subjects. But, however, Cd was detected in the 10 blood and 5 abdominal fluid samples of the patients and it was detected in the 6 blood and 4 abdominal fluids samples of the control group. Pb couldn't been detected in one blood sample from both study and control groups, however Pb could be detected in 6 and 7 abdominal fluid samples from study and control group, respectively. In our study, whole blood nickel levels were detected in the blood of 7 patients, all of whom were in the control group; none of the participants could be detected in the peritoneal fluid. On the contrary, a case control study conducted by Silva et al in Sri Lankan women indicated that whole blood nickel levels

were higher in women with endometriosis compared to healthy women²⁵.

For our study, higher mean values for Cd and Pb in endometriosis group are consistent with the literature^{15, 17, 19}. In the literature, no study has been reported about the average Cd and Pb concentrations in the healthy people. Mostly, the data are getting from the comparisons of the study and control groups. In this regard, it couldn't have been possible to compare measured values with other healthy/patient groups. However, as is known, Cd and Pb are non-essential elements and they accumulate on the soil and plants by spreading with an evaporation and condensation²⁶. Therefore, Cd and Pb accumulations in human body are strictly depends on their environment, living conditions and dietary habits. This can explain the accumulation of the Cd and Pb and their different concentrations in human tissues^{26, 27}. Cd and Pb are also soft metals and tends to complex with soft ligands. Cd and Pb usually accumulate in hair, keratin and the tissues rich from sulphur but they are in equilibrium at the blood and body fluids. When upper limit levels of Cd and Pb in control group, patient and control groups' different level of income and selection of the subjects from different social environments taken into the account, it can be said that dietary and food selection habits of the Turkish women living in the city center or suburbs of the Ankara are the same.

Nearly all of the studies have shown that metal analysis in various tissues of women with endometriosis results in higher Pb and Cd levels than control groups^{15, 16, 19}. It has been found that the accumulation of

these heavy metals in endometriosis patients is associated with the use of cigarettes or environmental factors in time. In our study patients with current smoker were not included, but the status of passive smoking or the possible effects of being a smoker in the past has not been questioned.

As a result, although it is not possible to show the exact role of heavy metals and trace elements in the pathogenesis of endometriosis in this study due to the small sample size, the detection of some heavy metals, even in the peritoneal fluid, is of importance.

CONCLUSION

Residing near Ankara in Turkey and in patients with endometriosis in blood and peritoneal lavage fluid samples some heavy metal and trace elements levels were determined but, the fact that the number of samples was not large did not allow for a statistical evaluation. However, in parallel with literature, it was determined by atomic absorption spectroscopy that the average of Cd and Pb values of soft metals in endometriosis patients is higher than that of control group.

REFERENCES

1. Giudice Linda C, Kao Lee C. Endometriosis. *Lancet* 2004; 364:1789-99.
2. Van Langendonckt A, Casanas-Roux F, Dolmans MM, Donnez J. Potential involvement of hemoglobin and heme in the pathogenesis of peritoneal endometriosis. *Fertil Steril* 2002; 77(3): 561-570.
3. Heilier JF, Donnez J, Lison D. Organochlorines and endometriosis:A mini-review. *Chemosphere*. 2008; 71:203-10.
4. Ryzimski Piotr, Ryzimski Pavel, Tomczyk K, Niedzielski P, Jakubowski K, Poniedzialek B, Opala T. Metal status in human endometrium: Relation to cigarette smoking and histological lesions. *Environ Res* 2014; 132: 328-33.
5. Duffus JH. “Heavy Metals”- A meaningless term. *Pure Appl Chem* 2002; 74:793-807.
6. Newton DE. *Chemistry of the Environment. Facts on File*. 2007; 119-24.
7. Jang DH, Hoffman RS. Heavy Metal Chelation in Neurotoxic Exposures. *Neurol Clin* 2011; 29:607-22.
8. Youness ER, Mohammed NA, Morsy FA. Cadmium impact and osteoporosis: mechanism of action. *Toxicol Mech Methods* 2012; 22: 560-67.
9. Hu H. Human health and heavy metals exposure. McCally M. (ed.). *Life support: the environment and human health*. MIT press, Massachusetts 2002; 4: 65–82.

10. Sharpe RM, Franks S. Environment, lifestyle and infertility – an intergenerational issue. *Nat Cell Biol* 2002; 4(S1): 33–40.
11. Pillai A, Priya L, Gupta S. Effects of combined exposure to lead and cadmium on the hypothalamic-pituitary axis function in proestrous rats. *Food Chem Toxicol* 2003; 41:379–384.
12. Chattopadhyay S, Ghosh D. The involvement of hypophyseal gonadal and hypophyseal-adrenal axes in arsenic-mediated ovarian and uterine toxicity: modulation by hCG. *J Biochem Mol Toxicol* 2010; 24:29–41.
13. Rahman SN, Fatima P, Chowdhury AQ, Rahman MW. Blood level of lead in women with unexplained infertility. *Mymensingh Medical Journal* 2013; 22:508–512.
14. Borja-Aburto V, Hertz-Picciotto I, Rojas Lopez M, Farias P, Camilo Rios, Blanco J. Blood lead levels measured prospectively and risk of spontaneous abortion. *Am J Epidemiol* 1999; 150:590–597.
15. Jackson LW, Zullo MD, Goldberg JM. The association between heavy metals, endometriosis and uterine myomas among premenopausal women: National Health and Nutrition Examination Survey 1999– 2002. *Human Reprod* 2008; 23(3): 679–687.
16. Nalinda S, Roshini PJ, Wickremasinghe R, Senanayake H, Sathiakumar N. Cadmium a metalloestrogen: are we convinced? *J Appl Toxicology* 2012; 32: 318-32.
17. Itoh H, Iwasaki M, Nakajima Y, Endo Y, Hanaoka T, Sasaki H, Tanaka T, Yang B, Tsugane S. A case–control study of the

- association between urinary cadmium concentration and endometriosis in infertile Japanese women. *Sci Total Environ* 2008; 402: 171-75.
18. Pollack AZ, Louis GMB, Chen Z, Peterson CM, Sundaram R, Croughan MS, Sun L, Hediger ML, Stanford JB, Varner MW, Palmer CD, Steurwald AJ, Parsons PJ. Trace elements and endometriosis: the ENDO study. *Reprod Toxicol* 2013; 42: 41-48.
 19. Rzymiski P, Tomczyk K, Rzymiski P, Poniedzialek B, Opala T, Wilczak M. Impact of heavy metals on the female reproductive system. *Ann Agric Environ Med* 2015; 22: 259-64.
 20. Silva N, Senanayake H, Peiris-John R, Wickremasinghe R, Sathiakumar N, Waduge V. Presence of metalloestrogens in ectopic endometrial tissue. *J Pharm Biomed Sci* 2012; 24: 1-5.
 21. Skoog DA, Leary JJ. Application of molecular ultraviolet/visible absorption spectroscopy. *Principles of Instrumental Analysis* 1992, 150-173.
 22. Armbruster DA, Tillman MD, Hubbs LM. Limit of detection (LQD)/limit of quantitation (LOQ): comparison of the empirical and the statistical methods exemplified with GC-MS assays of abused drugs. *Clin Chem* 1994; 40: 1233-38.
 23. Kaim W, Schwederski B. Eisen-Schwefel-und andere Nichthäm-Eisen-Proteine. In *Bioanorganische Chemie* 2004, pp. 136-157. Vieweg+ Teubner Verlag.

24. Akesson A, Julin B, Wolk A. Long-term Dietary Cadmium Intake and Postmenopausal Endometrial Cancer Incidence. *Cancer Res* 2008; 68: 6435-41.
25. Silva N, Senanayake H, Waduge V. Elevated levels of whole blood nickel in a group of Sri Lankan women with endometriosis: a case control study. *BMC Res Notes* 2013; 6(1): 13.
26. Spiro TG, Stigliani WM. *Chemistry of the Environment*, Prentice Hall, 1996; 311-329.
27. Hwang Y, Ko Y, Chiang C, Hsu S, Lee Y, Yu C, Chiou C, Wang J, Chuang H. Transition of cord blood lead level, 1985-2002, in the Taipei area and its determinants after the cease leaded gasoline use. *Environ Res* 2004; 96: 274-82.

CHAPTER 2

**DEEP DETECTION OF CERVICAL CANCER FROM PAP
SMEAR IMAGES**

Zehra KARAPINAR ŞENTÜRK¹, Nagihan ÇEKİÇ²

¹ Duzce University, Faculty of Engineering, Computer Engineering Dept., Duzce, Turkey, zehrakarapinar@duzce.edu.tr

² Duzce University, Institute of Science, Computer Engineering Dept., Duzce, Turkey, nagihanncekic@gmail.com

INTRODUCTION

Cancer is the name given to a mortal disease group and it may occur in any organ or tissue of the body with an increasing number of abnormal cells and these abnormal cells may invade the whole body [1]. 9.6 million people around the world died from cancer in 2018 according to the data provided by WHO [1]. Cervical cancer is the fourth common cancer type among women and in 2018 about 570000 women are diagnosed and 311000 women died because of cervical cancer worldwide [2]. According to WHO, cervical cancer is the most successfully treatable cancer type once it is diagnosed. Therefore, prevention efforts like screening and treating precancerous lesions prevent most of the women with cervical cancer.

The researchers are intensively working on the accurate computer aided diagnosis methods for cancer. Machine learning is the leading technology in this field. There are many papers in the literature related to early diagnosis of cancer based on machine learning in the last ten years. Breast cancer [3], [4], prostate cancer [5], lung cancer [6], pancreatic cancer [7], etc. Also, there are papers related to cervical cancer. In the rest of the paragraphs, cervical cancer diagnosis related papers based on machine learning will be elaborated.

One of the screening methods for cervical cancer detection cervicography was used in [8] and a web-based segmentation method for specific tissue types has been proposed. This novel segmentation method was developed using Matlab and Java for a lightweight implementation. Biomedically important parts of cervix tissues were

extracted automatically via their web-based tool. They developed a generic application in order to use it for other medical image processing tasks. Another cervix screening method is PAP's smear test and [9] used the multiple cell images obtained by the Pap smear test. They aimed to eliminate the errors caused by the interpretations of human observers. Some morphological operations were realized for cell segmentation and a Support Vector Machine (SVM) was trained for cancer classification using MATLAB image processing toolbox. 50 PAP smear slides obtained from a national hospital have been used by the method.

Nucleus which reveal if the cell is normal or abnormal in a single cell PAP smear image has been segmented by fuzzy c-means clustering in [10]. Harlev dataset with 70 single cell PAP smear images was used in this 7-class classification problem and they 93% and 94% precision and recall respectively. The most common cancer screening method PAP test was again exploited in [11] for cancer detection. They constituted a cervical cell database from their patients and used deep learning to determine pre-malignant and benign cells with 78% accuracy, 84% specificity, and 72% sensitivity. Nucleus region extraction from whole cervical cell was also studied in [12] using a database that the authors created. 12 shape features were used in the classification by linear SVM. They performed feature selection in order to improve the classification performance and they improved it from 92% to 97%. Deep learning was exploited in [13] for the detection and segmentation of nuclei. Two convolutional neural network models were developed to

distinguish and remove background noise. Liquid-based cytology (LBC), a method for preparing cervical samples, slides obtained from 6 hospitals were used. 100 images for training and 45 images for test were used. Nuclei was detected with 87% sensitivity by the proposed deep model.

Cancer detection process was improved by noise reduction in [14] using deep learning and handcraft features to help human experts for final diagnosis. Inflammatory cells, nuclei, cytoplasm and background were classified by a hybrid architecture of ResNet and U-Net. The research results showed that noise removal reduces the number of false positives in cancer detection. Deep learning was used as a feature extractor in [15] for cervical cancer detection on PAP smear images and these features were used as the input of a multi-layer perceptron (MLP) classifier. The cells were detected first and they were segmented. Then, the segmented cells were classified. They used Herlev dataset and obtained the best test accuracy as 89.22% by ResNet50.

The risk factors of cervical cancer were analyzed in [16] using the data collected from a hospital in Venezuela. 36 attributes of 858 records were investigated and the main inducers of cervical cancer such as “Age”, “Number of Sexual Partners”, and “Hormonal Contraceptives” were determined. They first developed a MLP classifier and analyzed the weights during prediction of each risk factor by random forest. 96.2% biopsy accuracy was obtained by the developed method.

Different from the above diagnosis methods, cervical cancer was detected by an improvement on colposcopy images [17]. Colposcopy is

a medical diagnostic process which provides an illuminated and magnified view of cervix. The proposed cancer screening method was based on multi-spectral narrow-band imaging. Cervical tissue images were obtained under different illumination sources and preprocessed. After preprocessing, the classification was performed by K-means clustering. They achieved 89% accuracy and 84% sensitivity for cancer diagnoses.

Cervical cancer was intended to be diagnosed via immunohistochemistry images in [18]. Immunohistochemistry involves the operation of identifying proteins in cells of a tissue [19]. Cervical histopathology images were classified benefited from transfer learning with 77.3% accuracy. Pap smear images were again included in a study given in [20] in order to detect cervical cancer. Random forests method was used for feature extraction and bagging ensemble classifier was used to detect cancer cases. 5 classification methods were used including Linear Discriminant Analysis, Support Vector Machines, K-Nearest Neighbor, boosted trees, and bagged trees. The best accuracy was obtained as 97.83% for 2-class problem, and 81.54% for 7-class problem using Herlev dataset.

A new Pap smear dataset was presented in [21] with five classes. Several features of cervical cells were extracted from the images and they were used for the classification by MLP and SVM. Deep features were also extracted and the results were compared. The best detection accuracy was obtained by Convolutional Neural Networks (CNN) as 95%.

In this paper, we developed a deep learning based model to distinguish probable precancerous cervical cells from the normal cells using a very recent database, SIPaKMeD [21]. Different from [21] we handled the problem as a two-class classification problem. This paper is organized as follows: Section 2 presents the details of the dataset used in the experiments and the details of the proposed method. Section 3 describes obtained results and finally in Section 4 conclusions are presented.

MATERIALS AND METHODS

Pap Smear Image Dataset

In this classification problem, we used the Pap smear images provided by SIPaKMeD database. There are 4049 separate cell images cropped manually from 966 tissue images that includes multiple cervical cells. 1618 of this 4049 cells are normal and the remaining 2431 are precancerous cells. We investigated this cell classification problem as a 2-class classification problem. Superficial-intermediate and parabasal cells were included in normal cells cluster and koilocytotic, dyskeratotic, and metaplastic cells constitute the abnormal cells cluster. Normal and abnormal cells were intended to be distinguished. Sample images are shown in Figure 1.

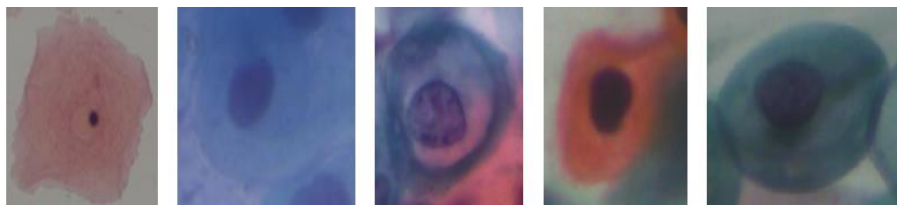


Figure 1. From left to right: Superficial-Intermediate, Parabasal, Koilocytotic, Dyskeratotic, Metaplastic cell images [21]

CNN-Based Classification of Cancerous Cells from Pap Smear Images

In this study, cervical cancer was diagnosed using a convolutional neural network. The size of the images in the first layer of the architecture is 100×100 color (RGB) images. Totally 5 convolutional filters (conv2D) and 5 pooling layers (max-pooling) were used. All the convolutional filters were 3×3 and the size of the filters in the pooling layer is 2×2 . The layers in each filter were 32-64-128-256-512-512 respectively. ReLU activation function was used in all of the layers. Dropout layer was applied to all neurons after filtering in order to prevent from overfitting. Softmax activation function was used in the last layer and the cervical cell images were classified as cancerous or non-cancerous. Architecture of the proposed deep learning model is given in Figure 2.

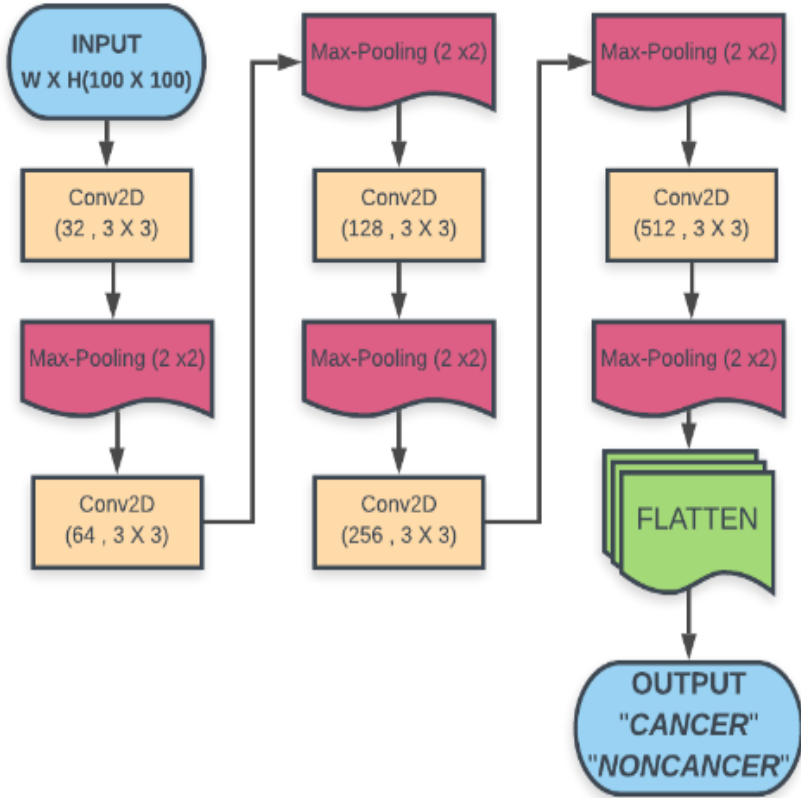


Figure 2. Layered architecture of the proposed CNN-based cancer detection method

In order to increase the amount of data available in the training set of the deep learning model that we proposed, we used Image Data Generator, a data augmentation method. The size of the dataset that we worked on was quadrupled by resizing, width shift, height shift, and horizontal rotation. The batch size of the proposed deep classification method was 80, learning rate was 0.0001, and epoch number was 50. After the mentioned adjustments were performed we trained the deep model and record its performance after many trials.

RESULTS

For the classification of cancerous cervical cells and non-cancerous ones from Pap smear images, above mentioned CNN model was trained. Before data augmentation, there were 4049 images in total and half of them was used in the training and the remaining images were used in the test and validation phases with the same sample rate. The accuracy of the model before augmentation was obtained as 93.13% for training and 72.80% for validation. To improve the performance of the proposed cervical cancer detection method. Table 1 shows the number of images in each class with and without data augmentation. Accuracy after augmentation was obtained as 95.73% for training and 88.84% for validation. Table 2 shows the effect of data augmentation on the classification performance of CNN.

Table 1. Number of samples before and after data augmentation

	Cancerous	Non-Cancerous	Total images
Without data augmentation	2431	1618	4049
With data augmentation	9724	6472	16196

Table 2. Accuracy before and after data augmentation

	Training Accuracy (%)	Validation accuracy (%)
Before data augmentation	93.13	72.80
After data augmentation	95.73	88.84

CONCLUSION

Early detection of cervical cancer is vital since it is the most treatable cancer type once it is diagnosed. Lives of hundreds of thousands of women can be saved by early detection and treatment in time. But early detection may not always be possible because of the low accessibility to medical facilities, low amount of experts in the region and expensive cancer screening processes. Computer aided decision support systems eliminate most of these issues. People may have cheap and reliable medical services thanks to computer aided early detection systems. This study showed that CNN can detect the abnormalities in cervical cells and may warn about the precancerous cells in women cervix. Therefore, it can be used for the diagnosis of cervical cancer with an acceptable accuracy rate. Also, the importance of data augmentation for CNN-based classification was shown in the paper. In the future studies, transfer learning will be investigated for the classification of cervical cells. Besides, other types of cancers will be examined by the abilities of CNN and other neural structures.

REFERENCES

- [1] World Health Organization, “Cancer.” https://www.who.int/health-topics/cancer#tab=tab_1 (accessed Apr. 21, 2020).
- [2] World Health Organization, “Cervical cancer.” https://www.who.int/health-topics/cervical-cancer#tab=tab_1 (accessed Apr. 21, 2020).
- [3] Z. K. Senturk and R. Kara, “Breast Cancer Diagnosis Via Data Mining: Performance Analysis of Seven Different Algorithms,” *Comput. Sci. Eng. An Int. J.*, vol. 4, no. 1, pp. 35–46, Feb. 2014, doi: 10.5121/cseij.2014.4104.
- [4] S. Ekici and H. Jawzal, “Breast cancer diagnosis using thermography and convolutional neural networks,” *Med. Hypotheses*, vol. 137, p. 109542, Apr. 2020, doi: 10.1016/j.mehy.2019.109542.
- [5] S. Nitta *et al.*, “Machine learning methods can more efficiently predict prostate cancer compared with prostate-specific antigen density and prostate-specific antigen velocity,” *Prostate Int.*, vol. 7, no. 3, pp. 114–118, Sep. 2019, doi: 10.1016/j.pnil.2019.01.001.
- [6] H. Li, M. Galperin-Aizenberg, D. Pryma, C. B. Simone, and Y. Fan, “Unsupervised machine learning of radiomic features for predicting treatment response and overall survival of early stage non-small cell lung cancer patients treated with stereotactic body radiation therapy,” *Radiother. Oncol.*, vol. 129, no. 2, pp. 218–

226, Nov. 2018, doi: 10.1016/j.radonc.2018.06.025.

- [7] Y. Hashimoto *et al.*, “590 – High Diagnostic Yield Using Advanced Artificial Intelligence in Cytology of Pancreatic Cancer by Eus-Fna,” *Gastroenterology*, vol. 156, no. 6, pp. 115–116, May 2019, doi: 10.1016/s0016-5085(19)37081-7.
- [8] Z. Xue, S. Antani, L. R. Long, and G. R. Thoma, “An online segmentation tool for cervicographic image analysis,” in *IHI’10 - Proceedings of the 1st ACM International Health Informatics Symposium*, 2010, pp. 425–429, doi: 10.1145/1882992.1883056.
- [9] M. Arya, N. Mittal, and G. Singh, “Cervical cancer detection using segmentation on pap smear images,” in *ACM International Conference Proceeding Series*, 2016, vol. 25-26-Aug, pp. 1–5, doi: 10.1145/2980258.2980311.
- [10] Indrabayu, A. R. Fatmasari, and I. Nurtanio, “A colour space based detection for cervical cancer using fuzzy C-means clustering,” in *ACM International Conference Proceeding Series*, 2017, pp. 137–141, doi: 10.1145/3121138.3121196.
- [11] J. Martínez-Más *et al.*, “Deep learning approach for classifying papanicolau cervical smears,” in *ACM International Conference Proceeding Series*, 2018, doi: 10.1145/3229710.3229732.
- [12] M. K. Bhowmik, S. D. Roy, N. Nath, and A. Datta, “Nucleus region segmentation towards cervical cancer screening using AGMC-TU Pap-smear dataset,” in *ACM International Conference Proceeding Series*, 2018, pp. 44–53, doi: 10.1145/3243250.

3243258.

- [13] J. Ke, Z. Jiang, C. Liu, T. Bednarz, A. Sowmya, and X. Liang, “Selective Detection and Segmentation of Cervical Cells,” in *ICBBT'19*, 2019, doi: <https://doi.org/10.1145/3340074.3340081>.
- [14] J. Ke, J. Deng, and Y. Lu, “Noise Reduction with Image Inpainting: An Application in Clinical Data Diagnosis,” in *SIGGRAPH'19*, 2019.
- [15] W. Mousser and S. Ouadfel, “Deep Feature Extraction for Pap-Smear Image Classification: A Comparative Study,” in *ICCTA 2019*, 2019, doi: <https://doi.org/10.1145/3323933.3324060>.
- [16] W. Yang, X. Gou, T. Xu, X. Yi, and M. Jiang, “Cervical Cancer Risk Prediction Model and Analysis of Risk Factors based on Machine Learning,” in *ICBBT'19*, 2019.
- [17] Z. Yang, D. Yi, and J. Shen, “Computer-aided cervical cancer screening method based on multi-spectral narrow-band imaging,” in *ICBIP '19*, 2019, pp. 62–66, doi: [10.1145/3354031.3354037](https://doi.org/10.1145/3354031.3354037).
- [18] C. Li *et al.*, “Transfer Learning Based Classification of Cervical Cancer Immunohistochemistry Images,” in *ISICDM'19*, 2019, pp. 24–26, doi: <https://doi.org/10.1145/3364836.3364857>.
- [19] “Immunohistochemistry,” *Wikipedia*, 2020. .
- [20] K. P. Win, Y. Kitjaidure, M. Phyu, and K. Hamamoto, “Cervical Cancer Detection and Classification from Pap Smear Images,” in *ICBSP '19*, 2019, pp. 47–54, doi: <https://doi.org/10.1145/>

3366174.3366178.

- [21] M. E. Plissiti, P. Dimitrakopoulos, G. Sfikas, C. Nikou, O. Krikoni, and A. Charchanti, “Sipakmed : A New Dataset For Feature And Image Based Classification Of Normal And Pathological Cervical Cells In Pap Smear Images” in *25th IEEE International Conference on Image Processing (ICIP)*, 2018, pp. 3144–3148, doi: 10.1109/ICIP.2018.8451588.

CHAPTER 3

**SPECIES IDENTIFICATION ABILITIES OF NUCLEAR AND
PLASTID DNA REGIONS, THEIR IMPORTANCE IN
PHYLOGENETIC RELATIONSHIPS AMONG *Colchicum L.*
Species**

Asst. Prof. Aykut YILMAZ¹

¹Uşak University, Faculty of Science and Arts, Department of Molecular Biology and Genetics, Uşak, Turkey. aykut.yilmaz@usak.edu.tr

INTRODUCTION

The genus *Colchicum* L. belonging to the family Colchicaceae is represented by about 100 species (Kahraman & Celep 2010, Rocchetti *et al.* 2019). The species of the genus show mainly distribution in Turkey, Balkans, Mediterranean countries and Caucasus. It can be additionally said that the genus have uneven distribution in the world (Dinç Düşen & Sümbül 2007, Kahraman & Celep 2010, Fridlender *et al.* 2014, Rocchetti *et al.* 2019). Turkey is one of the most important countries according to species number and high endemism rates for the genus (Toplan *et al.* 2016, Rocchetti *et al.* 2019). Turkey containing about 50 species belonging to the genus *Colchicum* is one of the major centres in aspect of diversity and speciation, together with Balkans. (Güner *et al.* 2000, Toplan *et al.* 2016, Rocchetti *et al.* 2019).

Colchicum species have been used for their medical value from ancient Greek to present time (Rocchetti *et al.* 2019). In other words, the species of the genus are very important and valuable owing to the presence of alkaloids, flavonoids, phenolic acids and tannins (Metin *et al.* 2014, Toplan *et al.* 2016, Rocchetti *et al.* 2019). Especially colchicine isolated by Pelletier & Caventou in 1820 is well known alkaloid for its antitumoral, antiinflammatory activity and cytotoxic effects (Kahraman & Celep 2010, Toplan *et al.* 2016).

Diagnostic characters provided from morphology of *Colchicum* species are few and vaguely. This is a problematic situation for taxonomy and determination of the phylogenetic relations within the genus.

Identification of hysteroanthous *Colchicum* species are very difficult due to leaves appear in spring whereas flowers appear in autumn for short period. On the contrary of hysteroanthous species, identification of synanthous *Colchicum* species that flowers and leaves appear together in spring are more easy (Fridlender *et al.* 2014, Toplan *et al.* 2016). Furthermore, chromosome numbers of the *Colchicum* species are very variable with $n=7, 8, 10, 11, 12, 18, 19, 20, 21, 22, 23, 25, 26, 27, 36$ and similarly different polyploidy levels are observed within the genus. (Şık *et al.* 2009, Persson *et al.* 2011, Chacon *et al.* 2014, Peruzzi *et al.* 2016). The studies based on the determination of chromosome numbers show that polyploidy is evolutionary direction of the genus (D'Amato 1955, Camarda 1978, Küçüker 1985, Şık *et al.* 2009). Furthermore polyploidy can provide contribution for the formation of new species (Abbott *et al.* 2013, Chacon *et al.* 2014) besides evolutionary dead end (Mayrose *et al.* 2011).

All of these make the necessary the determination of taxonomic status and phylogenetic relationships of the species belonging to the genus *Colchicum*. For this aim, in this study, seven regions belonging to nuclear and plastid DNA were used for determination of the phylogenetic relationships among *Colchicum* species. Also, species discrimination abilities for each regions were assigned besides the determination of the most succesful barcodin greigions.

MATERIAL AND METHODS FOR PHYLOGENETIC ANALYSIS OF *COLCHICUM* TAXA

The regions belonging to nuclear DNA (ITS1-5.8S rRNA partial) and plastid DNA (mat K, atpB-rbcL IGS, trnH-psbA IGS, trnL-trnF IGS, rbcL gene, rps16 intron) were preferred and examined for phylogenetic analysis. Sequence informations of *Colchicum* taxa for each related DNA regions were separately obtained from National Centre of Biotechnology Information (NCBI).

After the sequence informations for related taxa were obtained, multiple sequence alignments for each regions analysed were separately performed by using Molecular Evolutionary Genetics Analysis (MEGA). These alignment sequence informations were used for each barcoding regions to assign the variable sites, transitional substitutions (%), transversional substitutions (%), transition/transversion rates for purines-pyrimidines and nucleotide frequencies (%) (A+T/U and G+C).

Then, Neighbour-joining dendrograms showing bootstrap values reported on branches for each examined regions were provided to find out the species identification abilities and phylogenetic relations among *Colchicum* taxa. All positions containing gaps and missing data were eliminated for effective analyses results with complete deletion option of the program. The analyses results provided from examined DNA regions and their comparisons were showed in Table1.

NUCLEAR AND PLASTID DNA REGIONS USED FOR *COLCHICUM* TAXA AND THEIR ANALYSIS RESULTS

The seven regions belonging to nuclear and plastid DNA were preferred and examined for phylogenetic analysis.

Table 1: The Comparisons Of All Studied DNA Regions.

DNA regions	Taxon (number)	Alignment length (bp)	Variable site	Transitional	Transversional	Transition/Transversion rate			Nucleotide	
				substitutions (%)	substitutions (%)	Purin (k ₁)	Pyrimid. (k ₂)	Overall (R)	A+T/U freq. (%)	G+C
matK	47	608	49	62.06	37.94	4.35	2.34	1.34	70.30	29.70
ITS1-5.8S rRNA	47	201	73	59.78	40.22	1.09	5.20	1.03	33.68	66.32
atpB-rbcL IGS	110	755	67	49.50	50.50	1.75	2.15	0.83	69.56	30.44
trnH-psbA IGS	48	297	188	74.17	25.83	8.26	3.21	2.47	66.63	33.37
trnL-trnF IGS	109	329	87	58.04	41.96	3.91	1.73	1.16	69.46	30.54
rbcL	60	228	8	79.71	20.29	14.58	1.34	3.80	55.91	44.09
rps16	115	708	96	48.37	51.63	1.66	2.13	0.83	67.22	32.78
Total	325									

Analysis Results For matK Gene

The sequence informations belonging to 47 taxa were provided from NCBI (Altinkut Uncuoglu *et al.* 2017). Alignment length of *Colchicum* taxa studied for matK gen was determined as 608 bp. Variable sites showing the relationships among taxa were detected in 49 nucleotides. The rates of transitional substitutions and transversional substitutions were computed by the probability of substitution from one base to another base. The rates of transitional and transversional substitutions were determined as 62.06 % and 37.94 %, respectively. Furthermore, transition/transversion rates for purines (k_1) and pyrimidines (k_2) were assigned as 4.35 and 2.34, respectively. The overall transition/transversion rate (R) was additionally determined as 1,34 ($R = [A * G * k_1 + T * C * k_2] / [(A + G) * (T + C)]$) (Kumar *et al.* 2018). The nucleotide frequencies containing A+T/U % and G+C % of *Colchicum* taxa for mat K were analysed. As a result of this, it can be stated that the percentage of A+T/U bases (70.3 %) for the region examined is higher than the percentage of G+C bases (29.7 %). All analysis results are shown in Table 1.

Finally, Neighbor-Joining (NJ) dendrogram showing the evolutionary distances with the Maximum Composite Likelihood method (Tamura *et al.* 2004) was drawn to understand the species discrimination ability of matK region and to determine the phylogenetic relationships of *Colchicum* taxa (Fig. 1). In addition to the species identification ability of matK region, its grouping ability for the *Colchicum* species was

observed to be quite high although the second lowest variable sites among the seven regions studied were detected (Table 1).

Analysis Results For ITS1-5.8S rRNA (Partial)

Firstly, the DNA sequence informations for the region which is covering ITS1-5.8S rRNA (partial) of the 47 taxa belonging to the genus *Colchicum* were provided from NCBI (Altinkut Uncuoglu *et al.* 2019). These nDNA regions were aligned for taxa studied. Alignment length was determined as 201 bp and variable site was observed in 73 nucleotides. After the determination of the alignment length, the rates of transitional and transversional substitutions for related DNA region were determined as 59.78 % and 40.22 %, respectively. In addition to transitional and transversional substitutions, transition/transversion rates for purines (k_1), pyrimidines (k_2) and overall transition/transversion rate (R) were assigned as 1.09, 5.20 and 1.03, respectively. The nucleotide frequencies for the region containing ITS1-5.8S rRNA (partial) were determined as 33.68 % for A+T/U and 66.32 % for G+C. All analysis results are shown in Table 1.

Neighbor-Joining (NJ) dendrogram was prepared for the grouping the *Colchicum* taxa according to evolutionary distances and phylogenetic relationships (Fig. 2). The examination of NJ dendrogram showed that the sequence information of the DNA region containing ITS1 was sufficient for the separation of *Colchicum* species. In other words, all taxa studied were clearly identified in different branches. Consequently,

it can be stated that related DNA region has the enough sequence information with 73 variable sites to evaluate the *Colchicum* taxa.

Analysis Results For atpB-rbcL IGS

The DNA sequences of 110 taxa belonging to the genus *Colchicum* for atpB-rbcL IGS were obtained from NCBI (Vinnersten & Reeves 2003, Del Hoyo *et al.* 2009, Persson *et al.* 2011) and than the sequence informations were aligned by MEGA X for further analysis. Alignment length for 110 *Colchicum* taxa was established as 755 bp, after the exclusion of the positions containing gaps and missing data for effective analyses. Totally 67 variable sites were determined among the taxa studied (Table 1). Transitional substitutions showing the changes between same base groups (purines; A ↔ G or pyrimidines; C ↔ T) and transversional substitutions between different base groups were determined as 49.5 % and 50.5 %, respectively (Table 1). The transition/transversion rates were assigned as 1.75 for purines (k_1) and 2.15 for pyrimidines (k_2). The overall transition/transversion rate (R) is 0.83. The nucleotide frequencies of A+T/U and G+C were determined as 69.56 % and 30.44, respectively (Table 1).

Neighbor-Joining (NJ) dendrogram was prepared to show the phylogenetic relationships and the grouping of the *Colchicum* taxa. It revealed that atpB-rbcL IGS region belonging to chloroplast DNA is not enough with 67 variable sites for the separation of species and phlogenetic relationships among the *Colchicum* taxa (Fig. 3). However, it can be stated that some *Colchicum* taxa were clearly separated from

the others and identified such as *C. atticum*, *C. paschei*, *C. kotschyi* and *C. speciosum*.

Analysis Results For trnH-psbA IGS

The sequence informations of trnH-psbA IGS belonging to plastid DNA were provided (NCBI, Bruni *et al.* 2010, Altinkut Uncuoglu *et al.* 2017) and aligned for 48 *Colchicum* taxa. Alignment length of *Colchicum* taxa examined was established as 297bp. 188 variable sites were observed for related DNA region in 48 taxa belonging to the genus *Colchicum* (Table 1). The rate of transitional substitutions for trnH-psbA IGS sequence is higher with 74.17 % than transversional substitution determined as 25.83 %. Moreover, the transition/transversion rate for purines show the higher value with 8.26 than pyrimidines (3.21). The overall transition/transversion rate was determined as 2.47 in the evaluation of all nucleotide positions in final dataset (Table 1). The nucleotide frequencies are 66.63 % for A+T/U and 33.37 % for G+C.

When the NJ dendrogram was examined to understand the grouping based on evolutionary distances and phylogenetic relationships of *Colchicum* taxa, it can be stated that species identification and separation ability of this barcoding region is quite low in spite of the 188 variable sites (Fig. 4). In other words, trnH-psbA IGS is not enough for the evaluation of the *Colchicum* species although this barcoding region has the high variable sites. It can be stated as the basic reason of this situation that most variable sites are caused from only three species

such as *C. autumnale*, *C. chalcedonicum* and *C. imperatoris-friderici*. NJ dendrogram show that these species were clearly separated from other *Colchicum* taxa (Fig. 4).

Analysis Results For trnL-trnF IGS

DNA sequence informations for the regions which is covering trnL-trnF IGS were obtained from NCBI for 109 *Colchicum* taxa (Del Hoyo & Pedrola-Monfort 2008, Del Hoyo *et al.* 2009, Persson *et al.* 2011). The DNA sequences of totally 109 taxa were aligned for the subsequent analyses and alignment length of the region belonging to plastid DNA for *Colchicum* taxa was established as 329 bp. Variable sites that are important in understanding of phylogenetic relationships among taxa studied were detected in 87 nucleotides. The total rate of transitional substitutions between A ↔ G and C ↔ T were determined as 58.04 %, while transversional substitution observed between different base groups were determined as 41,96 %. The transition/transversion rates for purines, pyrimidines and also the overall transition/transversion rate were assigned as 3.91, 1.73 and 1.16, respectively. The nucleotide frequencies for the region which is covering trnL-trnF IGS belonging to chloroplast DNA for 109 *Colchicum* taxa were determined as 69.46 % for A+T/U and 30.54 % for G+C. All analysis results are shown in Table 1.

Finally, Neighbor-Joining (NJ) dendrogram for *Colchicum* taxa was drawn to understand the species identification ability and to determine the importance in phylogenetic relationships and DNA barcoding of

trnL-trnF IGS (Fig. 5). NJ dendrogram show to us that the sequence informations for trnL-trnF IGS are not enough to identification of all species, although some taxa were clearly separated from others and 109 taxa studied belonging to the genus *Colchicum* were grouped in different branches. However, it is suggested that the using of the related region together with other barcoding regions showing the positive results will be useful.

Analysis Results For rbcL Gene

The sequence informations of 60 *Colchicum* taxa for the rbcL gene were obtained from NCBI (Bruni 2013, Chacon *et al.* 2012, Chacon & Renner 2014, Altinkut Uncuoglu *et al.* 2017) and after that the alignment length for the rbcL gene of 60 *Colchicum* taxa was established as 228 bp. Variable sites showing the differences among the taxa were observed in only 8 nucleotides. The rates of transitional and transversional substitutions were determined as 79.71% and 20.29 %, respectively. The transition/transversion rates are 14.58 for purines and 1.34 for pyrimidines. The overall transition/transversion rate is 3.8 (Table 1). The nucleotide frequencies for A+T/U and G+C are 55.91 % and 44.09 %, respectively.

The lowest variable site among the all regions examined belonging to nuclear and plastid DNA was observed in rbcL gene (Table 1). Furthermore, Fig. 6 show that species identification and taxonomic classification ability for *Colchicum* taxa of rbcL gene is quite

inadequate. The fundamental reason of this can be caused by the highly protection of related gene region among *Colchicum* taxa.

Analysis Results For rps 16 Intron

115 *Colchicum* taxa were examined for rps16 intron based on DNA sequence informations (NCBI, Vinnersten & Reeves 2003, del Hoyo *et al.* 2009, Persson *et al.* 2011). After the sequence informations were aligned, alignment length was established as 708 bp. 96 variable sites were observed in rps16 intron belonging to *Colchicum* taxa examined. The rates of transitional and transversional substitutions for rps16 intron were determined as 48.37 % and 51.63 %, respectively. In addition to transitional and transversional substitutions, transition/transversion rates for purines, pyrimidines and overall transition/transversion rate were assigned as 1.66, 2.13 and 0.83, respectively. The nucleotide frequencies for the region containing rps16 intron of *Colchicum* taxa were determined as 67.22 % for A+T/U and 32.78 % for G+C. All analysis results are shown in Table 1.

Although the rps16 intron can not separate all species with strict limits, it is suggested according to the results of NJ dendrogram that the using of rps16 intron containing 96 variable sites with other detected barcoding regions will provide enormous data in the solution of taxonomic problems and in the determination of phylogenetic relationships among *Colchicum* taxa (Fig. 7).

CONCLUSION

Although Persson *et al.* (2011) were used the 6 plastid DNA regions for the phylogenetic analysis of *Colchicum* species, their phylogenetic trees did not completely separated species examined and not clearly determine species relationships. This situation also reveals the importance of the choice of DNA regions used, although it is very important to use many DNA regions together.

In this study, species identification and separation abilities of different DNA regions were determined. It is suggested as a result of this study, the preference of five regions containing matK, ITS1, atpB-rbcL IGS, trnL-trnF IGS and rps16 for further studies and especially the using together of these regions.

Vaguely and few of diagnostic characters produce problematic situation for the taxonomy and pylogenetic relations of the genus, for example in the identification of hysteranthous species. Because of the difficulty in identification of *Colchicum* species, Fridlender *et al.* (2014) state that their aim was to find some vegetative characters suitable for distinguishing the hysteranthous *Colchicum* species for a new taxonomic approach. Furthermore, many studies on the cytogenetic of the genus show that basic chromosome numbers of the *Colchicum* species are very variable and polyploidy is the situation frequently observed in the genus (D'Amato 1955, Camarda 1978, Küçüker 1985, Şık *et al.* 2009, Persson *et al.* 2011, Chacon *et al.* 2014, Peruzzi *et al.* 2016). Although the genus is represented by about 100 species in the

world, the most of the species belonging to the genus spread in the restricted locations. For example, Turkey contains about 50 species and shows high endemism. This distribution can be one of important reasons of the polyploidy and the new species caused by polyploidy.

Abbott *et al.* (2013) and Chacon *et al.* (2014) states that polyploidy can provide contribution for the formation of new species. All of these show that the genus is still problematic and the determination of the new characters is necessary to understand the evolutionary history and phylogenetic relationships of the genus. The studies based on molecular approaches are very common to solve these problems stated (Vinnersten & Reeves 2003, Manning *et al.* 2007, Del Hoyo & Pedrola-Monfort 2008, Del Hoyo *et al.* 2009, Persson *et al.* 2011, Chacon & Renner 2014, Metin *et al.* 2014). While some of these are PCR based studies (Metin *et al.* 2014), the most of these are studies based on sequence informations belonging to the plastid, mitochondrial and nuclear DNA (Manning *et al.* 2007, Persson *et al.* 2011).

Metin *et al.* (2014) states in their studies containing the AFLP analysis of *Colchicum* species that it is hard to determine the exact phylogenetic positions of species based on one marker type. Moreover, Persson *et al.* (2011) in the phylogenetic analysis of the genus *Colchicum* used the nucleotide sequences belonging to six plastid regions containing trnL intron, trnL-trnF IGS, trnY-trnD IGS, trnH-psbA IGS, atpB-rbcL IGS and rps16 intron. It was observed as a result of this study that the most of the species were not separated from each others and DNA sequence informations were not enough for phylogenetic analysis of the genus

Colchicum. Additionally, they suggested that it is necessary utilization the addition sequence informations containing nuclear DNA in addition to other plastid sequence data. Furthermore, similar result was proposed by Metin *et al.* (2014). They stated as a result of their studies that combination of all informations could be usefull in species identification and in the solution of phylogenetic relations among *Colchicum* taxa (Metin *et al.* 2014).

For this reason, here both of regions belonging to nuclear and plastid DNA were used for more effective pyhlogenetic analysis.

It can be stated as the main objectives of this study:

- determination of species identification ability for different regions belonging to plastid and nuclear DNA,
- as a result of the datas provided from these regions, determination the more advantageous region combinations and the selection of these regions in further studies for the genus *Colchicum*.
- contributing in the drawing of the best phylogenetic tree using different and usefull region combinations,
- finally the solution of taxonomic problems and understanding the phylogenetic relationships among the *Colchicum* species.

Acknowledgements

The author would like to thank to NCBI for sequence informations used in this study and the authors sharing the sequence informations in NCBI.

REFERENCES

- Abbott, R., Albach, D., Ansell, S., Arntzen, J.W., Baird, S.J.E., Bierne, N., Boughman, J., Brelsford, A., Buerkle, C.A., Buggs, R., Butlin, R.K., Dieckmann, U., Eroukhmanoff, F., Grill, A., Cahan, S.H., Hermansen, J.S., Hewitt, G., Hudson, A.G., Jiggins, C., Jones, J., Keller, B., Marczewski, T., Mallet, J., Martinez-Rodriguez, P., Möst, M., Mullen, S., Nichols, R., Nolte, A.W., Parisod, C., Pfennig, K., Rice, A.M., Ritchie, M.G., Seifert, B., Smadja, C.M., Stelkens, R., Szymura, J.M., Vainola, R., Wolf, J.B.W., Zinner, D. (2013). Hybridization and speciation. *Journal of Evolutionary Biology*, 26: 229 -246.
- Altinkut-Uncuoglu, A., Aydin, Y., Cabuk-Sahin, E. (2017). Bioengineering, Marmara University, Goztepe Campus, Istanbul, Kadikoy 34722, Turkey.
- Altinkut-Uncuoglu, A., Aydin, Y., Cabuk-Sahin, E. (2019). Bioengineering, Marmara University, Goztepe Campus, Istanbul, Kadikoy 34722, Turkey.
- Bruni, I. (2013). University of Milano Bicocca, Biotechnologies and Biosciences, P.zza della Scienza 2, 20126, Italy.
- Bruni, I., De Mattia, F., Galimberti, A., Galasso, G., Banfi, E., Casiraghi, M., Labra, M. (2010). Identification of poisonous plants by DNA barcoding approach. *International Journal of Legal Medicine*, DOI 10.1007/s00414-010-0447-3.
- Camarda, I. (1978). Numeri cromosomici per la flora Italiana: pp. 420-405. *Informatore Botanica Italiano*, 10(1): 84-90.

- Chacon, J., Camargo de Assis, M., Meerow, A.W., Renner, S.S. (2012). From east Gondwana to Central America: historical biogeography of the Alstroemeriaceae. *Journal of Biogeography*, 39: 1806-1818.
- Chacon, J., Cusimano, N., Renner, S.S. (2014). The Evolution of Colchicaceae, with a Focus on Chromosome Numbers. *Systematic Botany*, 39(2): 415-427.
- Chacon, J., Renner, S.S. (2014). Assessing model sensitivity in ancestral area reconstruction using LAGRANGE: a case study using the Colchicaceae family. *Journal of Biogeography*, 41: 1414-1427.
- D'Amato, F. (1955). Revisione citosistemica del genere *Colchicum* L. I: *C. autumnale* L., *C. lusitanum* Brot. E, *C. neapolitanum* Ten. *Caryologia*, 7(2): 292-349.
- Del Hoyo, A., Pedrola-Monfort, J. (2008). Phylogeny of *Androcymbium* (Colchicaceae) based on morphology and DNA sequences. *Plant Syst. Evol.*, 273: 151-167.
- Del Hoyo, A., Garcia-Marin, J.L., Pedrola-Monfort, J. (2009). Temporal and spatial diversification of the African disjunct genus *Androcymbium* (Colchicaceae). *Molecular Phylogenetics and Evolution*, 53: 848-861.
- Dinç-Düşen, O., Sümbül, H. (2007). A Morphological Investigation of *Colchicum* L. (Liliaceae) Species in the Mediterranean Region in Turkey. *Turk J Bot.*, 31: 373-419.
- Fridlender, A., Pustahija, F., Soliç, M.E., Abadžić, S., Bourge, M., Pech, N., Siljak-Yakovlev, S., Brown, S.C. (2014). Is it possible

- to identify *Colchicum neapolitanum* s.l. and *C. autumnale* s.l. in vegetative stage? Biometry and Aflow cytometry approaches. *Botanica Serbica*, 38(1): 43-56.
- Güner, A., Özhatay, N., Ekim, T., Canbaşer, K.H. (2000). *Flora of Turkey and the East Aegean Islands*, Vol. 11, Edinburgh, UK: Edinburgh University Press.
- Kahraman, A., Celep, F. (2010). Anatomical properties of *Colchicum kurdicum* (Bornm.) Stef. (Colchicaceae). *Australian Journal of Crop Science*, 4(5): 369-371.
- Kumar, S., Stecher, G., Li, M., Knyaz, C., Tamura, K. (2018). MEGA X: Molecular Evolutionary Genetics Analysis across computing platforms. *Molecular Biology and Evolution*, 35: 1547-1549.
- Küçükler, O. (1985). The morphological, anatomical and cytological studies on some *Colchicum* species of Istanbul area. *J. Sci. Istanbul University*, 50(B): 87-111.
- Manning, J., Forest, F., Vinnersten, A. (2007). The genus *Colchicum* L. redefined to include *Androcymbium* Willd. based on molecular evidence. *Taxon*, 56(3): 872-882.
- Mayrose, I., Zhan, S.H., Rothfels, C.J., Magnuson-Ford, K., Barker, M.S., Rieseberg, L.H., Otto, S.P. (2011). Recently formed polyploid plants diversify at lower rates. *Science*, 333: 1257.
- Metin, Ö.K., Türktaş, M., Ertuğrul, F., Kaya, E. (2014). Use of fluorescent-based amplified fragment length polymorphism to resolve phylogenetic relationships of *Colchicum* species from Turkey. *Genetics and Molecular Research*, 13(1): 1480-1490.

- NCBI, National Centre of Biotechnology Information, <https://www.ncbi.nlm.nih.gov/genbank>.
- Persson, K., Petersen, G., Del Hoyo, A., Seberg, O., Jorgensen, T. (2011). A phylogenetic analysis of the genus *Colchicum* L. (Colchicaceae) based on sequences from six plastid regions. *Taxon*, 60 (5): 1349-1365.
- Peruzzi, L., Astuti, G., Bartolucci, F., Conti, F., Rizzotto, M., Roma-Marzio, F. (2016). Chromosome numbers for the Italian flora: I. *Italian Botanist*, 1: 39-53.
- Rocchetti, G., Senizza, B., Zengin, G., Okur, M.A., Montesano, D., Yildiztugay, E., Lobine, D., Mahomoodally, M.F., Lucini, L. (2019). Chemical Profiling and Biological Properties of Extracts from Different Parts of *Colchicum szovitsii* subsp. *szovitsii*. *Antioxidants*, 8: 632.
- Şık, L., Kesercioğlu, T., Candan, F. (2009). Chromosome numbers of two *Colchicum* L. species, *C. burttii* and *C. balansae*, from Turkey. *African Journal of Biotechnology*, 8(18): 4358-4362.
- Tamura, K., Nei, M., Kumar, S. (2004). Prospects for inferring very large phylogenies by using the neighbor-joining method. *Proceedings of the National Academy of Sciences (USA)*, 101: 11030-11035.
- Toplan, G.G., Gürer, Ç., Mat, A. (2016). Importance of *Colchicum* species in modern therapy and its significance in Turkey. *J. Fac. Pharm. Istanbul / Istanbul Ecz. Fak. Dergisi*, 46(2): 129-144.
- Vinnersten, A., Reeves, G. (2003). Phylogenetic relationships within Colchicaceae. *Am. J. Bot.*, 90 (10): 1455-1462.

Appendix (DNA regions and their gene bank accession numbers)

MatK gene;

KX139823, KX139898, KX139890, KX139888, KX139886, KX139883, KX139882, KX139867, KX139863, KX139852, KX139850, KX139849, KX139841, KX139838, KX139837, KX139833, KX139830, KX139829, KX139828, KX139826, KX139825, KX139822, KX139819, KX139818, KX139817, KX139816, KX139815, KX139810, KX139809, KX139808, KX139807, KX139806, KX139804, KX139803, KX139799, KX139792, KX139789, KX139788, KX139780, KX139778, KX139774, KX139770, KX139767, KX139758, KX139752, KX139749, KX139747

ITS1-5.8S rRNA partial;

MF596408, MF596483, MF596475, MF596473, MF596471, MF596468, MF596467, MF596452, MF596448, MF596437, MF596435, MF596434, MF596426, MF596423, MF596422, MF596418, MF596415, MF596414, MF596413, MF596411, MF596410, MF596407, MF596404, MF596403, MF596402, MF596401, MF596400, MF596395, MF596394, MF596393, MF596392, MF596391, MF596389, MF596388, MF596384, MF596377, MF596374, MF596373, MF596365, MF596363, MF596359, MF596355, MF596352, MF596343, MF596337, MF596334, MF596332

atpB-rbcL IGS;

JF933998, JF934042, JF934036, JF934031, JF934014, JF933984, JF933978, JF933964, JF933950, JF933948, JF933944, JF933937, AJ554255, AJ554254, AJ554253, AJ554252, JF934057, JF934056, JF934055, JF934054, JF934053, JF934052, JF934051, JF934050, JF934049, JF934048, JF934045, JF934040, JF934039, JF934038, JF934034, JF934033, JF934032, JF934028, JF934025, JF934023, JF934022, JF934021, JF934020, JF934019, JF934018, JF934017, JF934016, JF934015, JF934013, JF934012, JF934010, JF934009, JF934008, JF934007, JF934006, JF934005, JF934004, JF934003, JF934002, JF934000, JF933999, JF933996, JF933994, JF933993, JF933992, JF933991, JF933990, JF933989, JF933988, JF933987, JF933986, JF933985, JF933983, JF933982, JF933981, JF933980, JF933979, JF933976, JF933975, JF933974, JF933973, JF933972, JF933971, JF933970, JF933968, JF933967, JF933966, JF933962, JF933961, JF933960, JF933959, JF933958, JF933957, JF933956, JF933955, JF933954, JF933953, JF933952, JF933951, JF933946, JF933945, JF933941, JF933939, JF933938, JF933935, JF933934, JF933933, JF933932, EU237025, EU237024, EU237023, EU237022, EU237021, EU237020

trnH-psbA IGS;

KX139975, KX140050, KX140042, KX140040, KX140038, KX140035, KX140034, KX140019, KX140015, KX140004, KX140002, KX140001, KX139993, KX139990, KX139989, KX139985, KX139982, KX139981, KX139980, KX139978, KX139977, KX139974, KX139971, KX139970, KX139969, KX139968, KX139967, KX139962, KX139961, KX139960, KX139959, KX139958, KX139956, KX139955, KX139951, KX139944, KX139941, KX139940, KX139932, KX139930, KX139926, KX139922, KX139915, KX139910, KX139904, KX139901, KX139899, FN675817

trnL-trnF IGS;

JF934545, JF934540, JF934534, JF934517, JF934501, JF934487, JF934481, JF934453, JF934451, JF934447, JF934440, JF934560, JF934559, JF934558, JF934557, JF934556,

JF934555, JF934554, JF934553, JF934552, JF934551, JF934548, JF934546, JF934542, JF934541, JF934537, JF934536, JF934535, JF934532, JF934531, JF934528, JF934526, JF934525, JF934524, JF934523, JF934522, JF934521, JF934520, JF934519, JF934518, JF934516, JF934515, JF934514, JF934513, JF934512, JF934511, JF934510, JF934509, JF934508, JF934507, JF934506, JF934505, JF934503, JF934502, JF934499, JF934498, JF934497, JF934496, JF934494, JF934493, JF934492, JF934491, JF934490, JF934489, JF934488, JF934486, JF934485, JF934484, JF934483, JF934482, JF934479, JF934478, JF934477, JF934476, JF934475, JF934474, JF934473, JF934471, JF934470, JF934469, JF934466, JF934465, JF934464, JF934463, JF934462, JF934461, JF934460, JF934459, JF934458, JF934457, JF934456, JF934455, JF934454, JF934449, JF934448, JF934444, JF934442, JF934441, JF934438, JF934437, JF934436, JF934435, AY622727, AY622726, AY622724, AY622722, EU237048, EU237047, EU237046

rbcl gene;

KX139641, KX139715, KX139708, KX139706, KX139704, KX139701, KX139700, KX139682, KX139681, KX139669, KX139668, KX139667, KX139659, KX139656, KX139655, KX139651, KX139648, KX139647, KX139646, KX139644, KX139642, KX139640, KX139637, KX139636, KX139635, KX139634, KX139633, KX139628, KX139627, KX139626, KX139625, KX139624, KX139622, KX139621, KX139617, KX139610, KX139607, KX139606, KX139597, KX139595, KX139592, KX139588, KX139585, KX139576, KX139570, KX139567, KX139565, HF572821, HF572820, JQ404764, JQ404749, JQ404748, KC899464, KC899462, KC899460, KC899459, KC899457, KC899455, KC899454, KC899453,

rps16;

JF934293, JF934287, JF934282, JF934216, JF934202, JF934200, JF934196, AJ551206, JF934308, JF934307, JF934306, JF934305, JF934304, JF934303, JF934302, JF934301, JF934300, JF934299, JF934295, JF934292, JF934290, JF934289, JF934285, JF934284, JF934283, JF934280, JF934279, JF934276, JF934274, JF934273, JF934272, JF934271, JF934270, JF934269, JF934268, JF934267, JF934266, JF934265, JF934264, JF934263, JF934262, JF934261, JF934260, JF934259, JF934258, JF934257, JF934256, JF934255, JF934254, JF934252, JF934251, JF934249, JF934248, JF934247, JF934246, JF934245, JF934244, JF934243, JF934242, JF934241, JF934240, JF934239, JF934238, JF934237, JF934235, JF934234, JF934233, JF934232, JF934231, JF934229, JF934228, JF934227, JF934226, JF934225, JF934224, JF934223, JF934222, JF934221, JF934220, JF934219, JF934218, JF934214, JF934213, JF934212, JF934211, JF934210, JF934209, JF934208, JF934207, JF934206, JF934205, JF934204, JF934203, JF934198, JF934197, JF934193, JF934191, JF934190, JF934188, JF934187, JF934186, JF934185, JF934184, EU237103, EU237102, EU237101, EU237100, EU237099, EU237098, AJ551212, AJ551211, AJ551210, AJ551209, AJ551208, AJ551207

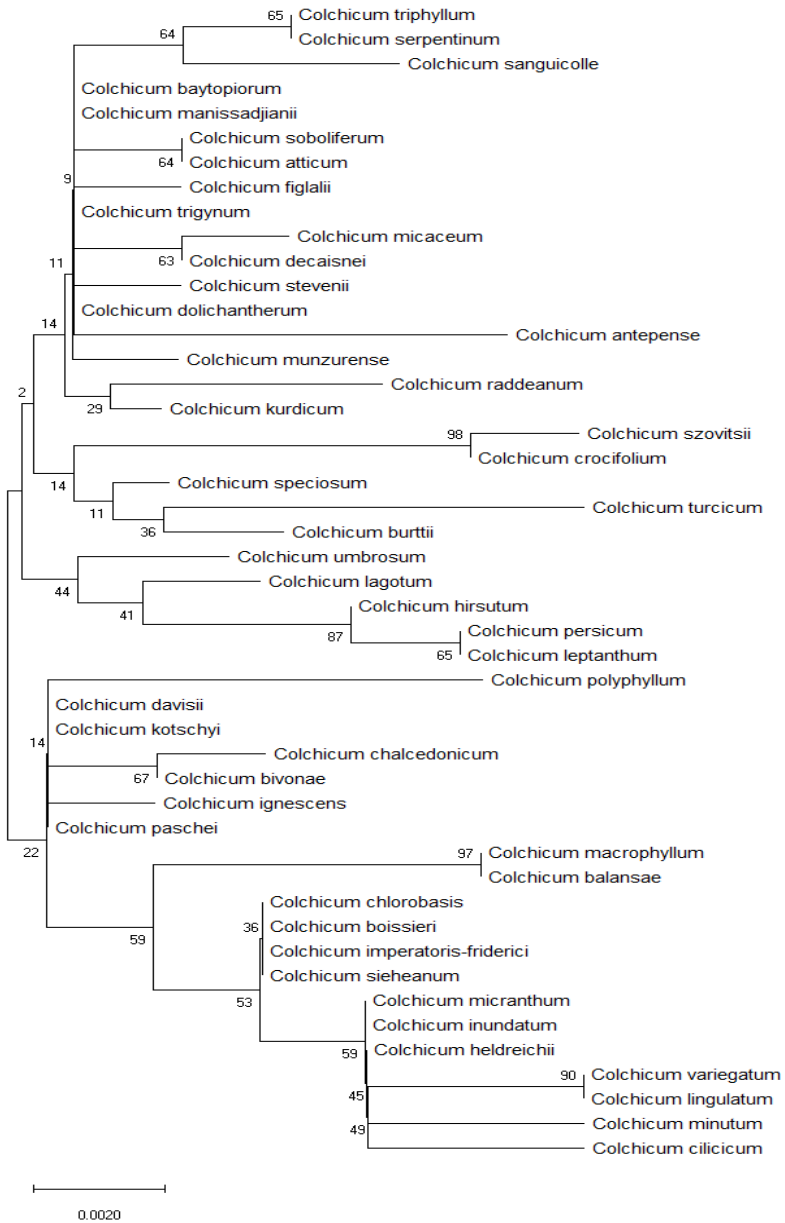


Figure 1: Neighbor-Joining Dendrogram Provided From matK Region For 47 *Colchicum* Taxa (Bootstrap values are reported in the branches. All positions containing gaps and missing data were eliminated with complete deletion option)

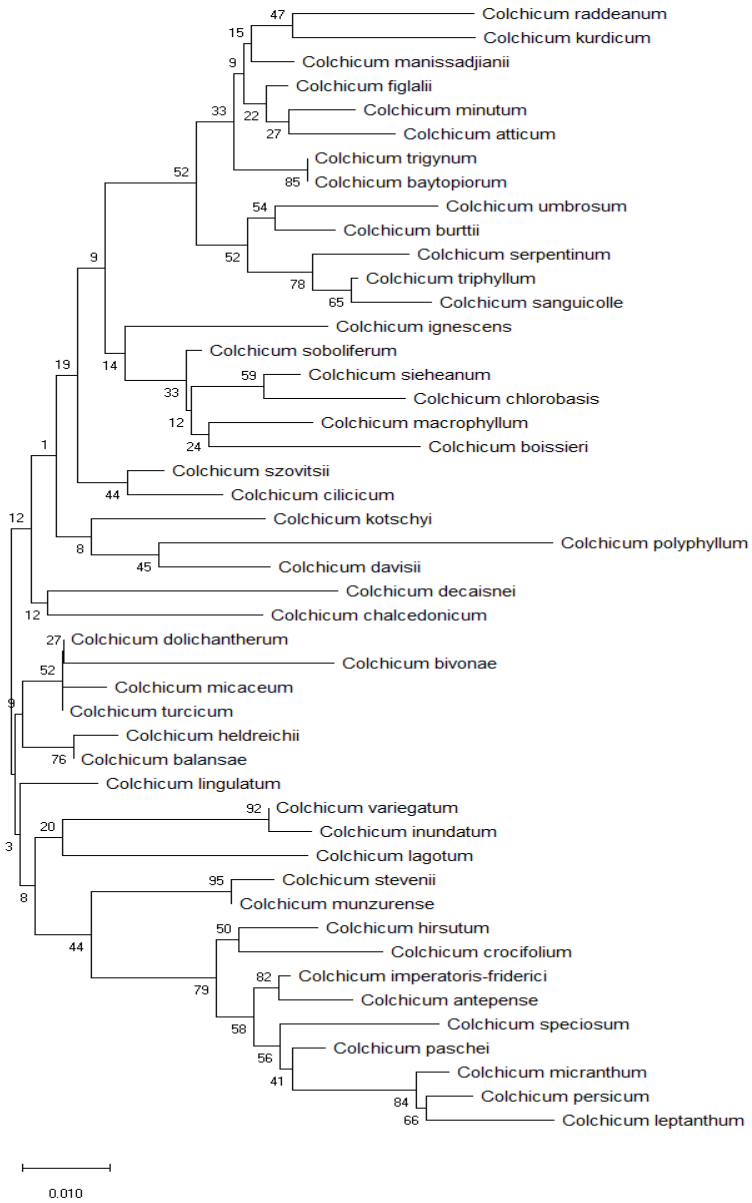


Figure 2: Neighbor-Joining Dendrogram Provided From ITS1-5.8S rRNA Partial Region For 47 *Colchicum* Taxa (Bootstrap values are reported in the branches. All positions containing gaps and missing data were eliminated with complete deletion option)

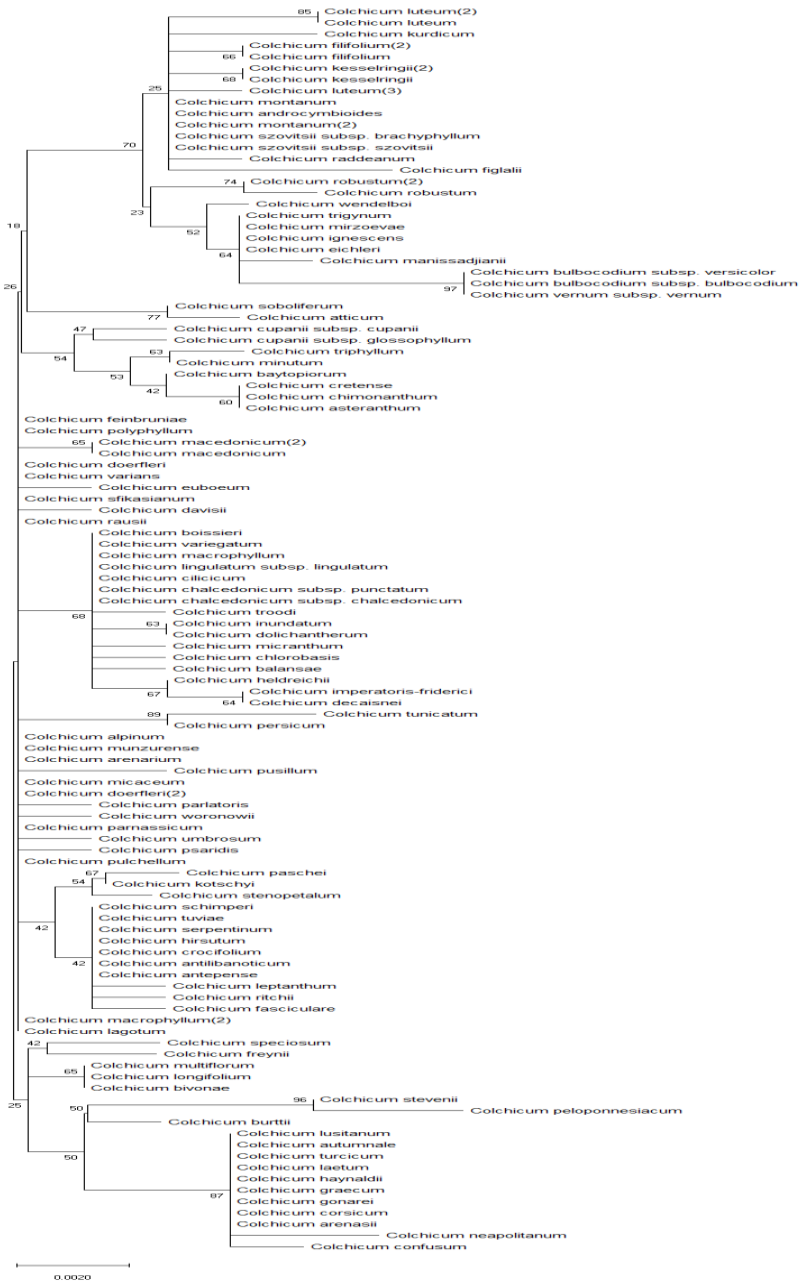


Figure 3: Neighbor-Joining Dendrogram Provided From atpB-rbcL IGS Region For 110 *Colchicum* Taxa (Bootstrap values are reported in the branches. All positions containing gaps and missing data were eliminated with complete deletion option)

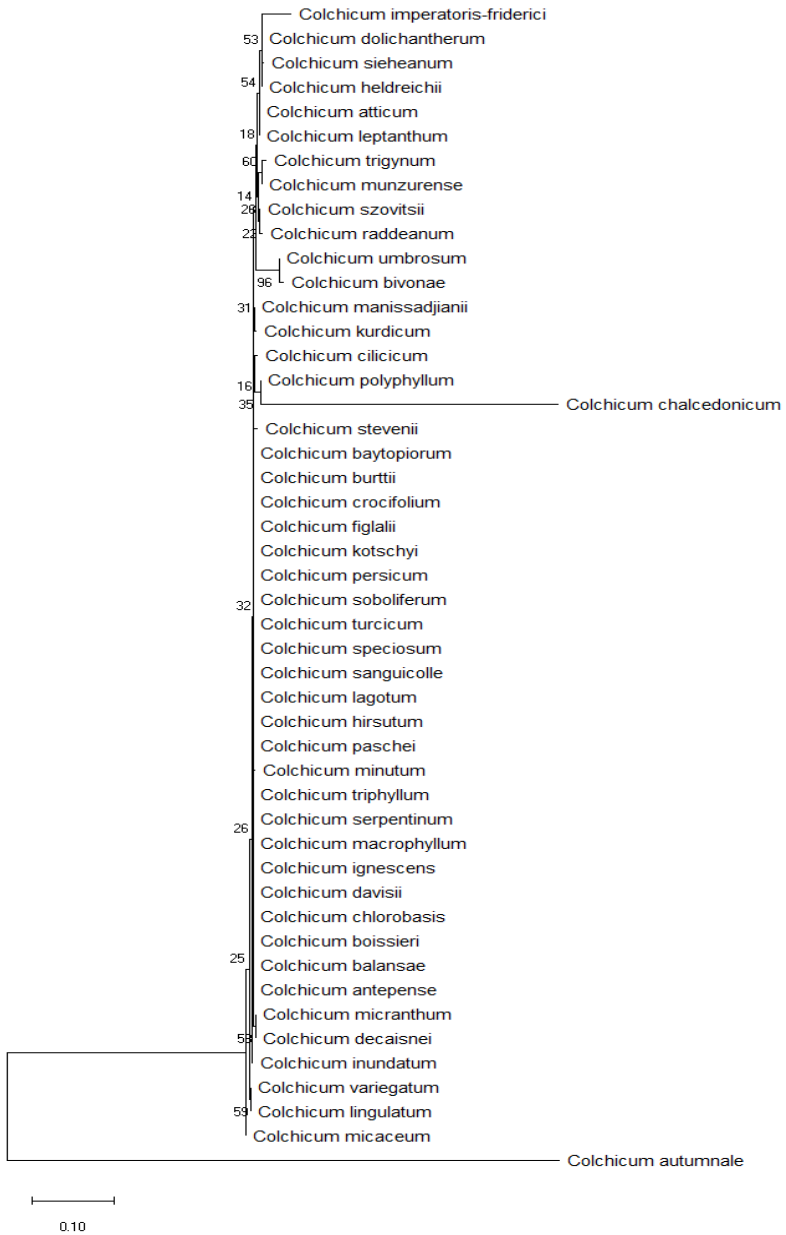


Figure 4: Neighbor-Joining Dendrogram Provided From trnH-psbA IGS Region For 48 *Colchicum* Taxa (Bootstrap values are reported in the branches. All positions containing gaps and missing data were eliminated with complete deletion option)

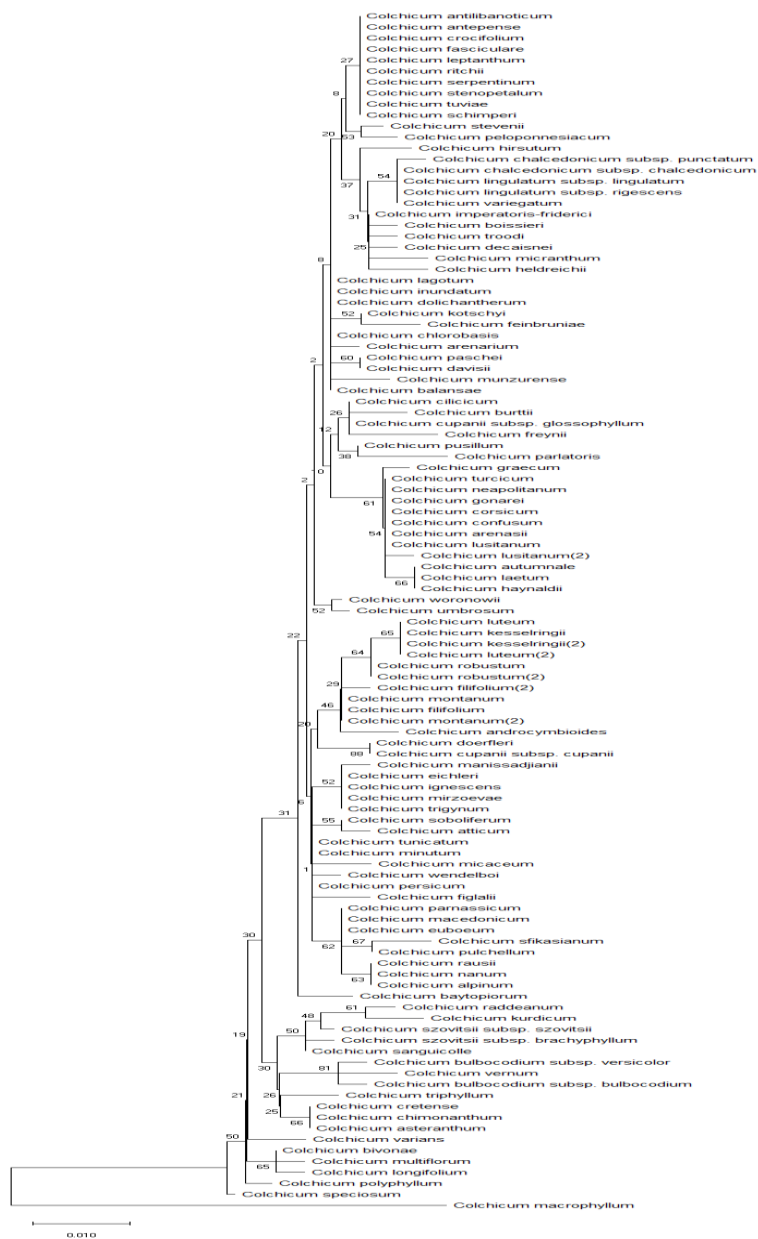


Figure 5: Neighbor-Joining Dendrogram Provided From trnL-trnF IGS Region For 109 *Colchicum* Taxa (Bootstrap values are reported in the branches. All positions containing gaps and missing data were eliminated with complete deletion option)

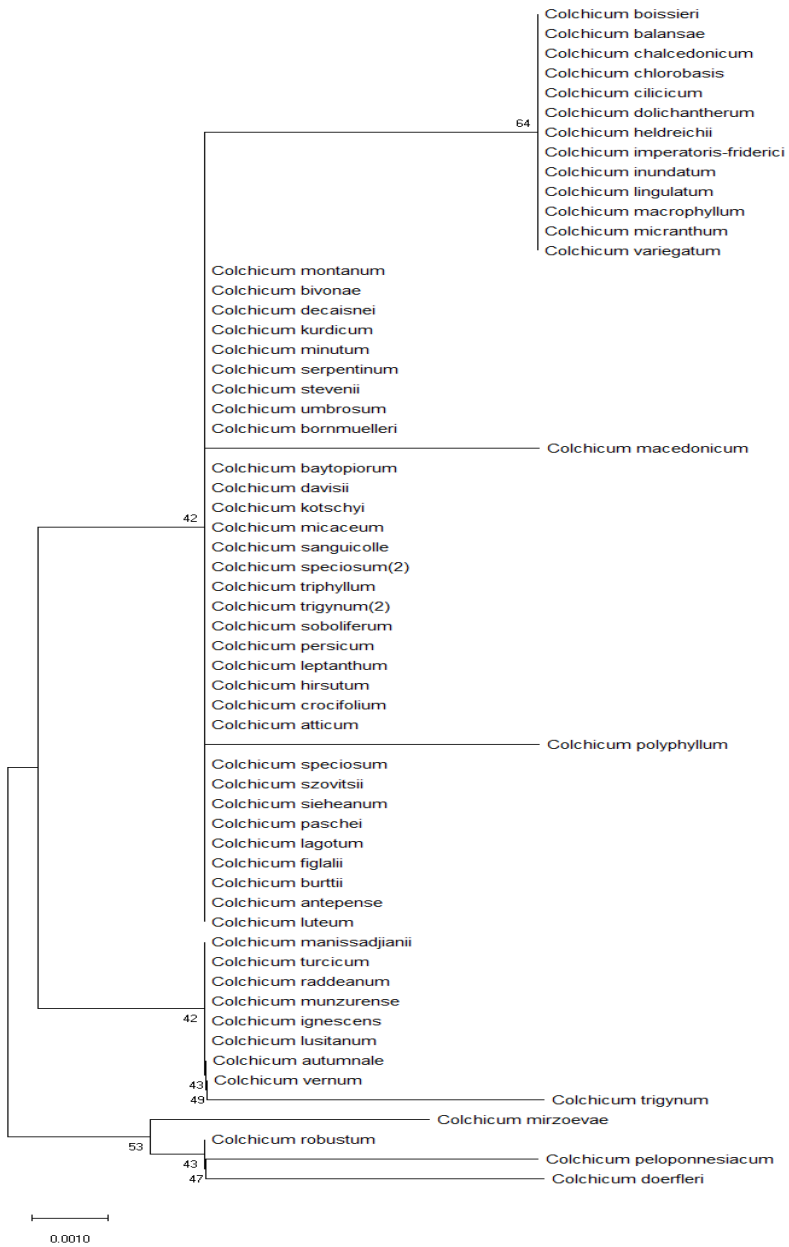


Figure 6: Neighbor-Joining Dendrogram Provided From *rbcL* Gene Region For 60 *Colchicum* Taxa (Bootstrap values are reported in the branches. All positions containing gaps and missing data were eliminated with complete deletion option)

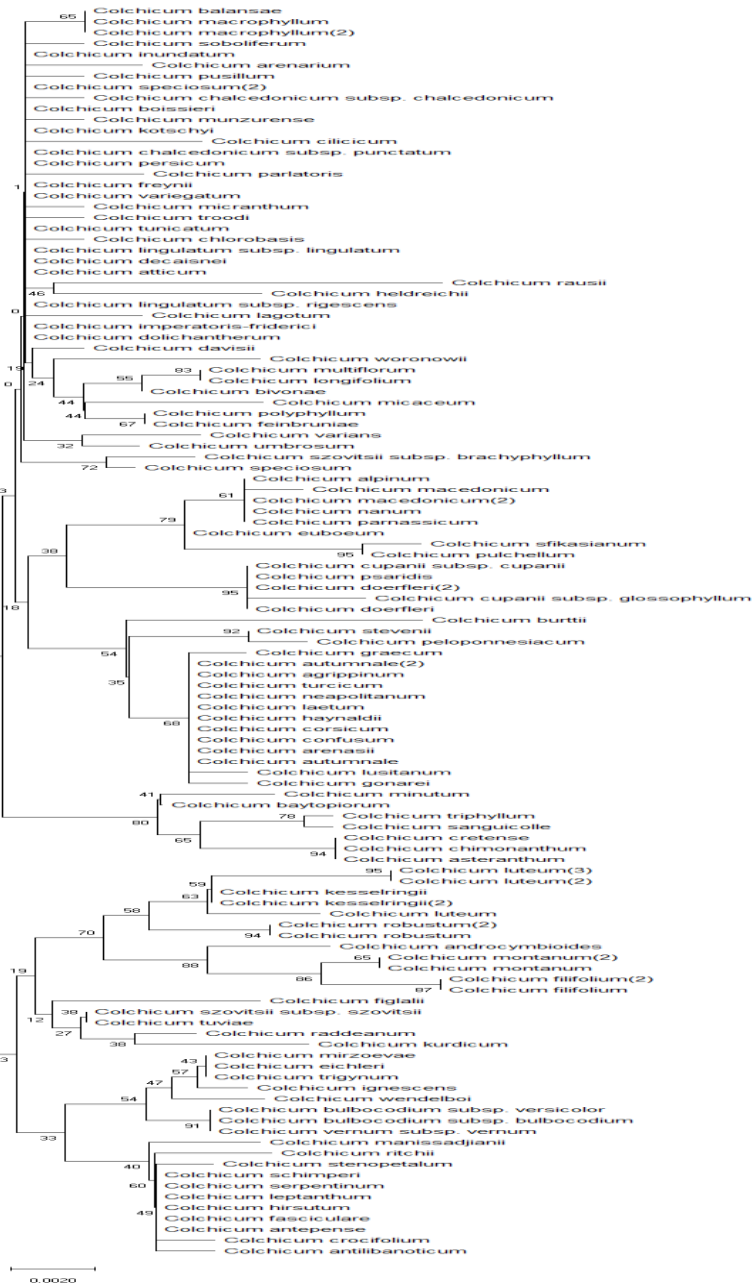


Figure 7: Neighbor-Joining Dendrogram Provided From rps16 Intron Region For 115 *Colchicum* Taxa (Bootstrap values are reported in the branches. All positions containing gaps and missing data were eliminated with complete deletion option)

CHAPTER 4

STRUCTURE AND FUNCTION OF THREE CLASSES OF C₂H₂ ZINC FINGER (ZNF) PROTEINS

Kemal YUCE¹, Ahmet Ismail OZKAN²

¹ Selcuk University, Medicine Faculty, Department of Physiology, Konya, Turkey.
yuce@selcuk.edu.tr

² Dicle University, Faculty of Science, Department of Biology, Diyarbakir, Turkey.
aiozkan.13801509@ogr.dicle.edu.tr

INTRODUCTION

Zinc (Zn) is essential for connective tissue, hair growth, immune system, nervous system and learning. Zn can stimulate or inhibit oxidative stress and apoptosis depending on its concentration (1). In addition, Zn can prevent ischemia-induced muscle lipid peroxidation and may perform endogenous neuromodulator task in synaptic neurotransmission (2, 3). Zn is involved in the structure of ZNF proteins. ZNF proteins are important in the recognition of DNA, packaging of RNA, transcriptional activity, regulation of apoptosis, folding and aggregation of proteins, and binding of lipids. ZNF proteins are also involved in the structure of RNA polymerase and ribosomal proteins. It is stated that ZNF proteins have different topologies. This provides important information about the relationship between their structure and functions. ZNF contain protected cysteine and histidine ligands binded to Zn. In recent years, studies on the design of new Cys₂His₂ finger proteins targeting important regions in the human genome have intensified. Such studies are important for human gene therapy. It is an important problem in these studies to accomplish high affinity and binding specificity. The presence of an excessive amounts of Zn stimulates the synthesis of metallothionein. Metallothionein synthesis is arranged by MTF-1 (MRE-binding transcription factor-1), which have six Cys₂His₂ZNF(4). The main structural feature of ZNF proteins is the use of cysteine and histidine around Zn to create a ZNF folding (5). Zn binding is necessary for stability and specific protein-DNA binding (6). Each of the ZNF proteins contains repeating cysteine (±

histidine) from 2 to 37 (7). ZNF proteins form a finger-like structure. It is named in the order of the first repeating unit, such as C₂H₂ (8). DNA methylation is an essential epigenetic marker (9). Various missions of ZNF motifs make them versatile in many biological processes (including autophagy, growing, metabolism and differentiation,). ZNF proteins are coded by 2% of human genes. Eight different classes of ZNF motifs have been recorded. These include Metallothionein, Treble clef, Gag knuckle, TAZ2 domain like, Zn ribbon, Zinc binding loops, Zn₂/Cys₆, and Cys₂His₂ (C₂H₂) like. C₂H₂ type ZNF motif is the biggest group among all ZNF motif classes (10). There are many C₂H₂ZNF proteins (**Table.1**) in lower eukaryotes, even in prokaryotes. A Zn atom in C₂H₂ is coordinated with protected cysteines (within β-turn) and histidines (within α-helix). In addition, finger structures are stabilized by interactions between protected hydrophobic arrays. This was confirmed by NMR studies (11). Cys₂-His₂ (C₂H₂) ZNF proteins recognize methylated DNA and bind preferably to methylated CpG in a broader specific sequence (12).

1. TRIPLE-C₂H₂ (TC₂H₂) FINGER PROTEINS

1.1. KLFs (The kruppel-like factor)

The KLF family of the gene regulating proteins are transcription factors involved in many biological processes (including proliferation, apoptosis, differentiation, growing and tumor growth, obesity,

cardiovascular diseases and inflammation) (13, 14). Krüppel-like ZNF regulate the suppression and activation of transcription. They also bind to CACCC amino acids and GC-rich regions of DNA (15). KLFs play a role in maternal endometrial development during embryo implantation (16). KLF2 is important in maintaining endothelial barrier integrity and preventing podocyte injury in diabetic mice. KLF4 is a proteinuria regulator in mice and humans. KLF5 and KLF6 prevent podocyte apoptosis. KLF15 protects against podocyte damage. While loss of KLF4 and KLF15 increased renal fibrosis, the expression of KLF5 and KLF6 increased in fibrotic kidneys (17).

1.2. Sp1 (Specificity protein 1)

SP1 is a very common transcription factor that performs a critical function in supporting oncogenes necessary for tumor survival, progression, and metastasis (18). SP1 also includes SP2, SP3 and SP4 (19). SP1 regulates the transcription of many genes in tumors and normal tissues. There are increasing evidences that many SP proteins are involved in the metastasis and growth of many tumor by arranging the transcription of vascular endothelial growth factors (VEGF). SP1 has been found to clearly regulate the transcription of VEGF in pancreatic cancer cells. SP1 is involved in regulating some genes related to the continuation of cell growth and cycle, purine and pyrimidine synthesis and metabolism, angiogenesis and anti-apoptosis in breast cancer cells (20).

1.3. Zif268

Zif268 belongs to a subgroup of regulatory IEGs (Immediate early genes). Zif268 mRNAs have been shown to be upregulated during different forms of contextual learning after tetanic stimuli that stimulate long-term potential. There is a consensus that Zif268 can have a critical mechanism for encoding long-term memory (21). Gonadectomy has been shown to cause a decrease in Zif268 protein in mPFC (Medial prefrontal cortex). This was paralleled with impaired memory in spontaneous object recognition test and the y-maze, depression-like behaviors in the forced swim test and reduced social interaction time. Re-establishment of mPFC Zif268 by using a new adeno-associated-viral construct abolished gonadectomy-induced working memory disorders, long-term memory impairments, and reduction in social interaction times. But it did not affect gonadectomy induced depression-like behaviors (22). Brain-derived neurotrophic factor is required for consolidation of fear memory. Zif268 is required for re-consolidation. Infusion of Zif268 antisense oligodeoxynucleotide into the dorsal hippocampus was sufficient to induce critical memory (amnesia) losses (23).

2. MULTIPLE-ADJACENT-C₂H₂ (MAC₂H₂) FINGER PROTEINS

2.1. Jaz

The JAZ is located in the nucleus, primarily the nucleolus and contains four C₂H₂ZNF motifs (24, 25). ZNF346 (JAZ) preferably

(but unequally specifically) binds to RNA hybrids and DNA on double chain DNAs, single chain DNAs and single chain RNAs (26). ZNF346 (JAZ) has low affinity for single chain RNAs and double chain DNAs (27). It has been reported that JAZ binds Exportin-5 in a dependent manner to Ran-GTP and dsRNA. Exportin-5 is a nuclear receptor for some double stranded RNA (dsRNA) classes, including some tRNAs, viral hairpin RNAs, and pre-micro-RNAs. Exportin-5 stimulates the JAZ shuttle and silencing exportin-5 reduces the shuttle service (28). Increased expression of JAZ has been found to induce apoptosis in rodent fibroblast cells (25).

2.2. WT1 (The transcription factor Wilms' Tumor-1)

WT1 is essential for heart development. Deletion of WT1 in mice results in death-due to epicardial and myocardial formation problems and cardiovascular deficiencies. WT1 expression is found in epicardial, endothelial and endocardial cells. WT1 expression differs in atrium and ventricles (29). WT1, which selectively binds to DNA and RNA, is also essential for the development of the genitourinary system (30).

2.3. Prdi-Bf1/Prdm1/Blimp1

Histon methyltransferase Blimp1 contains five C_2H_2 ZNF, the c terminal acidic domain, a proline-rich region at the N terminal (31). PRDI-BF1/Blimp1/PRDM1 is a basic regulator for B cell differentiation and can serve as a tumor suppressor in the pathogenesis

of diffuse large B-cell lymphomas (DLBCL). In this pathogenesis, PRDM1 is often inactivated by deletions and mutations. In a current study it was stated that this suppressor effect of PRDM1 shows that it has an important function in the loss of HGAL and LMO2 transcription on transformation of GC B cells to plasma cells and may give rise to lack of HGAL and LMO2 expression in post-GC lymphoid tumors (32) (33, 34). In a mouse model (TBlimp) in which an interfering truncated form of Blimp1 were produced transgenically, the deficiencies were found in development of mature B cells in the spleen. These mice have an increased serum IgM and long-term IgM response. It is stated that this effect is due to the increasing number of short-lived and IgM-secreting plasma cells (35). Blimp1 plays an important role not only for B cells but also for differentiation of T cells. There are studies also involved in dendritic cells and macrophages. Blimp1 was found to be expressed at a higher rate in memory CD4⁺T cells than naïve CD4⁺T cells and Blimp1 suppresses Tat-mediated HIV-1 transcription (36, 37).

2.4. Gfi-1 (Growth factor independence-1)

Hereditary gene variants play an important role in malignant diseases. Gfi is a transcriptional repressor and regulates proliferation and differentiation of HSCs. A single nucleotide polymorphism of Gfi-1 (rs34631763) produces a protein with asparagine instead of serine at position 36 and the prevalence of this situation is about 3-5% among Caucasians. Although Gfi-1 regulates myeloid development, it has not

been established as a definitive diagnostic marker for myelodysplastic syndrome (38). Epigenetic changes are involved in acute myeloid leukemia (AML). AML is a malignant disease. This amino acid change is associated with de novo AML in humans. Gfi-1 increased the ratio of AML in rodent models and led to the development of AML in a shorter time. This changes stimulated epigenetic changes that led to the expression of AML-related genes. The use of histone acetyl transferase inhibitors prevented growth in human and rodent cells that have this changes in vivo and in vitro (39). Gfi controls the self-renewal of these cells by limiting the proliferation of HSCs. Gfi-1 deficient HSCs also increased proliferation rate. P21 is dramatically lower in Gfi deficient HSCs. The Gfi-1 cell cycle inhibitor can reveal its effect on HSC proliferation by regulating p21^{CIP1/WAF1}. The p21^{CIP1/WAF1} is involved in the regulation of HSCs (40). Gfi-1 is found in rodent and human pancreas. In Gfi-1 suppressed mouse models, Gfi-1 has been found to fulfill an significant function in regulating the development and formation of pancreatic centroacinar cells. Gfi-1 regulates the maintenance of HSCs, pre-T cell differentiation, granulocytes formation, development of inner ear hair cells and organize the development process of secretory cell types in the intestine (41). The cyclin dependent kinase inhibitor p57^{Kip2} regulates the function of Gfi-1 that promotes survival and differentiation of hair cells in inner ear (42). The populations of HSCs, myeloid and lymphoid are regulated by Gfi-1 α while the developments of HSCs, megakaryocytes and erythroid are regulated by Gfi-1 β in mammals(43). Gfi-1 is a six ZNF transcriptional suppressor

oncoprotein (44). Gfi genes encode a nuclear protein. This sub protein contains a carboxy terminal ZNF domain and a new N terminal domain with 20 amino acids called the SNAG domain. Expression of Gfi is seen in many places from hematopoietic and lymphoid systems to parts of the sensory epithelium, lung and central nervous system. Gene suppression studies have revealed that Gfi-1 is required for the development of granulocytes and involved in T cell differentiation and macrophage-induced cytokine production. This suggests that these proteins take responsibility for defending against pathogens. Gfi-1 is required for more accurate functioning of inner ear hair cells. Because as a result of suppression of Gfi-1 in mice, the ataxia and deafness caused by hair cells have developed. However, hereditary hearing loss with Gfi-1 has not been associated so far (45).

2.5. Ikaros

The Ikaros protein family, which is a ZNF transcription factor, includes Pegasus, Aiolos, Eos, Ikaros and Helios. These proteins interact with gene-regulating elements. Pegasus, Aiolos, Eos, Ikaros and Helios contains four DNA-binding ZNF that recognize the GGAAA sequence. Pegasus recognizes the typical DNA binding region GNNNGNNG due to its N terminal containing three ZNF. Ikaros is highly expressed in myelocytes and metamyelocytes. It is also expressed in erythroid and myeloid precursors. Ikaros family members regulate cell-fate during hematopoiesis, especially for the adaptive immune system. It is stated that Ikaros expression is limited

to peripheral blood leukocytes, spleen, thymus and lymphopoietic tissues in adults (46). All Ikaros isoforms share a common C-terminal domain, but the number of N-terminal ZNF domains varies. At least three N-terminal ZNF are necessary for an Ikaros protein to bind specifically to DNA. In addition, the C-terminal domain is necessary for dimerization and high affinity DNA binding (47). Mice with a homozygous mutation related to the Ikaros DNA binding domain fail to produce mature lymphocytes (48). Follicular B cells, in which Ikaros is deficient, become wider and they enter the cell cycle faster after anti-IgM stimuli. Therefore, Ikaros is stated to be a negative regulator of follicular B cell activation (49). Ikaros is an important transcription factor involved in the development and differentiation of HSCs. Ikaros has been shown to have many functions (such as activation, suppression and rearrangement of chromatin) (50). The Ikaros gene encodes a DNA binding protein belonging to the C₂H₂ZNF gene family. Lack of Ikaros in mice leads to a decreased number of T cells and the absence of B, NK and dendritic cells. Ikaros is a substrate for CK2 kinase. CK2 kinase phosphorylates Ikaros in many steps. Excessive phosphorylation of Ikaros mediated by CK2 results in its inability to control the G1-S cell cycle. It is suggested that phosphorylation of Ikaros by CK2 kinase may be an significant way for inactivating Ikaros' tumor suppression service in lymphocytes (51). Ikaros is a tumor suppressor that is inactivated in leukemia. It forms a complex with nucleosome deacylase complex and positive transcription elongation factor b (P-TEFb). This is necessary

for a healthy transcription to continue. Ikaros has been shown to interact with factors involved in ending transcription (52).

2.6. MTF-1 (Metal-response element binding transcription factor-1)

MTF-1 is a important regulator of Zn found in many eukaryotes, from insects to humans. MTF-1 coordinate the expression of many genes related to intracellular transport and separation of metallothioneins and Zn. The most protected area of MTF-1 is the ZNF DNA binding region, which is similar in mice and humans (53). Dnmt1 is a protein that contributes significantly to the silencing of tumor suppressor genes and is highly expressed in cancer. Nuclear receptor SHH antagonizes MTF-1 to inhibit zinc stimulation of Dnmt1. Zn treatment stimulates Dnmt1 transcription by decreasing SHH expression and increasing the settle of MTF-1 on the Dnmt1 promoter. Thus, MTF-1 expression is suppressed by SHH and eliminates Zn-mediated changes in the chromatin configuration of the Dnmt1 promoter. Dnmt1 increases in mice in which SHH is suppressed. Increased Dnmt1 expression in human hepatocellular carcinoma is negatively related to the level of SHH (54). MTF-1 is a pluripotent arranger involved in the adaptation of the cell to some stress situations (such as hypoxia, heavy metal and oxidative stress). MTF-1 is also required for liver development. Because mice lacking MTF-1 die because of liver problems (55). MTF-1 is also found in prokaryotes. MTF-1 functions

in drosophila under high and low copper conditions and protects cells from copper (56).

2.7. dsRBP-ZFa

dsRBP-ZFa is a *Xenopus*ZNF protein that binds to RNA and dsRNA. DNA binds to dsRBP-ZFa with sequence-independent and high affinity. It contains 7 C₂H₂ZNF proteins in the N terminal domain (57, 58). ZNF distributions in dsRBP-ZFa are similar to ZNF in Wig-1(a Cys₂His₂-type ZNF protein) (59).

2.8. P43

P43 protein is an important component of the xenopus 42 S ribonucleoprotein storage. The 5S RNA binding protein is structurally similar to TFIIIA containing nine ZNF proteins (58, 60). 5S rRNA and related genes have been found to be highly replicated in the ovaries with previtellogenic (PV) oocytes. As oocytes developed, the transcriptional levels related to 5S rRNA production (gtf3a), accumulation (gtf3a, 42sp43), nucleostoplasmic transport (rpl5, rpl11) and 5S / 18S rRNA index decreased (PV> EV “early vitellogenesis” > MV “mid vitellogenesis” > LV “late-vitellogenesis” > MN “migratory nucleus stage “).P43 transcript level is high in oocytes. P43, together with the 5S rRNA, forms 42 S ribonucleoprotein particles (RNP) in the cytosol (61).

2.9. TFIIIA (Transcription factor IIIA)

TFIIIA in *Xenopus* oocytes serves as an important RNA polymerase III transcription factor for the expression of the 5S rRNA gene. TFIIIA binds to 5S rRNA to form 7S ribonucleoprotein particles and stabilizes this RNA. It is essential for the collection of ribosomes and facilitates the transport of 5S rRNAs to the nucleus. It contains nine C₂H₂ZNF used to recognize RNA and DNA targets and it regulates 5S rRNA synthesis (62). TFIIIA is necessary for the transcription of 5S ribosomal RNA. And TFIIIA is an essential component of ribosomes. TFIIIA is found in all organisms (63). TFIIIA binds to the RNA transcript and functions in the storage and transport of 5S RNA. TFIIIA performs two functions in eukaryotic cells. Firstly, it functions as transcription factor. TFIIIA acts as a transcription factor that arranges the expression of the 5S ribosomal gene by RNA polymerase III via specifically binding to an inner central region within the 5S RNA gene. Secondly, TFIIIA functions as a 5S RNA transcript chaperone required for RNA storage and nucleocytoplasmic transport (64).

2.10. Roaz

Roaz is involved in regulating olfactory neuron differentiation through interaction with the Olf-1/EBF transcription factor family (65). Roaz mRNA was found in the olfactory epithelium, brain, heart, spleen and eye. It has been reported that Roaz is located in the basal layer of neural precursor cells and olfactory epithelium immature sensory

neurons, but not in mature receptor cells. It is stated that Roaz encode a protein which contains TFIIIA's 29C₂H₂ZNF (66).

3. SEPARATED-PAIRED-C₂H₂ (SPC₂H₂) FINGER PROTEINS

The third group of ZNF proteins are grouped as spC₂H₂ (separated-paired-C₂H₂) ZNF as they are far apart from each other throughout the polypeptide sequence. There is little known about this group of ZNF (67).

3.1. Ttk (Tramtrack)

TTK is a common expressed transcription factor. It is mainly related to cell cycle regulation, cell proliferation and cell fate (68). The TTK gene encodes two alternatively truncated proteins. These proteins are 69 kDa and 88 kDa. They have different ZNF pairs and a common N-terminal region (69). TTK is effective in many differentiation processes from early embryonic formation to organogenesis (70). Both dysfunction and overexpression of TTK affect the fate of the SOP (sensory organ precursor) lineage. Loss of TTK function transforms support the cells into neurons, while TTK overexpression results in inverse transformation (71).

3.2. Prdii-Bf1 (Positive regulatory domain II-binding factor 1, also named as CIRIP, ZFP40, GAAP, HIV-EP1, MBP-1)

PRDII-BF1 is a ZAS1 member protein which is one of the three paralogous proteins of the ZAS family in mammals (Yakovich et al., 2011). The gene of PRDII-BF1 expresses a 298 kDa cellular protein. Inside this protein, separated two ZNF that bind to the same DNA sequence are detected. This gene is called ZNF40 (Gaynor et al., 1991). PRDII-BF1 is a DNA binding protein that positively regulates interferon (IFN) expression (72). Previous studies have investigated the suppression effect of PRDI-BF1 and PRDII-BF1 proteins on IFN β expression. Both proteins specifically bind to the IFN β promoter and functioned as suppressors in vivo. The transient overexpression of both suppressors in cultured cells, potentially inhibiting IFNB reporter expression, strongly demonstrated that IFN expression had a role in post-induction suppression. However, contrary to expectation, reducing or eliminating PRDI-BF1 or PRDII BF1 expression has little effect on induction kinetics of the IFN β gene. For this reason, it has been determined that PRDI-BF1 or PRDII BF1 is not required for the post-induction suppression of IFN(73).

3.3. Bnc (Basonuclin)

BNC, a cell-type-specific ZNF protein, has been discovered in cultured human epidermal cells. BNC is a protein that contains three pairs of C₂H₂ZNF. BNC gene is highly expressed in fast growing cultured human keratinocytes. Protein is mostly found in the cell

nucleus. However, due to cultural conditions that weakly support cell growth, it may be moved to cytoplasm. Intracellular localization of BNC depends on the regulation mediated by phosphorylation. BNC is also limited to certain cells in the hair follicles of humans and mice. In mouse testicle cells, BNC is concentrated in the nucleus of germ cells. During the formation of spermatozoa, which transcription is inactive, BNC leaves the nucleus and becomes cytoplasmic. BNC is also concentrated in the nucleus of female germ cells (74). BNC is a cell-type-specific ZNF protein that is highly conserved in evolution. BNC has two genes (BNC1 and BNC2). Abnormal expression of transcription factor BNC has been reported in different tumor types. BNC1 has been found to be silenced by promoter methylation in a wide variety of tumors such as renal cell carcinoma, pancreatic cancer, primary breast tumors, lymphocytic leukemia, lung cancer, and metastatic brain tumors. Over-expression of BNC1 in pancreatic cancer cell lines has been reported to inhibit in vitro cell proliferation and colony formation. Therefore, BNC1 is thought to be a potential tumor suppressor gene in these tumors (75). In addition, scientists have determined that a 5 bp deletion in the BNC1 gene encoding bazonuclin-1 causes a decrease in meiosis in oocytes (76).

BNC2 has been related with color change and cancer risk of skin. In addition, BNC2 gene deletion and decreased expression of BNC2 mRNA were found in Barrett esophageal tumor tissues. Stable transcription of BNC2 in esophageal adenocarcinoma cells is suggesting that BNC2 may also be a tumor suppressor gene (75). It

has been suggested that human BNC2, an evolutionarily conserved C₂H₂ZNF protein, plays a role in regulating the truncation, processing, or transcription of mRNA. BNC2 has been detected in a wide variety of tissues. It is abundantly expressed in the ovaries, skin, uterus and kidneys. Expression has also been found in the testes, lung and prostate. BNC2 expression was detected in keratinocyte cell line HaCaT, HeLa and HEK293 cells, including primary human keratinocytes (77). It is stated that BNC2 mRNA is abundant in cell types with BNC1. It has even been reported to be found in tissues without BNC1 such as uterus, kidney and intestine. The size of genes is quite different for BNC1 and BNC2. Although they are located on different chromosomes, it is clear that they have a common evolutionary origin. It has been stated that the conservation of BNC2 evolutionarily is much larger than that of BNC1 (78).

Compliance with the ethical standards

Conflict of interest The authors declare that they have no conflict of interest.

Ethical approval For this type of study formal consent is not required.

REFERENCES

1. Baltaci AK, Yuce K, Mogulkoc R. Zinc Metabolism and Metallothioneins. *Biological Trace Element Research*. 2017;183(1):22-31.
2. Takeda A. Zinc homeostasis and functions of zinc in the brain. *Biometals*. 2001;14(3):343-51.

3. Celer M, Mogulkoc R, Baltaci AK, Dasdelen D. The effects of zinc and melatonin on muscle ischaemi-reperfusion injury in rat. *Cell Mol Biol (Noisy-le-grand)*. 2018;64(3):1-4.
4. Laity JH, Lee BM, Wright PE. Zinc finger proteins: new insights into structural and functional diversity. *Curr Opin Struct Biol*. 2001;11(1):39-46.
5. Vanden Heuvel J. Receptor-Mediated Carcinogenesis. 142010. p. 349-69.
6. Huang M, Shaw Iii CF, Petering DH. Interprotein metal exchange between transcription factor IIIa and apo-metallothionein. *Journal of Inorganic Biochemistry*. 2004;98(4):639-48.
7. Baldwin M, Benz C. Redox Control of Zinc Finger Proteins. *Methods in enzymology*. 2002;353:54-69.
8. Ramos KS, Naney A. Introduction and Overview of Receptor Systems. *Comprehensive Toxicology: Second Edition*. 2-142010. p. 71-80.
9. Sasai N, Nakao M, Defossez P-A. Sequence-specific recognition of methylated DNA by human zinc-finger proteins. *Nucleic Acids Research*. 2010;38(15):5015-22.
10. Jen J, Wang Y-C. Zinc finger proteins in cancer progression. *Journal of Biomedical Science*. 2016;23(1).
11. Papworth M, Kolasinska P, Minczuk M. Designer zinc-finger proteins and their applications. *Gene*. 2006;366(1):27-38.
12. Patel A, Hashimoto H, Zhang X, Cheng X. Characterization of How DNA Modifications Affect DNA Binding by C2H2 Zinc Finger Proteins. 2016;573:387-401.
13. Wu Z, Wang S. Role of kruppel-like transcription factors in adipogenesis. *Developmental Biology*. 2013;373(2):235-43.
14. Xie W, Li L, Zheng X-L, Yin W-D, Tang C-K. The role of Krüppel-like factor 14 in the pathogenesis of atherosclerosis. *Atherosclerosis*. 2017;263:352-60.
15. Pearson R, Fleetwood J, Eaton S, Crossley M, Bao S. Krüppel-like transcription factors: A functional family. *The International Journal of Biochemistry & Cell Biology*. 2008;40(10):1996-2001.
16. Shen X, Hu Y, Jiang Y, Liu H, Zhu L, Jin X, et al. Krüppel-like factor 12 negatively regulates human endometrial stromal cell decidualization. *Biochemical and Biophysical Research Communications*. 2013;433(1):11-7.
17. Rane MJ, Zhao Y, Cai L. Krüppel-like factors (KLFs) in renal physiology and disease. *EBioMedicine*. 2019;40:743-50.
18. Bajpai R, Nagaraju GP. Specificity protein 1: Its role in colorectal cancer progression and metastasis. *Critical Reviews in Oncology/Hematology*. 2017;113:1-7.

19. Vizcaíno C, Mansilla S, Portugal J. Sp1 transcription factor: A long-standing target in cancer chemotherapy. *Pharmacology & Therapeutics*. 2015;152:111-24.
20. Safe S, Abdelrahim M. Sp transcription factor family and its role in cancer. *European Journal of Cancer*. 2005;41(16):2438-48.
21. Davis S, Bozon B, Laroche S. How necessary is the activation of the immediate early gene zif268 in synaptic plasticity and learning? *Behavioural Brain Research*. 2003;142(1-2):17-30.
22. Dossat AM, Jourdi H, Wright KN, Strong CE, Sarkar A, Kabbaj M. Viral-mediated Zif268 expression in the prefrontal cortex protects against gonadectomy-induced working memory, long-term memory, and social interaction deficits in male rats. *Neuroscience*. 2017;340:243-57.
23. Lee JLC. Memory reconsolidation mediates the strengthening of memories by additional learning. *Nature Neuroscience*. 2008;11(11):1264-6.
24. Brown RS. Zinc finger proteins: getting a grip on RNA. *Current Opinion in Structural Biology*. 2005;15(1):94-8.
25. Yang M, May WS, Ito T. JAZ requires the double-stranded RNA-binding zinc finger motifs for nuclear localization. *J Biol Chem*. 1999;274(39):27399-406.
26. Sen S, Kundu S, Dutta SK. Proteomic analysis of JAZ interacting proteins under methyl jasmonate treatment in finger millet. *Plant Physiology and Biochemistry*. 2016;108:79-89.
27. Burge RG, Martinez-Yamout MA, Dyson HJ, Wright PE. Structural Characterization of Interactions between the Double-Stranded RNA-Binding Zinc Finger Protein JAZ and Nucleic Acids. *Biochemistry*. 2014;53(9):1495-510.
28. Chen T, Brownawell AM, Macara IG. Nucleocytoplasmic Shuttling of JAZ, a New Cargo Protein for Exportin-5. *Molecular and Cellular Biology*. 2004;24(15):6608-19.
29. Duim SN, Smits AM, Kruithof BPT, Goumans M-J. The roadmap of WT1 protein expression in the human fetal heart. *Journal of Molecular and Cellular Cardiology*. 2016;90:139-45.
30. Nurmammedov E, Yengo RK, Ladomery MR, Thunnissen MMGM. Kinetic behaviour of WT 1's zinc finger domain in binding to the alpha-actinin-1 mRNA. *Archives of Biochemistry and Biophysics*. 2010;497(1-2):21-7.
31. Ewen-Campen B, Schwager EE, Extavour CGM. The molecular machinery of germ line specification. *Molecular Reproduction and Development*. 2009;77(1):3-18.

32. Cubedo E, Maurin M, Jiang X, Lossos IS, Wright KL. PRDM1/Blimp1 downregulates expression of germinal center genes LMO2 and HGAL. *FEBS Journal*. 2011;278(17):3065-75.
33. Turner CA, Mack DH, Davis MM. Pillars Article: Blimp-1, a Novel Zinc Finger-Containing Protein That Can Drive the Maturation of B Lymphocytes into Immunoglobulin-Secreting Cells. *Cell*. 1994. 77: 297–306. *The Journal of Immunology*. 2010;185(1):5-14.
34. Ying H-Y, Su S-T, Hsu P-H, Chang C-C, Lin IY, Tseng Y-H, et al. SUMOylation of Blimp-1 is critical for plasma cell differentiation. *EMBO reports*. 2012;13(7):631-7.
35. Angelin-Duclos C, Johnson K, Liao J, Lin KI, Calame K. An interfering form of Blimp-1 increases IgM secreting plasma cells and blocks maturation of peripheral B cells. *Eur J Immunol*. 2002;32(12):3765-75.
36. Kaczmarek Michaels K, Natarajan M, Euler Z, Alter G, Viglianti G, Henderson AJ. Blimp-1, an Intrinsic Factor that Represses HIV-1 Proviral Transcription in Memory CD4+ T Cells. *The Journal of Immunology*. 2015;194(7):3267-74.
37. Kim SJ. Immunological function of Blimp-1 in dendritic cells and relevance to autoimmune diseases. *Immunologic Research*. 2015;63(1-3):113-20.
38. Botezatu L, Michel LC, Makishima H, Schroeder T, Germing U, Haas R, et al. GFI136N as a therapeutic and prognostic marker for myelodysplastic syndrome. *Experimental Hematology*. 2016;44(7):590-5.e1.
39. Botezatu L, Michel LC, Helness A, Vadnais C, Makishima H, Hönes JM, et al. Epigenetic therapy as a novel approach for GFI136N-associated murine/human AML. *Experimental Hematology*. 2016;44(8):713-26.e14.
40. Akala OO, Clarke MF. Hematopoietic stem cell self-renewal. *Current Opinion in Genetics & Development*. 2006;16(5):496-501.
41. Qu X, Nyeng P, Xiao F, Dorantes J, Jensen J. Growth Factor Independence-1 (Gfi1) Is Required for Pancreatic Acinar Unit Formation and Centroacinar Cell Differentiation. *Cellular and Molecular Gastroenterology and Hepatology*. 2015;1(2):233-47.e1.
42. Kirjavainen A, Sulg M, Heyd F, Alitalo K, Ylä-Herttuala S, Möröy T, et al. Prox1 interacts with Atoh1 and Gfi1, and regulates cellular differentiation in the inner ear sensory epithelia. *Developmental Biology*. 2008;322(1):33-45.
43. Cooney JD, Hildick-Smith GJ, Shafizadeh E, McBride PF, Carroll KJ, Anderson H, et al. Teleost growth factor independence (gfi) genes differentially regulate successive waves of hematopoiesis. *Developmental Biology*. 2013;373(2):431-41.

44. Duan Z, Horwitz M. Gfi-1 takes center stage in hematopoietic stem cells. *Trends in Molecular Medicine*. 2005;11(2):49-52.
45. Möröy T. The zinc finger transcription factor Growth factor independence 1 (Gfi1). *The International Journal of Biochemistry & Cell Biology*. 2005;37(3):541-6.
46. John LB, Ward AC. The Ikaros gene family: Transcriptional regulators of hematopoiesis and immunity. *Molecular Immunology*. 2011;48(9-10):1272-8.
47. Fan Y, Lu D. The Ikaros family of zinc-finger proteins. *Acta Pharmaceutica Sinica B*. 2016;6(6):513-21.
48. Winandy S, Wu P, Georgopoulos K. A dominant mutation in the Ikaros gene leads to rapid development of leukemia and lymphoma. *Cell*. 1995;83(2):289-99.
49. Heizmann B, Sellars M, Macias-Garcia A, Chan S, Kastner P. Ikaros limits follicular B cell activation by regulating B cell receptor signaling pathways. *Biochemical and Biophysical Research Communications*. 2016;470(3):714-20.
50. He L-C, Xu H-Z, Gu Z-M, Liu C-X, Chen G-Q, Wang Y-F, et al. Ikaros is degraded by proteasome-dependent mechanism in the early phase of apoptosis induction. *Biochemical and Biophysical Research Communications*. 2011;406(3):430-4.
51. Dovat S, Payne KJ. Tumor suppression in T cell leukemia—The role of Ikaros. *Leukemia Research*. 2010;34(4):416-7.
52. Bottardi S, Mavoungou L, Milot E. IKAROS: a multifunctional regulator of the polymerase II transcription cycle. *Trends in Genetics*. 2015;31(9):500-8.
53. Laity JH, Andrews GK. Understanding the mechanisms of zinc-sensing by metal-response element binding transcription factor-1 (MTF-1). *Archives of Biochemistry and Biophysics*. 2007;463(2):201-10.
54. Zhang Y, Andrews GK, Wang L. Zinc-induced Dnmt1 expression involves antagonism between MTF-1 and nuclear receptor SHP. *Nucleic Acids Research*. 2012;40(11):4850-60.
55. Günther V, Lindert U, Schaffner W. The taste of heavy metals: Gene regulation by MTF-1. *Biochimica et Biophysica Acta (BBA) - Molecular Cell Research*. 2012;1823(9):1416-25.
56. Balamurugan K, Schaffner W. Copper homeostasis in eukaryotes: Teetering on a tightrope. *Biochimica et Biophysica Acta (BBA) - Molecular Cell Research*. 2006;1763(7):737-46.

57. Finerty PJ, Jr., Bass BL. A *Xenopus* zinc finger protein that specifically binds dsRNA and RNA-DNA hybrids. *J Mol Biol.* 1997;271(2):195-208.
58. Ryan RF, Darby MK. The role of zinc finger linkers in p43 and TFIIIA binding to 5S rRNA and DNA. *Nucleic acids research.* 1998;26(3):703-9.
59. Mendez-Vidal C, Wilhelm MT, Hellborg F, Qian W, Wiman KG. The p53-induced mouse zinc finger protein wig-1 binds double-stranded RNA with high affinity. *Nucleic Acids Res.* 2002;30(9):1991-6.
60. Zang WQ, Romaniuk PJ. Characterization of the 5 S RNA binding activity of *Xenopus* zinc finger protein p43. *J Mol Biol.* 1995;245(5):549-58.
61. Rojo-Bartolomé I, Martínez-Miguel L, Lafont A-G, Vílchez MC, Asturiano JF, Pérez L, et al. Molecular markers of oocyte differentiation in European eel during hormonally induced oogenesis. *Comparative Biochemistry and Physiology Part A: Molecular & Integrative Physiology.* 2017;211:17-25.
62. Ogilvie MK, Hanas JS. Molecular biology of vertebrate transcription factor IIIA: cloning and characterization of TFIIIA from channel catfish oocytes. *Gene.* 1997;203(2):103-12.
63. Layat E, Probst AV, Tourmente S. Structure, function and regulation of Transcription Factor IIIA: From *Xenopus* to *Arabidopsis*. *Biochimica et Biophysica Acta (BBA) - Gene Regulatory Mechanisms.* 2013;1829(3-4):274-82.
64. Lee BM, Xu J, Clarkson BK, Martinez-Yamout MA, Dyson HJ, Case DA, et al. Induced Fit and "Lock and Key" Recognition of 5S RNA by Zinc Fingers of Transcription Factor IIIA. *Journal of Molecular Biology.* 2006;357(1):275-91.
65. Tsai RY, Reed RR. Identification of DNA recognition sequences and protein interaction domains of the multiple-Zn-finger protein Roaz. *Mol Cell Biol.* 1998;18(11):6447-56.
66. Tsai RY, Reed RR. Cloning and functional characterization of Roaz, a zinc finger protein that interacts with O/E-1 to regulate gene expression: implications for olfactory neuronal development. *J Neurosci.* 1997;17(11):4159-69.
67. Laity JH. Cys2His2 Zinc Finger Proteins. *Encyclopedia of Inorganic and Bioinorganic Chemistry.* 2011.
68. Araujo SJ, Cela C, Llimargas M. Tramtrack regulates different morphogenetic events during *Drosophila* tracheal development. *Development.* 2007;134(20):3665-76.

69. Guo M, Bier E, Jan LY, Jan YN. tramtrack acts downstream of numb to specify distinct daughter cell fates during asymmetric cell divisions in the *Drosophila* PNS. *Neuron*. 1995;14(5):913-25.
70. Samakovlis C, Rotstein B, Molnar D, Adryan B, Llimargas M. Tramtrack Is Genetically Upstream of Genes Controlling Tracheal Tube Size in *Drosophila*. *PLoS ONE*. 2011;6(12):e28985.
71. Guo H, Raza SHA, Schreurs NM, Khan R, Wei D, Wang L, et al. Genetic variants in the promoter region of the KLF3 gene associated with fat deposition in Qinchuan cattle. *Gene*. 2018;672:50-5.
72. Zhang L, Das P, Schmolke M, Manicassamy B, Wang Y, Deng X, et al. Inhibition of pyrimidine synthesis reverses viral virulence factor-mediated block of mRNA nuclear export. *The Journal of Cell Biology*. 2012;196(3):315-26.
73. Stoddart CA, Ye J, Maniatis T. Negative Regulation of Interferon- β Gene Expression during Acute and Persistent Virus Infections. *PLoS ONE*. 2011;6(6):e20681.
74. Iuchi S, Green H. Basonuclin, a zinc finger protein of keratinocytes and reproductive germ cells, binds to the rRNA gene promoter. *Proceedings of the National Academy of Sciences*. 1999;96(17):9628.
75. Wu Y, Zhang X, Liu Y, Lu F, Chen X. Decreased Expression of BNC1 and BNC2 Is Associated with Genetic or Epigenetic Regulation in Hepatocellular Carcinoma. *International Journal of Molecular Sciences*. 2016;17(2):153.
76. Atabiekov I, Hobeika E, Sheikh U, El Andaloussi A, Al-Hendy A. The Role of Gene Therapy in Premature Ovarian Insufficiency Management. *Biomedicines*. 2018;6(4):102.
77. Urgard E, Reigo A, Reinmaa E, Rebane A, Metspalu A. Human basonuclin 2 up-regulates a cascade set of interferon-stimulated genes with anti-cancerous properties in a lung cancer model. *Cancer Cell International*. 2017;17(1).
78. Vanhoutteghem A, Djian P. Basonuclins 1 and 2, whose genes share a common origin, are proteins with widely different properties and functions. *Proceedings of the National Academy of Sciences*. 2006;103(33):12423-8.

CHAPTER 5

A VERY RARE REASON OF NASAL OBSTRUCTION: INFERIOR TURBINATE PNEUMATIZATION: REPORT OF TWO CASES

Assist. Prof. Dr. Kenan Selçuk TUNCAY¹

¹ Bahçeşehir University Faculty of Medicine Ear Nose Throat and Head Neck Surgery Department, Istanbul, Turkey, kenanselcuk.tuncay@med.bau.edu.tr

INTRODUCTION

Nasal obstruction is one of the most common problems experienced by Otolaryngology and Head and Neck Surgery specialists in daily practice. Nasal obstruction causes include physiological causes, endocrine and metabolic diseases, certain drugs, congenital anomalies, anatomical causes, mucosal causes, traumatic causes, neoplastic diseases, non-neoplastic enlargements and other diseases (Table 1).¹

Table 1. Classification of nasal obstruction.
1. Physiological Nasal cycle Positional Pregnancy Menstrual cycle Genitonasal reflex Psychosomatic
2. Endocrine and Metabolic Amyloidosis Gout Hypothyroidism Diabetes Mellitus Hormonal
3. Drugs

Systemic drugs (antihypertensives, anti-inflammatories, psychotropics, etc.

Rhinitis medicamentosa (topical nasal vasoconstrictor agents)

4. Congenital

Nasal aplasia (Arrhinia)

Polyrrhinia

Encephalocele

Nasal gliomas (intranasal, extranasal)

Choanal atresia

Nasal dermoid sinus cysts (NDSCs)

Lateral and medial nasal cleft

Proboscis lateralis

Congenital nasal pyriform aperture stenosis

5. Anatomical

Nasal septum deviation

Nasal valv collapse (Nasal vestibular stenosis)

Nasal septum perforation

Turbinate hypertrophies

Anatomical variations of turbinates (paradoxical middle turbinate, pneumatization of turbinates)

6. Mucosal

Acute inflammatory rhinitis

(Common cold, influenza)

Chronic inflammatory rhinitis

<p>(Tuberculosis, syphilis, rhinoscleroma, fungus)</p> <p>Allergic rhinitis</p> <p>Non-allergic rhinitis</p> <p>(Vasomotor rhinitis, atrophic rhinitis, non-allergic rhinitis with nasal eosinophilia syndrome-NARES)</p>
<p>7. Traumatic</p> <p>Nasal septal hematoma</p> <p>Nasal septal abscess</p> <p>Nasal foreign body</p> <p>Nasal fracture</p>
<p>8. Neoplastic</p> <p>Benign (inverted papilloma, juvenile nasopharyngeal angiofibroma, osteoma, lobular capillary hemangioma)</p> <p>Malignant (squamous cell carcinoma, adenoid cystic carcinoma, adenocarcinoma, lymphoma, melanoma, olfactory neuroblastoma, nasopharyngeal carcinoma)</p>
<p>9. Non-neoplastic</p> <p>Sinonasal polyposis</p> <p>Cystic fibrosis</p> <p>Kartagener syndrome (primary ciliary dyskinesia)</p> <p>Immotile cilia syndrome</p> <p>Asthma</p> <p>Young syndrome</p> <p>Secondary ciliary dyskinesia</p> <p>Congenital and acquired immune deficiencies</p>

10. Others

Sarcoidosis

Tuberculosis

Wegener's granulomatosis

Churg-Strauss syndrome

Rhinoscleroma

Cocaine and narcotics

When necessary, radiological and rhinomanometric evaluations should be performed in addition to anterior rhinoscopic and endoscopic examination after anamnesis in the evaluation of patients with nasal obstruction. Although there are many causes of nasal obstruction, the most common structural causes are nasal septum deviation, nasal valve collapse, turbinate hypertrophies and anatomical variations of turbinates.² Pneumatization of turbinates, which is considered among the anatomical variations of the turbinates, is most common in the middle turbinate, while it is rarely the cause of nasal obstruction in the upper turbinate and very rarely in the lower turbinate.^{3,4} In the retrospective evaluation of the coronal section paranasal sinus computed tomographies of 493 patients who underwent nasal surgery between January 2017 and March 2020 in our clinic, pneumatization of middle, superior and inferior turbinate were detected in 287, 9 and 2 patients respectively (Figure 1).



Figure 1. Paranasal sinus computed tomography image of superior, middle and inferior turbinate pneumatization in 3 different patients. (Marked areas)

The inferior concha bullosa formation, which is characterized by pneumatization of the inferior turbinate, may be associated with maxillary sinus pneumatization. Inferior concha bullosa can be unilaterally or bilaterally.⁵ Some anatomical variations such as excessive pneumatization of the inferior, middle and/or superior turbinates, hypertrophy of the uncinata bulla, secondary middle turbinate may cause significant obstruction in the nasal passage.⁶ Although they are generally asymptomatic, excessive pneumatization and hypertrophic turbinates can cause rhinorrhea and mucosal oedema, smell disorder, post nasal drainage, as well as contact headache due to pressure.⁷ Clinical, physical examination and nasal endoscopic findings

are not sufficient in the differential diagnosis of pneumatization of turbinate with turbinate hypertrophy. Pneumatization of turbinates can be easily detected with computed paranasal sinus tomography.⁸ Treatment is not needed as pneumatization of inferior turbinate is mostly asymptomatic, but in symptomatic cases, the goal of the treatment is to maintain nasal mucosa function and provide nasal airway patency. Although there is no consensus in the treatment of pneumatization of inferior turbinate, turbinate resection, 'outfracture' method or lateralization of the turbinate are frequently applied (Table 2).^{9,10}

Table 2. Methods used in the treatment of inferior turbinate pneumatization.
Injection of corticoid or submucosal sclerosing agent
Cryoturbinectomy
Cauterization
Radiofrequency ablation
Resection of the free edge of the turbinate
Turbinoplasty with microdebrider
‘‘Outfracture’’
Turbinate resection

CASE REPORTS

CASE 1

A 24-year-old female patient who presented with complaints of nasal obstruction, nasal deformity and rhinorrhea stated that she had these complaints for a very long time, but has increased very much in the last 1 year. The patient, who does not have any chronic diseases, smoking, alcohol or drug abuse in her background, also has no previous history of surgery, including nasal surgery. On physical examination and nasal endoscopy, hypertrophy in inferior and middle turbinates, bone and cartilage hump in nasal dorsum, ptosis in nasal type and volume increase in alar cartilage lateral cruras were detected also there was no deviation in nasal septum. In the coronal sectioned paranasal sinus computed tomography images, on both inferior and middle turbinates pneumatization were detected, on both inferior turbinates hypertrophy were detected and nasal septum was in the midline. In this tomographic images it was determined that the air sac remaining in the pneumatized right inferior turbinate was not associated with the maxillary sinus, and the air sac remaining in the pneumatized left inferior turbinate was associated with the maxillary sinus (Figure 2,3,4,5). After giving detailed information about the planned surgery and possible complications in preoperative preparations, both written and verbal consent was obtained from the patient. And then detailed photographs of the nose shape were done before surgery.

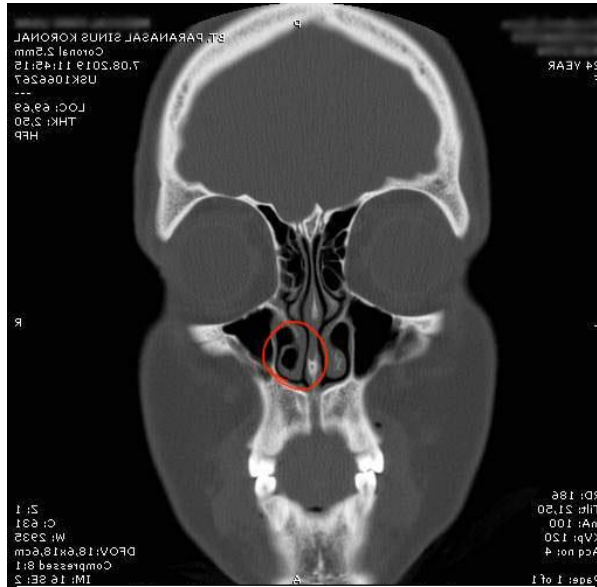


Figure 2. Paranasal sinus computed tomography image of the right inferior turbinate pneumatization. (Case 1, marked area)

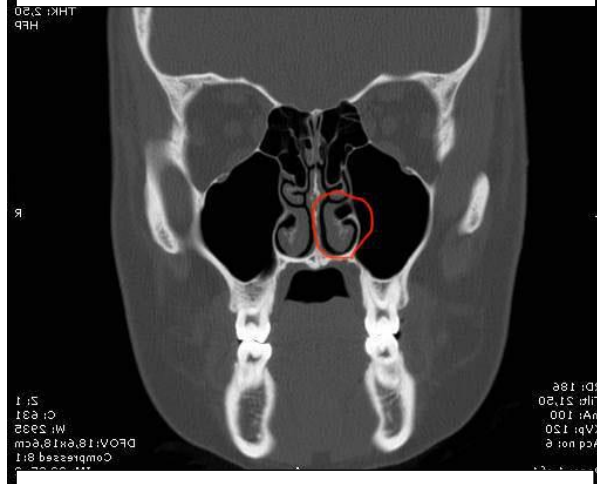


Figure 3. Paranasal sinus computed tomography image of the left inferior turbinate pneumatization. (Case 1, marked area)

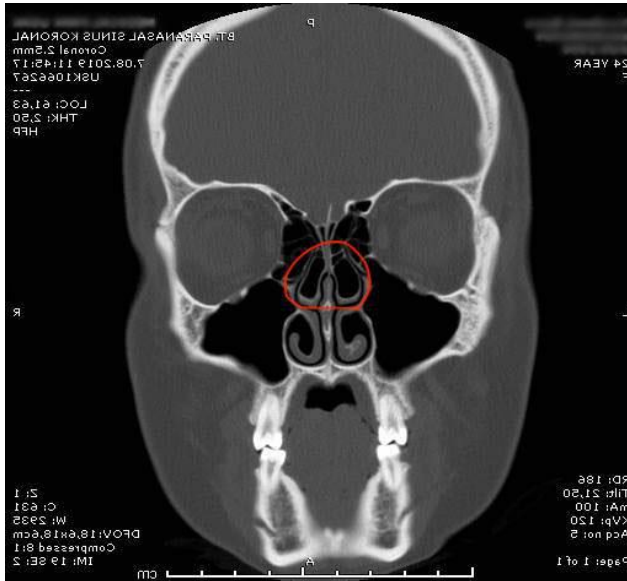


Figure 4. Paranasal sinus computed tomography image of both middle turbinates pneumatization. (Case 1, marked area)

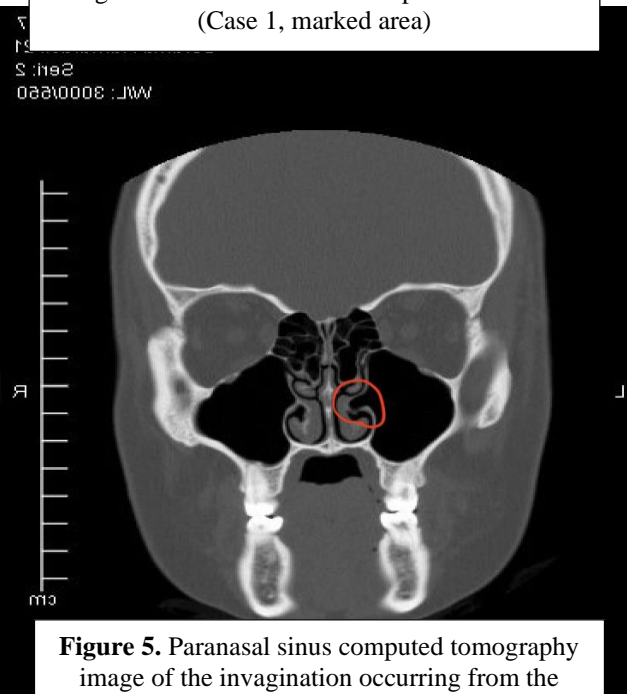


Figure 5. Paranasal sinus computed tomography image of the invagination occurring from the medial wall of the left maxillary sinus to the point where the left inferior turbinate is attached. (Case 1, marked area)

Under general anesthesia, the rhinoplasty was done and combined with an endoscopic approach that contains submucosally resection of the lateral part of both middle turbinates and the 'outfracture' technique of both pneumatized inferior turbinates. In addition at this operation, radiofrequency was applied with endoscopic approach for the treatment of hypertrophies in both inferior turbinate. No complications were observed after surgery and 6 months follow-up. During follow-ups, detailed photographing of the nose shape was made and it was seen that the nose shape improved objectively and subjectively (Picture 6,7). In addition, the patient stated that there was a significant improvement in nasal obstruction and rhinorrhea complaints.



Figure 6. Photographs taken from the right side before rhinoplasty and 10 days after the operation.



Figure 7. Photographs taken from the left side before rhinoplasty and 10 days after the operation.

CASE 2

A 29-year-old male patient who presented with complaints of nasal obstruction and post-nasal drainage stated that he received medical treatment for allergic rhinitis for a long time, but there was no improvement in these complaints. The patient, who does not have any chronic diseases, smoking, alcohol or drug abuse in his background, also has no previous history of surgery, including nasal surgery. On physical and nasal endoscopic examination, it was observed that the

nasal septum was deviated to the right side and on both inferior and middle turbinates were hypertrophic. For the differential diagnosis of turbinate hypertrophies, the diagnosis of accompanying paranasal sinus diseases, the detailed examination of the sinonasal anatomy and the relationship between nasal structures and adjacent anatomical structures, a coronal sectional paranasal sinus computerized tomographic examination was performed. Tomographic images showed that the nasal septum was deviated to the right side, on both middle turbinates and left inferior turbinate were pneumatized, on both inferior turbinate were hypertrophic and there was a retention cyst in the left maxillary sinus (Pictures 8,9,10,11). After giving detailed information about the planned surgery and possible complications in preoperative preparations, both written and verbal consent was obtained from the patient.

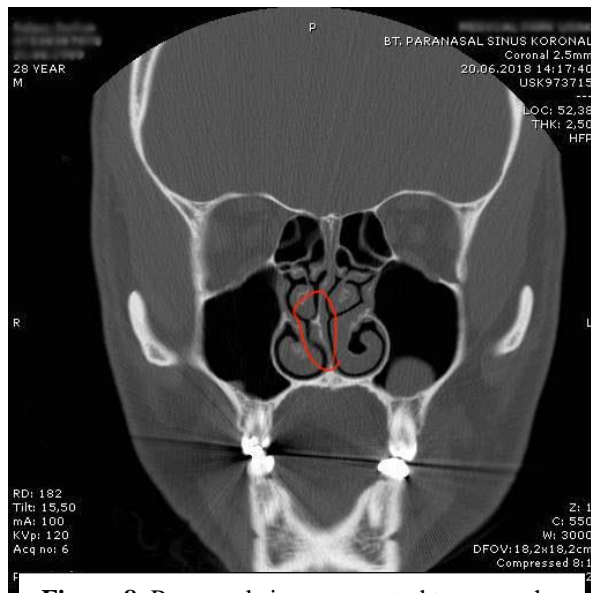


Figure 8. Paranasal sinus computed tomography image of the deviation of the nasal septum to the right.(marked area)

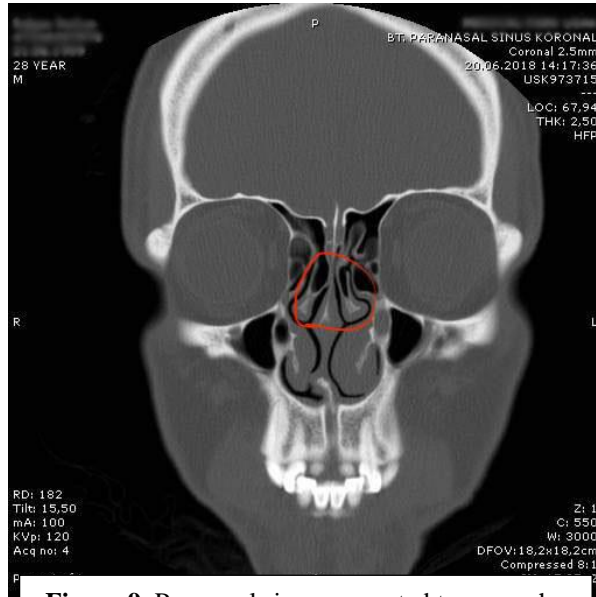


Figure 9. Paranasal sinus computed tomography image of bilateral middle turbinate pneumatization. (marked area)

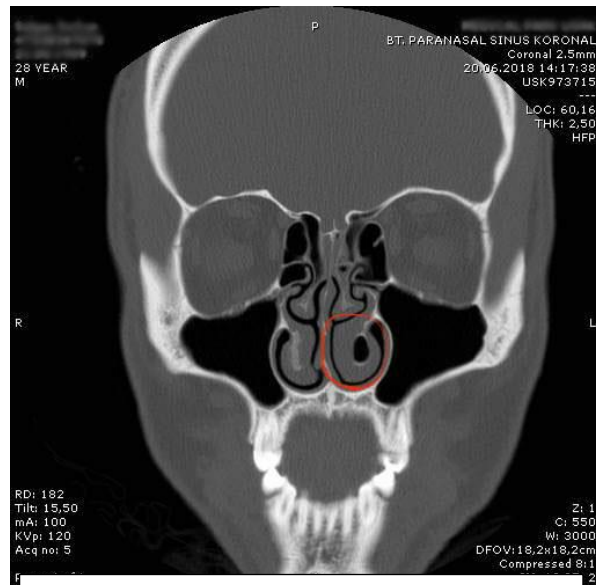
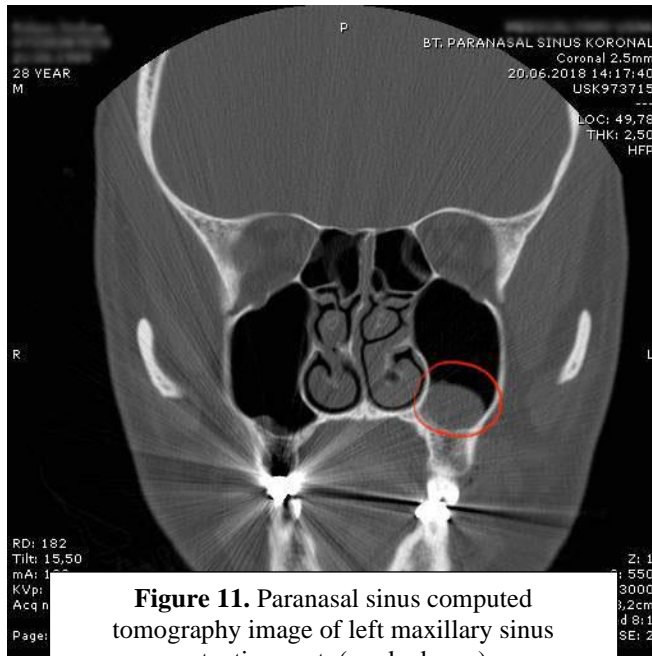


Figure 10. Paranasal sinus computed tomography image of left inferior turbinate pneumatization. (marked area)



Under general anesthesia, the septoplasty was done and combined with an endoscopic approach that contains submucosally resection of the lateral part of both middle turbinates, excision of the left maxillary sinus retention cyst by antrostomy. In addition at this operation, with the endoscopic approach, the 'outfracture' technique was applied for the treatment of pneumatized left inferior turbinate and radiofrequency was applied for the treatment of hypertrophy in both inferior turbinates. No complication was observed in the 1-year follow-up of the patient who did not develop any complications after the operation and the patient stated that there was a significant decrease in the complaints of nasal obstruction and post-nasal drainage.

DISCUSSION

While turbinate pneumatization is the second most common anatomical variation among the anatomical variations of the nose and paranasal sinuses, the septum deviation is the most common anatomical variation.³ While concha bullosa, which can be defined as pneumatized turbinate or concha in which air is present, is frequently seen in the middle turbinate, it is a rare anatomical variation in the inferior turbinate.^{11,12} Two different mechanisms are thought to play a role in the etiology of the inferior turbinate pneumatization, which was first described by Zinreich in 1988.^{7,10,11,13} In the first hypothesis, the inferior turbinate cartilage skeleton has two different ossification centers and two chondral lamellae which appears in the fifth and the seventh week of fetal life and begins to merge in the ninth week. It was suggested that pneumatization occurs as a result of epithelial intussusception between two lamellas during this merger. In the other hypothesis, it was suggested that pneumatization is towards to the inferior turbinate while the maxillary sinus was forming.^{9,10,11,13} Apuhan et al, in a study, they investigated the effect of the middle turbinate pneumatization on the inferior turbinate and they found that the distance of the inferior turbinate to the maxillary sinus wall on the side of the middle concha bullosa was less than the other side.³ Sapmaz et al, reported a case with superior, middle and inferior concha pneumatization ipsilateral.¹⁴ San et al, reported a case with inferior, middle and superior turbinate pneumatization bilaterally.¹⁵ Akagün et

al and Özcan et al, reported cases with inferior turbinate pneumatization bilaterally.^{11,16}

In our first case, middle and inferior concha pneumatization is observed bilaterally. In this case, it can be thought that the inferior turbinate and the maxillary sinus distance decrease on the right side with the effect of the middle turbinate to the inferior turbinate, therefore the maxillary sinus pneumatization may have extended towards to the inferior turbinate. However, since there are no clinical and radiological findings regarding the right maxillary sinus pathology, it indicates that both hypotheses may cause to the formation of the right inferior turbinate pneumatization. Again in our first case, on the left side, with the effect of the middle turbinate to the inferior turbinate, it suggests that the distance between the maxillary sinus and the inferior turbinate decreases, therefore the maxillary sinus pneumatization extends towards the inferior turbinate. Because, as shown in the computed tomography section in figure 4 above, there is an invagination from the medial wall of the left maxillary sinus to the place where the left inferior turbinate is connected.

In our second case, bilateral middle turbinate pneumatization and left inferior turbinate pneumatization is observed. In this case, it can be thought that the inferior turbinate and the maxillary sinus distance decrease on the left side with the effect of the middle turbinate to the inferior turbinate, therefore the maxillary sinus pneumatization may have extended towards to the inferior turbinate. However, since there

are no clinical and radiological findings regarding the left maxillary sinus pathology except retention cyst, it indicates that both hypotheses may cause to the formation of the left inferior turbinate pneumatization.

The inferior turbinate pneumatization is usually asymptomatic and is detected incidentally on paranasal sinus tomography.¹⁷ However, inferior turbinate pneumatization may cause nasal obstruction due to inferior turbinate hypertrophy, headache due to mucosal contact and epiphora due to nasolacrimal duct blockage.^{11,18} Christmas et al, reported three cases of inferior turbinate pneumatization that caused nasal obstruction.¹⁹ In our first case, we thought that complaints of nasal obstruction and rhinorrhea were caused by bilateral middle turbinate pneumatization, bilateral inferior turbinate pneumatization and hypertrophy. In our second case, we thought that complaints of nasal obstruction and post-nasal drainage were caused by nasal septum deviation, bilateral middle turbinate pneumatization, left inferior turbinate pneumatization and bilateral inferior turbinate hypertrophy.

Computed tomographic imaging provides more detailed information about nasal cavity and paranasal sinuses than classical radiological methods, and is preferred more frequently in this area. Since x-ray images of cases where the ethmoid infundibulum is deep may be confused with the inferior turbinate pneumatization in differential diagnosis, the coronal section computerized tomographic examination is very valuable in the detection of anatomical variations of the inferior turbinates.¹⁰ One of the two inferior turbinate pneumatization cases that

described by Aydın et al, was incidentally detected in the tomographic examination due to a mass in the palate.²⁰ In a retrospective study, Yang et al, had scanned the paranasal sinus tomographic images of 59238 patients and have reported 16 cases of inferior turbinate pneumatization.²¹ In the retrospective analysis of the paranasal sinus tomography images of 493 patients who underwent nasal surgery in our clinic between January 2017 and March 2020, we encountered inferior turbinate pneumatization in only 2 cases. While bilateral middle turbinate pneumatization was accompanied in two of these cases, we encountered bilateral inferior turbinate pneumatization in one case and unilateral inferior turbinate pneumatization in the other.

The inferior turbinate pneumatization is mostly asymptomatic and therefore does not need treatment. When it is symptomatic, treatment is needed and the purpose of the treatment is to maintain nasal mucosa functions and to provide nasal airway patency. Although there is no consensus in the treatment of the inferior turbinate pneumatization, the recommended methods include injection of corticoid or submucosal sclerosing agent, cryoturbinectomy, cauterization, radiofrequency ablation, resection of the free edge of the turbinate, turbinoplasty with microdebrider, turbinate resection and ‘‘outfracture’’.^{9,10,11,13,22,23,24} Ozcan et al, had applied the "outfracture" method in cases with inferior turbinate pneumatization.¹¹

In our first case, after the diagnoses of external nasal deformity, bilateral inferior turbinate hypertrophy, bilateral middle and inferior

turbinate pneumatization, under general anesthesia we performed the operation. The operation included the rhinoplasty and combined with an endoscopic approach that contains submucosally resection of the lateral part of both middle turbinates and the 'outfracture' technique of both pneumatized inferior turbinates. In addition at this operation, radiofrequency was applied with endoscopic approach for the treatment of hypertrophies in both inferior turbinates. In our second case, with the diagnoses of nasal septum deviation, bilateral middle turbinate pneumatization, retention cyst in the left maxillary sinus, left inferior turbinate pneumatization and bilateral inferior turbinate hypertrophy, under general anesthesia we performed the operation. The operation included the septoplasty and combined with an endoscopic approach that contains submucosally resection of the lateral part of both middle turbinates and excision of the left maxillary sinus retention cyst by antrostomy. In addition at this operation, with the endoscopic approach, the 'outfracture' technique was applied for the treatment of pneumatized left inferior turbinate and radiofrequency was applied for the treatment of hypertrophy in both inferior turbinates. The 'outfracture' method provides reducing turbinate volume by creating multiple fractures in the medial and lateral walls of the inferior turbinate and it is one of the most preferred methods because it is one of the least damaging methods to the nasal mucosa. Therefore we preferred this method for treatment of inferior turbinate pneumatization in our cases.

CONCLUSION

In the differential diagnosis of inferior turbinate hypertrophy that is a very common clinical condition, inferior turbinate pneumatization, a very rare anatomical variation, should also be considered. Tomographic examination is required in differential diagnosis and preparation for the surgical treatment. In symptomatic cases, appropriate surgical method should be planned. When planning surgical treatment, attention should be paid to the relationship of the inferior turbinate pneumatization with the maxillary sinus. Further studies are needed to better understand the formation mechanism of the inferior turbinate pneumatization.

REFERENCES

1. Gün, R. Nasal obstruction in patients: Evaluation of common assessment. *Türkiye Klinikleri J E. N. T. -Special Topics*. 2009;2(2):25-30.
2. Kaygusuz, İ. Depends on the structural causes of nasal obstruction. *Türkiye Klinikleri J E. N. T. -Special Topics*. 2009;2(2):55-60.
3. Apuhan T, Aksoy F, Yıldırım YS, Veyseller B, Özturan O. Unilateral konka büllozanın alt konka üzerine etkisi: CT değerlendirmesi. *Turk Arch Otolaryngol* 2011;49:25-9.
4. Hatipoğlu HG, Cetin MA, Yüksel E. Concha bullosa types: their relationship with sinusitis, ostiomeatal and frontal recess disease. *Diagn Interv Radiol* 2005;11:145-9.
5. Baykara M, Polat C, Uysal İÖ, Soylu E, Yüce S, Düzer S. İnförior konka bülloza: Olgu sunumu. *Cumhuriyet Tıp Derg* 2013;35:411-413
6. Kantarci M, Karasen RM, Alper F, Onbas O, Okur A, Karaman A. Remarkable anatomic variations in paranasal snus region and their clinical importance. *Eur J Radiol* 2004;50(3):296-302.
7. Zinreich SJ, Mattox DE, Kennedy DW, Chisholm HL, Diffley DM, Rosenbaum AE. Concha bullosa: CT evaluation. *J Comput Assist Tomogr* 1988;12(5):778-784.
8. Uzun L, Uğur MB, Savranlar A. Pneumatization of the inferior turbinate. *Eur J Radiol Extra* 2004;51:99-101.
9. Cankaya H, Egeli E, Kutluhan A, Kiriş M. Pneumatization of the concha inferior as a cause of nasal obstruction. *Rhinology* 2001;39:109-11.
10. Doğru H, Döner F, Uygur K, Gedikli O, Cetin M. Pneumatized inferior turbinate. *Am J Otolaryngol* 1999;20:139-41.
11. Ozcan C, Görür K, Duce MN. Massive bilateral inferior concha bullosa. *Ann Otol Rhinol Laryngol* 2002;111:100-1.
12. Grossman RI, Yousem DM (Eds). *Sinonasal disease*. 1 st ed. Mosby- Year Book Inc.; St. Lois 1994.

13. Ural A, Uslu S. Olgu sunumu: İinferior konka bülloza. KBB ve BBC Dergisi 2004; 12: 129-31.
14. Sapmaz E, Sapmaz HI, Toplu Y, Öçalın R, Karaer İÇ. A rare cause of nasal obstruction: concha bullosa of the inferior turbinate. J Turgut Ozal Med Cent 2014;21:145-7.
15. San T, San S, Gürkan E, Erdoğan B. Bilateral triple concha bullosa: a very rare anatomical variation of the intranasal turbinates. Case Rep Otolaryngol 2014;2014:851508.
16. Akagün F, Erdoğan BA, Bora F. Pneumatization of bilateral inferior turbinates: case report. Bakırköy Tıp Dergisi 2013;9:36-8.
17. Braun H, Stammberger H. Pneumatization of turbinates. Laryngoscope 2003; 113(4): 668-672.
18. Ingram WA, Richardson BE. Concha bullosa of an inferior turbinate. Ear Nose Throat J 2003; 82(8):605-607.
19. Christmas DA Jr, Merrel RA Jr, Mirante JP, Yanagisawa E. Pneumatized inferior turbinate: report of three cases. Ear Nose Throat J 2004;83:152-3.
20. Aydın O, Ustündağ E, Ciftçi E, Keskin IG. Pneumatization of the inferior turbinate. Auris Nasus Larynx 2001;28:361-3.
21. Yang BT, Chong VF, Wang ZC, Xian JF, Chen QH. CT appearance of pneumatized inferior turbinate. Clin Radiol 2008;63:901-5.
22. Dawlaty EE. Inferior concha bullosa—a radiological and clinical rarity. Rhinology 1999; 37: 133-5.
23. Blaugrund SM. Nasal obstruction. The nasal septum and concha bullosa. Otolaryngol Clin North Am 1989;22:291-306.
24. Fradis M, Golz A, Danino J, Gershinski M, Goldsher M, Gaitini L, Malatskey S, Armush W. Inferior turbinectomy versus submucosal diathermy for inferior turbinate hypertrophy. Ann Otol Rhinol Laryngol 2000; 109: 1040-5.

CHAPTER 6

COMPARATIVE EVALUATION OF IN-VITRO METHODS FOR ANTIMICROBIAL ACTIVITY DETERMINATION

Res. Asst. Tuba UNVER¹
Assoc. Prof. Dr. Ayse Sebnem ERENLER²

¹ Inonu University, Faculty of Pharmacy, Department of Pharmaceutical Microbiology, Malatya, Turkey, tuba.unver@inonu.edu.tr

² Inonu University, Faculty of Art and Science, Department of Biology, Malatya, Turkey, sebnem.erenler@inonu.edu.tr

INTRODUCTION

The term antimicrobial is used to describe substances that have the power to reduce the presence of microorganisms, such as bacteria and molds. Many substances, such as disinfectants, antibiotics, and natural antimicrobial additives, are described as antimicrobial. An antimicrobial agent is effective against a wide range of microorganisms: this includes bacteria, mold, and fungi.

After the discovery of penicillin in 1928, finding and developing antibiotics for treatment has taken a long time, and these studies are still ongoing. It is vital for the human being to find an effective antimicrobial agent because humankind faces a very variety of infections that cause serious illness from the beginning of life in the world. It is crucial to use appropriate antibiotics for patients suffering from infectious diseases. So especially turning to alternative sources for treatment can be useful. In this respect, emerging methods for antimicrobial activity has gained importance.

Various methods have been found after the Kirby-Bauer method, which was used as the first standard method for determining antimicrobial activity. Generally, tests that are divided into two groups as dilution and diffusion methods are used in determining in-vitro antimicrobial activity. Furthermore, these methods have been standardized by CLSI and EUCAST, thereby establishing criteria where joint evaluations can be made worldwide. The purpose of this chapter is to examine in-vitro methods for antimicrobial activity determination comparatively.

1. A SHORT HISTORY OF ANTIMICROBIAL ACTIVITY METHODS

In 1928, Alexander Fleming discovered penicillin. He found that *Staphylococcus aureus*, grown in the agar plate, was inhibited at the area of contaminated blue mold (a fungus from *Penicillium*). As a result of this, it was concluded that some microorganisms could produce substances that could inhibit the growth of another type of microorganism. Penicillin G was the first used for therapeutic purposes in 1941 [1, 2, 3]. In 1966, the Disk diffusion method was defined as the first standard method for determining antimicrobial activity by Kirby, Bauer and their friends [4]. In 1971, the agar dilution method was first used in a collective study by Ericsson and Sherris [5]. These methods were standardized by establishing the Clinical and Laboratory Standards Institute (CLSI) in 1968 and the European Committee on Antimicrobial Susceptibility Testing (EUCAST) in 1997 [6, 7].

2. PURPOSE OF USE OF ANTIMICROBIAL ACTIVITY

Antimicrobial susceptibility tests are used for drug discovery, epidemiology and therapeutic outcome estimation [8]. Antimicrobial susceptibility tests are essential in the use of many biotechnologically produced products and the development of industrially used products. It is used for the discovery of new substances that will affect a wide variety of microorganisms with minimum damage, with the smallest dose. It is a significant advantage to observe biological activity in vitro.

Microbial and herbal products constitute the majority of the antimicrobial compounds discovered so far. Recently, scientists have been researching the plant, animal and microbial extracts, pure primary or secondary metabolites, essential oils, and newly synthesized molecules as potential antimicrobial agents.

3. THE METHODS FOR DETERMINING ANTIMICROBIAL ACTIVITY

The methods for determining antimicrobial activity are technically the same. Media used and incubation conditions are different. Generally, the methods are divided into the Dilution Method and Diffusion Method (Figure 1).

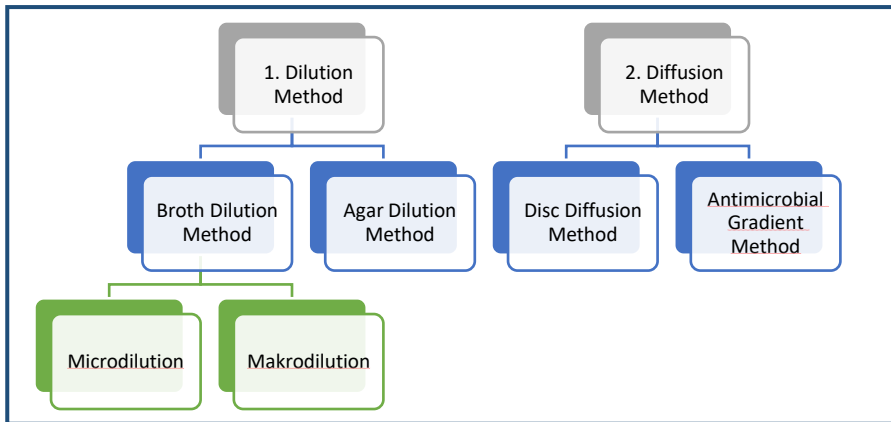


Figure 1: The Methods For Determining Antimicrobial Activity

3.1. Antibacterial and Antifungal agents according to their mechanism of action:

Antifungal agents are examined in four groups, including fungal sterol agents, nucleic acid inhibitors, agents affecting the fungal cell wall, and mitosis inhibitors [9]. Moreover, antibacterial agents are examined in five groups as follows.

- ***Cell wall synthesis inhibitors:*** Inhibition of cell wall synthesis occurs due to inhibition of the transpeptidase and carboxypeptidase enzyme, which serve in the last step of peptidoglycan synthesis. Besides that, Beta-lactamases are enzymes that break down the beta-lactam ring and inactivate the antimicrobial. To prevent degradation, beta-lactam antimicrobials can be administered in combination with beta-lactamase inhibitors [10, 11].

- ***Protein synthesis inhibitors:*** An antimicrobial agent can inhibit protein synthesis by binding to the 50s or 30s Ribosomal subunit of the microorganism. This effect is bacteriostatic [12].

- ***Nucleic acid synthesis inhibitors:*** An antimicrobial agent can disrupt DNA replication by inhibition of the DNA gyrase (topoisomerase II) enzyme, or inhibit nucleic acid synthesis by stopping RNA synthesis by inhibition of DNA-dependent RNA polymerase [13, 14].

• *Antimetabolite effect (Folate synthesis inhibitors)*: The bacterial cell synthesizes the folic acid required in DNA synthesis. DNA synthesis in bacteria is inhibited by inhibition of enzymes involved in the folic acid synthesis [15].

• *Impairment of membrane permeability-integrity*: An antimicrobial agent can act by disrupting membrane permeability-integrity [10].

3.2. Clinical and Laboratory Standards Institute (CLSI) and the European Antimicrobial Susceptibility Test Committee (EUCAST)

The most recognized standards are provided by the Clinical and Laboratory Standards Institute (CLSI) and the European Antimicrobial Susceptibility Test Committee (EUCAST). These standards provide a uniform procedure for tests applied in most clinical microbiology laboratories and allow a bio-analysis to be performed with a standardized approach to assess the clinical relevance of the results [6, 7]. On the other hand, these standards developed does not guarantee the clinical significance of such tests.

3.3. Dilution Methods

Broth and agar dilution methods are used most common applications for quantitatively antimicrobial activity measurement [16, 8]. Dilution

methods are the most suitable methods for the determination of MIC values because they provide to estimate the concentration of the antimicrobial agent tested in agar dilution or broth dilution medium. [16].

Minimum Inhibitory Concentration (MIC) value is defined as the lowest concentration of antimicrobial agent that inhibits the apparent growth of the microorganism tested and is usually expressed in mg/mL or $\mu\text{g/mL}$. Moreover, Minimum Bactericidal or Fungicidal Concentration Value (MBC or MFC), also called Minimum Lethal Concentration (MLC), is defined as the lowest antimicrobial agent concentration required to kill 99.9% of the original number of microorganisms. The MBC value is determined by making quantitative subcultures from tubes or wells without visible growth after incubation period. 10 μL is taken from tubes or wells that have no visible growth and spread over the surface of agar plates. After the incubation, the lowest antimicrobial agent concentration has no visible growth on the agar plate surface is considered to be the MBC value.

3.3.1. Broth Dilution Method

Broth micro-dilution or macro-dilution is one of the most basic antimicrobial susceptibility testing methods [8]. The procedure involves the preparation of two-fold or ten-fold dilutions of the antimicrobial agent in tubes containing a minimum of 2 mL (macro-dilution) or in a liquid growth medium distributed in smaller

volumes using 96-well microplates (microdilution) (Figures 2 and 3). After that, microbial suspension adjusted to 0.5 McFarland standard is inoculated into each tube or well. Then, the tubes or wells are incubated for a specified period at an appropriate temperature [17, 18].

McFarland standards are used as the turbidity standard for the preparation of microorganism suspensions. The McFarland 0.5 standard is mainly applied during the preparation of bacterial inoculum to perform antimicrobial susceptibility tests (at 625 nm OD: 0.08-0.1). In the case of the McFarland 0.5 standard is not used, too little bacterial inoculation can result in false-sensitive or too many bacterial inoculation results in false-resistant results.

In 1907, McFarland developed a series of barium sulfate solutions to estimate the number of bacteria in solutions of equal turbidity. Barium sulfate is prepared by adding sulfuric acid to the aqueous solution of barium chloride (adding 99,5 mL of 0,18 M Sulfuric acid to 0,5 mL of 0,048 M Barium chloride) [19].

The McFarland 0.5 standard corresponds to a homogeneous suspension containing approximately $1-2 \times 10^8$ cfu/mL bacteria and $1-5 \times 10^6$ cfu/mL *Candida*, which varies according to various bacteria and yeast species [20].

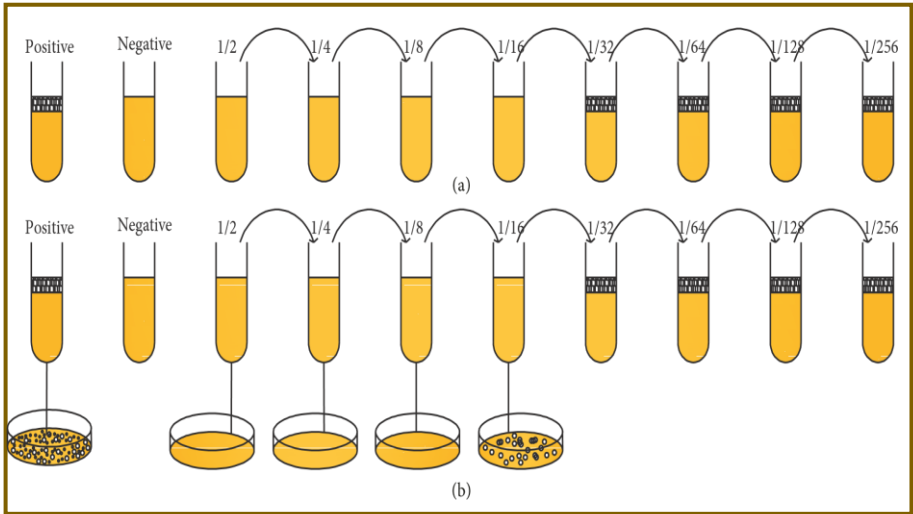


Figure 2: Picture of The Macrodilution Method Performed In Test Tubes A) Minimum Inhibition Concentration (MIC) B) Minimum Bacteriocidal-Fungicidal Concentration (MBC-MFC) [21].

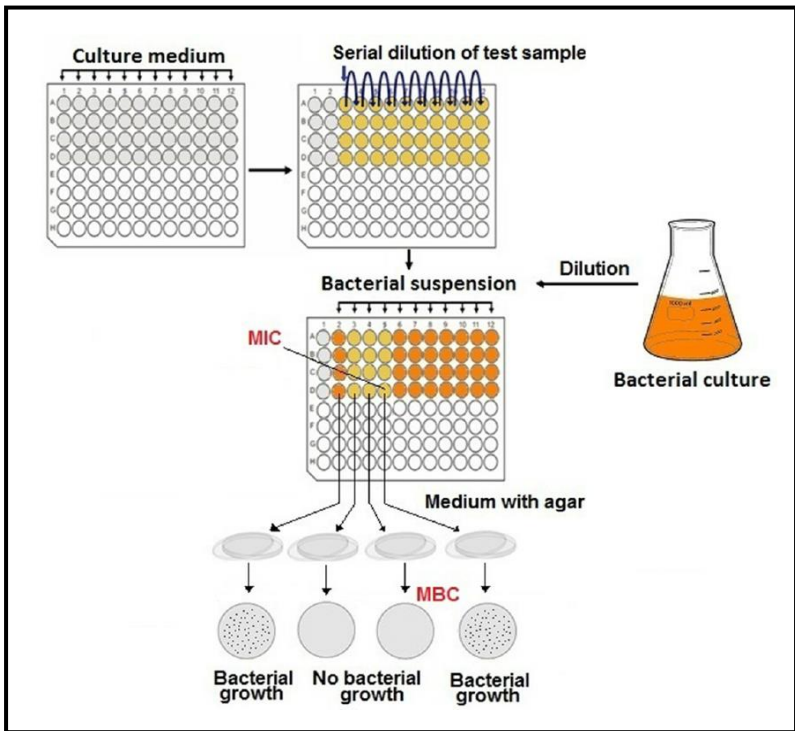


Figure 3: Schematic Representation of The Microdilution Method Carried Out In Microplates [22]

3.3.1.1. Determination of MIC value for microdilution assay

The determination of the MIC value for the interpretation of microdilution tests is mainly based on two methods. The first method is to determine the results by imaging devices that have a high ability to distinguish the growth in the wells. The second method is to determine the MIC value by various colorimetric methods based on the use of various dye reagents such as tetrazolium salts. Tetrazolium salts, 3-(4,5dimethylthiazol-2-yl)-2,5-diphenyltetrazolium bromide (MTT) and 2,3-bis {2-methoxy-4-nitro-5- [(sulfenylamino) carbonyl] -2H-tetrazolium - hydroxide} (XTT), are frequently used for the determination of MIC value for microdilution assays [16]. Resazurin (Alamar blue dye) is also an efficient living cell marker that can be used for this purpose (Figure 4) [23, 24].

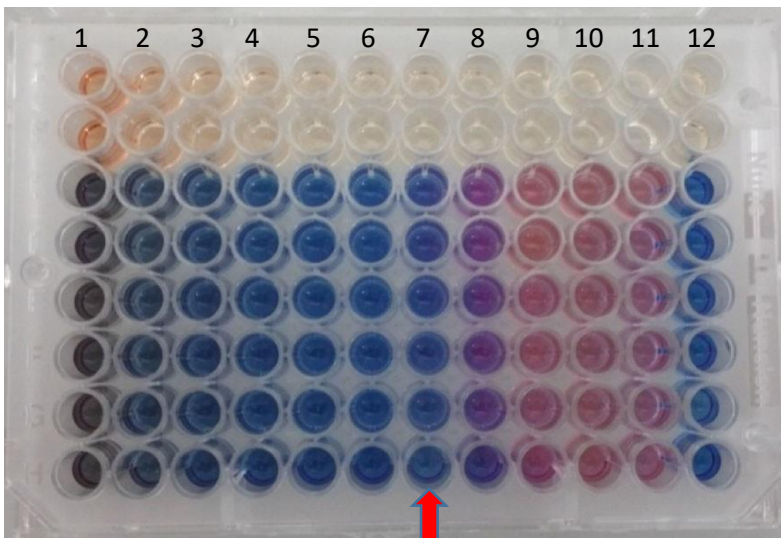


Figure 4: Microplate Image Where The Microdilution Method Is Applied. The Red Arrow Shows MIC Value Because There Is No Colour Changes In That Column [23].

3.3.2. Agar Dilution Method

The agar dilution method is based on the inclusion of various concentrations of the antimicrobial agent in an agar medium (molten agar medium) using dilutions, and then incubation of a particular microorganism on the agar plate surface. The MIC value is recorded as the plate value with the lowest concentration of antimicrobial agent, where growth is completely inhibited under appropriate incubation conditions. (Figure 5) [8,16].

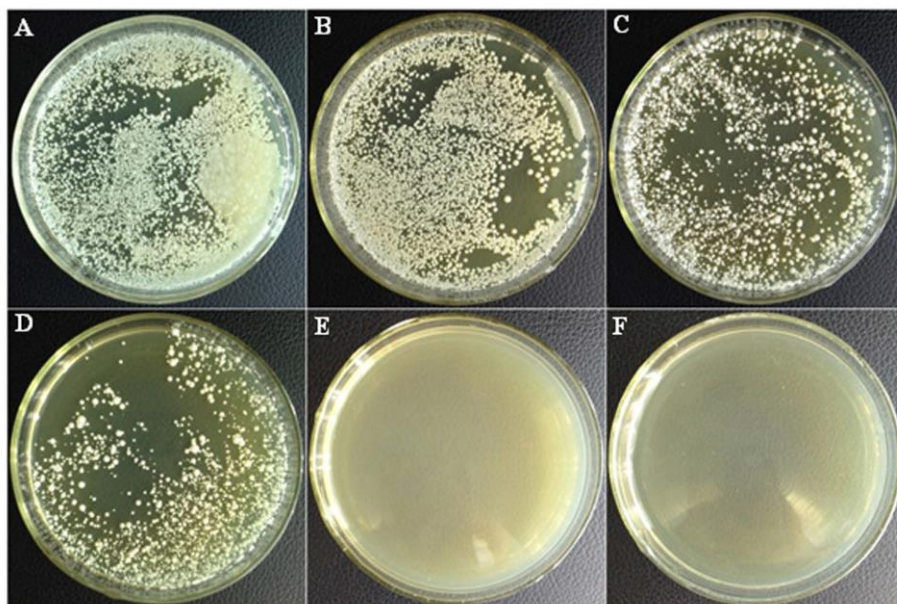


Figure 5: Petri Dish Pictures Of Garlic Oil Antifungal Activity Assay With Different Concentrations ($\mu\text{g}/\text{ml}$) Against *C. Albicans* In Overnight Incubation Using Agar Dilution Method. (A) Control, (B) 0.04, (C) 0.09, (D) 0.17, (E) 0.35, (F) 0.69 [25].

3.3.2.1. Advantages of Agar Dilution Method

This technique can be used appropriately for both antibacterial and antifungal activity testing. If the tested compound masks the detection of microbial growth in the liquid medium, the agar dilution method overcomes this problem, and it is the most suitable method for MIC determination. In the possible case, contamination cannot be easily detected in the broth dilution method, but it can be easily determined in the agar dilution method [26]. Moreover, this method offers a good correlation with E-test for antibacterial testing.

3.4. Diffusion Method

This test is based on the fact that paper discs impregnated with antimicrobial agents diffuse into the medium where the microorganism is inoculated.

3.4.1. Disc Diffusion Method (Kirby-Bauer Method)

Kirby, Bauer, and their friends defined the disc diffusion method as the first standard method for determining antimicrobial activity in 1966. Since then, this method has been used extensively for the detection of antimicrobial activity. This method creates a gradient of antimicrobial agent concentration as the antimicrobial agent radiates radially into the agar [4].

As the first step of this method, the microorganism to be tested is adjusted to 0.5 McFarland standard. After that, 10 μ l of this microorganism is inoculated on the Mueller-Hinton agar surface. Filter paper discs (around 6 mm in diameter) containing the test compound are placed on the agar surface, and then Petri dishes are incubated for a certain period under appropriate conditions. At the end of this period, the inhibition zones around the discs are measured with a ruler and compared to the standard zone table, they are evaluated as sensitive (S), intermediate (I), and resistant (R) (Figure 6 and Table 1). [27, 28].

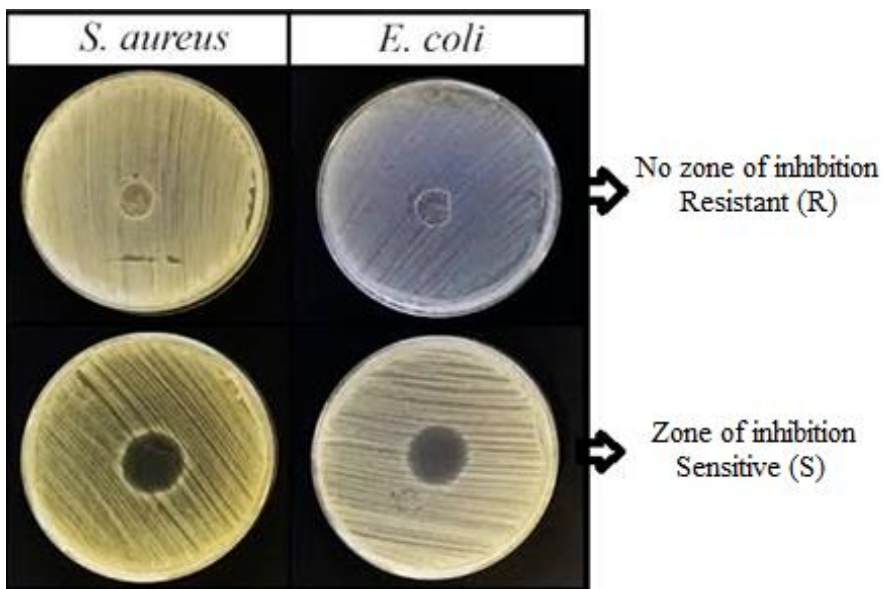


Figure 6: Petri Dishes Photos With Inhibition Zones Formed By Antimicrobial Agent Applied Using Disc Diffusion Method (Adapted From Marti et al. 2018) [29].

The assessment of inhibition zone sizes varies in different types of microorganisms. In table 1, *Staphylococcus* species, *E.coli*, and other

enteric Gram (-) rods are interpreted as resistant/medium/sensitive as the two examples of bacteria group against various antibiotic discs [28].

Table 1: According To CLSI Standards, Interpretable Zone Sizes Of *Staphylococcus* species, *E.coli* and Other Enteric Gram (-) Rods Against Different Antibiotic Groups (Adapted From Jorgensen and Turnidge 2015) [28,7].

<i>Staphylococcus</i> species (Zone Diameter, nearest whole mm)				<i>E.coli</i> and other enteric Gram Negative Rods (Zone Diameter, nearest whole mm)			
	Resistant	Intermediate	Susceptible		Resistant	Intermediate	Susceptible
Cefazolin (30 µg)	≤14	15-17	≥18	Amikacin (30 µg)	≤14	15-16	≤17
Clindamycin (2 µg)	≤14	15-20	≥21	Ampicillin (10 µg)	≤13	14-16	≤17
Erythromycin (15 µg)	≤13	14-22	≥23	Cefazolin (30 µg)	≤14	15-17	≤18
Gentamicin (10 µg)	≤12	13-14	≥15	Gentamicin (10 µg)	≤12	13-14	≤15
Oxacillin (1 µg)	≤10	11-12	≥13	Tetracycline (30 µg)	≤14	15-18	≤19
Penicillin G (10 µg)	≤28	-	≤29	Ticarcillin (75 µg)	≤14	15-19	≤20
Tobramycin (10 µg)	≤12	13-14	≤15	Trimethoprim (5 µg)	≤10	11-15	≤16
Vancomycin (30 µg)	-	-	≤15	Tobramycin (10 µg)	≤12	13-14	≤15

While applying the disc diffusion method, it is necessary to pay attention to some points. The maximum amount of 12 antibiotic discs can be placed on 150 mm plates, and this amount should be 5 discs for 100 mm plates [27]. Antibiotic discs should not be closer than 24 mm to each other. Moreover, the thickness of the medium should be 4 mm ± 0.5 mm. In the case of agar thickness on the plate is too thick or thin, the zone diameters would be narrow or large, respectively. Because of that, zone diameters can be misinterpreted [30]. Before placing a disc, a homogeneous inoculation should be performed on the surface of agar plates. If there is no homogeneous distribution on the agar surface and

the colonies are so rare that they appear individually, the inoculation should be repeated.

3.4.1.1. Advantages of the Disc Diffusion Method

It provides qualitative results by classifying bacteria as sensitive, medium, or resistant. Therefore, the resistance phenotype of the microbial strain tested is easily evaluated. Clinicians use the results of the method for the selection of antibiotics suitable for empirical treatments and specific patients in certain situations. Compared to other methods, it is simple and low cost. It also can test a large number of microorganisms and antimicrobial agents at the same time, and the results found allow simple and straightforward interpretation [26, 31].

3.4.1.2. Disadvantages of the Disc Diffusion Method

Since bacterial growth inhibition does not imply bacterial death, this method does not distinguish between bactericidal and bacteriostatic effects. In addition to that, MIC cannot be determined in the disc diffusion method because it is impossible to measure the amount of antimicrobial agents spread over the agar medium.

3.4.2. Antimicrobial Gradient Method (Etest)

The antimicrobial gradient method is a combination of dilution methods and disk diffusion methods for determining the MIC value. The method

is evaluated by generating a concentration gradient of the antimicrobial agent tested on the agar plate. [8,32].

In the procedure, the bacterial suspension is adjusted to the density of a 0.5 McFarland standard and then inoculated onto the agar surface. A strip penetrated by the increasing concentration gradient of the antimicrobial agent is then placed on the agar surface. Depending on the type of microorganism to be tested for sensitivity, agar plates are incubated under appropriate conditions for a specified period. At the end of this period, the MIC value is detected in the growth inhibition ellipse intersects (Figure 7).

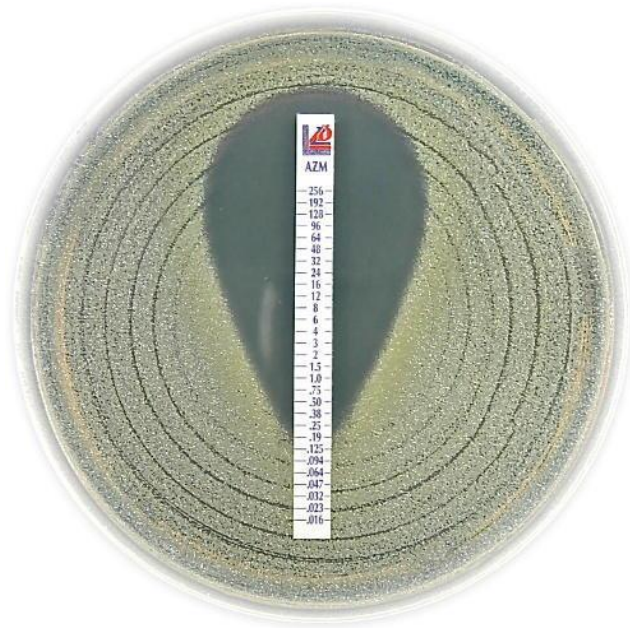


Figure 7: The Photo Of Inhibition Ellipse Resulting From Etest Applied On The Agar Plate [33].

3.4.2.1. Advantages and Disadvantages of Antimicrobial Gradient Method (Etest)

Etest is practically performed similarly by the disk diffusion method. It is, therefore, technically simple to apply. The versatility and ease of applicability make Etest more preferable than traditional sensitivity tests. The MIC value is read directly from the scale at the point of growth inhibition. Therefore, Etest is used in routine hospital laboratories to meet the needs of clinicians [32].

However, the cost of each of the Etest strips is about \$ 2-3 and is a financial burden when multiple samples are tested in routine laboratory studies. Besides, the application of the method requires technical experience [26].

3.5. Determination of Antimicrobial Susceptibility of Hard-Growing Microorganisms

Muller Hinton Agar (MHA) and Muller Hinton Broth (MHB) media, which are widely used in the determination of antimicrobial activity, are not suitable for hard-growing microorganisms.

3.5.1. Determination of Antimicrobial Susceptibility of *Haemophilus* spp.

Haemophilus Test Media (HTB) is used for the determination of the Antimicrobial Susceptibility of *Haemophilus* spp. It is applied only by the broth dilution method. The applicability of the agar dilution method has not been investigated. 15 µg / ml β-NAD (not autoclaved), 15 µg / ml beef hematin (autoclavable), and 5 g / L yeast extract are added to the MHB used.

3.5.2. Determination of Antimicrobial Susceptibility of *Neisseria gonorrhoeae*

GC-Lect Agar (Gonococcus agar) medium is used to determine the Antimicrobial Susceptibility of *Neisseria gonorrhoeae*. Only the agar dilution method is applied. After the medium is autoclaved, 1 % reproduction additive is added. The production additives in 1 liter of water are: 1.1g L-cysteine, 0.03g guanine HCl, 3 mg thiamine HCl, 13mg PABA, 0.01g B12, 0.1g co-carboxylase, 0.25g NAD, 1g adenine, 10g L-glutamine, 100g glucose 0.02g ferric nitrate. The bacterial suspension is adjusted to 0.5 McFarland turbidity by directly colony method and should be used within 15 minutes. The suspension is incubated for 20-24 hours in an environment of 5% CO₂ at 35 ° C.

3.5.3. Determination of Antimicrobial Susceptibility of *Streptococcus pneumonia* and other *Streptococcus* spp.

Mueller Hinton Agar or Broth supplemented with 2- 5 % sheep blood is used for determination of Antimicrobial Susceptibility of *Streptococcus pneumonia* and other *Streptococcus* spp. The bacterial suspension is taken from colonies grown in overnight blood agar and adjusted to 0.5 McFarland turbidity. The procedure specified for the broth dilution method is applied within 15 minutes. After that, the bacterial suspension is incubated at 35 ° C under normal atmospheric conditions for 20-24 hours.

4. CORRECT USAGE OF ANTIMICROBIAL SUBSTANCES AND MANAGEMENT OF THIS TARGET

Antibiotics used today are in danger of losing their effectiveness due to increased microbial resistance [34]. As a result, treatment failures associated with multidrug-resistant bacteria can be seen, which has become a global concern for public health [35]. The amount of death in infections caused by antibiotic-resistant microorganisms is approximately 700,000 people worldwide, and this amount is expected to be 10 million people by 2050 [36]. As a result, we can be able to lose our lives even from uncomplicated infections caused by multidrug-resistant bacteria. [37].

During treatment, a change occurs in the susceptibility of disease agents to antimicrobial drugs, and as a result, drugs against the disease agent become insufficient. In such cases, infection recurrences occur, and the prognosis of the infection shifts in different directions.

In all these cases, scientists tend to turn to alternative antimicrobial agents. In particular, natural antimicrobial agents are more preferred than chemical agents with intense side effects. Natural antimicrobial products are produced from prokaryotic and eukaryotic microorganisms, various plants, and animals. Thus, the discovery of new, natural, biocompatible antimicrobial agents is carried out by using antimicrobial determination methods.

5. ACCURATE AND RATIONAL ANTIMICROBIAL USE IN MEDICINES

The number of patients admitted to the hospital for systemic bacterial infection is almost half the total number of patients (45.1% for the service and 57.7% for the intensive care unit) [38]. In accordance with this, incorrect and irrational antimicrobial use can have negative consequences for the patient and the community. The risk of infection may increase with resistant bacteria. Damage caused by drug side effects may increase. At the same time, the economic burden increases as a result of unnecessary drug use.

Accurate and rational antimicrobial use in Medicine involves the use of the appropriate antibiotic for the patient with the right (narrowest spectrum) drug selection, the right dose, the right time, with the correct diagnosis, clinically and laboratory.

The positive effects of the improvements made on antimicrobial use on the patient and the society are as follows. Patients are ensured to benefit from antimicrobial treatment in the most appropriate way. Moreover, the spread of resistant microorganisms is prevented in hospitals. At the same time, adverse drug side effects on the patient and clinical cost are reduced [39].

CONCLUSION

Antimicrobial agents can be used in a wide variety of biotechnology fields. These agents can be used in food packaging, detergents, building paints and coating materials, coating of interior and exterior installation materials. It can also be used in cosmetics, disinfectant products, fabrics, carpets and upholstery materials, dental and body implants. Moreover, it can be used to accelerate growth, prevent, and treat diseases in farms and poultry.

Correct and appropriate use of antimicrobial agents is required by ensuring that the proper drug is selected in the proper time, in the adequate dose, for a suitable period. However, since uncontrolled and excessive use of antimicrobials in products created as a result of

bioengineering may have an allergic or toxic effect on living beings, it is crucial to apply antimicrobial management effectively not only in medicine but also in biotechnological applications.

Considering all the in-vitro methods described comparatively in this Chapter, the Disk diffusion method and Etest are more comfortable to apply than other methods. However, dilution methods should be preferred to obtain a quantitative result and to determine the MIC value. Etest can also be used to obtain results that are more satisfactory by determining the MIC value. However, we mentioned before that Etest is a more expensive method than other methods. Consequently, the most appropriate method should be preferred depending on the type of microorganism, the sensitivity of which will be measured, and the nature of the agent whose antimicrobial activity will be determined.

REFERENCES

1. Powers JH. Antimicrobial drug development – the past, the present, and the future. *Clin Microbiol Infect.* 2004 Nov;10 (4), 23–31.
2. Saga T, Yamaguchi K. History of Antimicrobial Agents and Resistant Bacteria. *Japan Med Assoc J.* 2009;52(2), 103–108.
3. Gaynes R. The Discovery of Penicillin—New Insights after More Than 75 Years of Clinical Use. *Emerg Infect Dis.* 2017 May; 23(5), 849–853.
4. Bauer AW, Kirby WM, Sherris JC, Turck M. Antibiotic susceptibility testing by a standardized single disk method. *Am J Clin Pathol.* 1966 Apr;45(4), 493-6.
5. Ericsson H, Sherris JC. Antibiotic sensitivity testing. Report of an international collaborative study. *Acta Pathol Microbiol Scand B Microbiol Immunol.* 1971 May;217(1), 1-90.
6. The European Committee on Antimicrobial Susceptibility Testing. Antimicrobial susceptibility testing. calibration and validation. 2020 (updated 1 Jan 2020) Available from: <http://www.eucast.org>
7. Clinical and Laboratory Standards Institute. Methods for Dilution Antimicrobial Susceptibility Tests for Bacteria that Grow Aerobically, Approved Standard, 11th ed., CLSI document M07. 2018 Available from: https://clsi.org/media/1928/m07ed11_sample.pdf

8. Balouiri M, Sadiki M, Ibsouda SK. Methods for in vitro evaluating antimicrobial activity: A review. *J Pharm Anal.* 2016 Apr;6, 71–79
9. Dixon DM, Walsh TJ. Antifungal Agents. In Baron S, editor. *Medical Microbiology.* 4th ed. Galveston: University of Texas Medical Branch at Galveston; 1996. Chapter 76.
10. Saran B, Karahan ZC. Antimikrobiyal Ajanlara Genel Bakış. *Turk Urol Sem.* 2010;1, 216-20.
11. Sarkar P, Yarlagadda V, Ghosh C, Haldar J. A review on cell wall synthesis inhibitors with an emphasis on glycopeptide antibiotics. *Med Chem Comm.* 2017 Mar;8(3), 516–533.
12. Poehlsgaard J, Douthwaite S. The bacterial ribosome as a target for antibiotics. *Nat Rev Microbiol.* 2005 Oct;3, 870–881.
13. Collin F, Karkare S, Maxwell A. Exploiting bacterial DNA gyrase as a drug target: current state and perspectives. *Appl Microbiol Biotechnol.* 2011 Nov;92(3), 479–497.
14. Hooper DC, Jacoby GA. Topoisomerase Inhibitors: Fluoroquinolone Mechanisms of Action and Resistance. *Cold Spring Harb Perspect Med.* 2016 Sep;6(9), a025320.
15. Villa DF, Aguilar MR, Rojo L. Folic Acid Antagonists: Antimicrobial and Immunomodulating Mechanisms and Applications. *Int J Mol Sci.* 2019 Oct;20(20), 4996.
16. Wiegand I, Hilpert K, Hancock RE. Agar and broth dilution methods to determine the minimal inhibitory concentration (MIC) of antimicrobial substance. *Nat Protoc.* 2008 Jan;3(2), 163-75.

17. Ingroff AE, Kerkering TM, Goldson PR, Shadomy S. Comparison study of broth macrodilution and microdilution antifungal susceptibility tests. *J Clin Microbiol.* 1991 Jun;29(6), 1089–1094.
18. Abbasoglu U. Antimikrobiyal Aktivite Araştırma Yöntemleri. *FABAD J Pharm Sci.* 1996 May;22, 111-118.
19. McFarland J. The nephelometer: an instrument for estimating the numbers of bacteria in suspensions used for calculating the opsonic index and for vaccines. *JAMA.* 1907 Oct;(49), 1176-1178.
20. Guinea J, Recio S, Escribano P, Torres-Narbona M, Peláez T, Sánchez-Carrillo C, Rodríguez-Créixems M, Bouza E. Rapid Antifungal Susceptibility Determination for Yeast Isolates by Use of Etest Performed Directly on Blood Samples from Patients with Fungemia. *J Clin Microbiol.* 2010 Jun;48(6), 2205–2212
21. Yilmaz T. Minimum inhibitory and minimum bactericidal concentrations of boron compounds against several bacterial strains. *Turk J Med Sci.* 2012 Dec;42(2), 1423-1429.
22. Paiva PMG, Pontual EV, Coelho LCBB, Napoleão TH. Protease inhibitors from plants: Biotechnological insights with emphasis on their effects on microbial pathogens, In book: *Microbial pathogens and strategies for combating them: science, technology and education, Microbiology Book Series – 2013th ed.* Formatex Research Centre; 2013. p. 641-649

23. Elshikh M, Ahmed S, Funston S, Dunlop P, McGaw M, Marchant R, Banat IM. Resazurin-based 96-well plate microdilution method for the determination of minimum inhibitory concentration of biosurfactants. *Biotechnol Lett.* 2016 Mar;38,1015–1019
24. Farkas A, Pap B, Kondorosi E, Maróti G. Antimicrobial Activity of NCR Plant Peptides Strongly Depends on the Test Assays. *Front Microbiol.* 2018 Oct;9, 1-10.
25. Li WR, Shi QS, Dai HQ, Liang Q, Xiao-BaoXie, Huang XM, Zhao GZ, Zhang LX. Antifungal activity, kinetics and molecular mechanism of action of garlic oil against *Candida albicans*. *Nature Sci Rep.* 2016 Mar;(6), 22805
26. Schofield CB. Updating antimicrobial susceptibility testing: Methods. *Clin Lab Sci.* 2012 Oct;25:233–239.
27. Hudzicki J. Kirby- Bauer disk diffusion susceptibility test protocol. American Society for Microbiology. 2009 Dec; Available from: <https://www.asm.org/getattachment/2594ce26-bd44-47f6-8287-0657aa9185ad/Kirby-Bauer-Disk-Diffusion-Susceptibility-Test-Protocol-pdf.pdf>
28. Jorgensen J, Turnidge J. (2015). Susceptibility Test Methods: Dilution and Disk Diffusion Methods, In Jorgensen J, Pfaller M, Carroll K, Funke G, Landry M, Richter S, Warnock D, editors, *Manual of Clinical Microbiology*, 11th ed. Washington: ASM Press; 2015. p 1253-1273.

29. Martí M, Frígols B, Serrano-Aroca A. Antimicrobial Characterization of Advanced Materials for Bioengineering Applications. *J Vis Exp*. 2018 Aug;138, e57710.
30. Flanagan JN, Steck TR. The Relationship Between Agar Thickness and Antimicrobial Susceptibility Testing. *Indian J Microbiol*. 2017 Dec;57(4), 503–506.
31. Bonev B, Hooper J, Judicaël P. Principles of assessing bacterial susceptibility to antibiotics using the agar diffusion method. *J Antimicrob Chemother*. 2008 Jun;61(6),1295-301.
32. Brown DFJ, Brown L. Evaluation of the E test, a novel method of quantifying antimicrobial activity. *J Antimicrob Chemother*. 1991 Feb;27(2), 185–190.
33. Liofilchem. MIC Test Strip. 2010. Available from <https://www.liofilchem.com/en-us/products/featured-products/mic-test-strip-liofilchem.html>
34. Ventola CL. The Antibiotic Resistance Crisis Part 1: Causes and Threats. *P T*. 2015 Apr;40(4), 277–283.
35. Prestinaci F, Pezzotti P, Pantosti A. Antimicrobial resistance: a global multifaceted phenomenon. *Pathog Glob Health*. 2015 Oct;109(7), 309–318.
36. Dadgostar P. Antimicrobial Resistance: Implications and Costs. *Infect Drug Resist*. 2019 Dec;12: 3903–3910.
37. Guschin A, Ryzhikh P, Rumyantseva T, Gomberg M, Unemo M. Treatment efficacy, treatment failures and selection of macrolide resistance in patients with high load of *Mycoplasma*

genitalium during treatment of male urethritis with Josamycin. *BMC Infect Dis.* 2015 Feb;15, 1–7.

38. Alemkere G, Tenna A, Engidawork E. Antibiotic use practice and predictors of hospital outcome among patients with systemic bacterial infection: Identifying targets for antibiotic and health care resource stewardship. *PLoS One*, 2019 Feb;14(2), e0212661.
39. Sultana J, Cutroneo P, Trifirò G. Clinical and economic burden of adverse drug reactions. *Pharmacol Pharmacother.* 2013 Dec;4(Suppl1), S73–S77.



IKRAF
Publishing House



ISBN: 978-625-7897-22-8